Spring 2013

Efficient uncertainty quantification in aerospace analysis and design

Yi Zhang

Department: Mechanical and Aerospace Engineering

EFFICIENT UNCERTAINTY QUANTIFICATION IN AEROSPACE ANALYSIS AND DESIGN

by

YI ZHANG

A DISSERTATION

Presented to the Faculty of the Graduate School of the

MISSOURI UNIVERSITY OF SCIENCE AND TECHNOLOGY

In Partial Fulfillment of the Requirements for the Degree

DOCTOR OF PHILOSOPHY

in

AEROSPACE ENGINEERING

2013

Approved by

Dr. Serhat Hosder, Advisor
Dr. Xiaoping Du
Dr. David W. Riggins
Dr. Fathi Finaish
Dr. Leifur Thor Leifsson

ABSTRACT

The main purpose of this study is to apply a computationally efficient uncertainty quantification approach, Non-Intrusive Polynomial Chaos (NIPC) based stochastic expansions, to robust aerospace analysis and design under mixed (aleatory and epistemic) uncertainties and demonstrate this technique on model problems and robust aerodynamic optimization. The proposed optimization approach utilizes stochastic response surfaces obtained with NIPC methods to approximate the objective function and the constraints in the optimization formulation. The objective function includes the stochastic measures which are minimized simultaneously to ensure the robustness of the final design to both aleatory and epistemic uncertainties. For model problems with mixed uncertainties, Quadrature-Based and Point-Collocation NIPC methods were used to create the response surfaces used in the optimization process. For the robust airfoil optimization under aleatory (Mach number) and epistemic (turbulence model) uncertainties, a combined Point-Collocation NIPC approach was utilized to create the response surfaces used as the surrogates in the optimization process. Two stochastic optimization formulations were studied: optimization under pure aleatory uncertainty and optimization under mixed uncertainty. As shown in this work for various problems, the NIPC method is computationally more efficient than Monte Carlo methods for moderate number of uncertain variables and can give highly accurate estimation of various metrics used in robust design optimization under mixed uncertainties. This study also introduces a new adaptive sampling approach to refine the Point-Collocation NIPC method for further improvement of the computational efficiency. Two numerical problems demonstrated that the adaptive approach can produce the same accuracy level of the response surface obtained with oversampling ratio of 2 using less function evaluations.

ACKNOWLEDGMENTS

First of all, I would like to express my deepest gratitude to my academic advisor, Dr. Serhat Hosder, and thank him for his excellent guidance, patience, caring and providing me the opportunity to work on this research. This work was possible because of his constant stimulation and full support. I feel honored to have been a part of his group for the past three years and I am sure that his example as a teacher and a scientist will continue to inspire me in the future.

I am also grateful to Dr. Xiaoping Du, Dr. Leifur Thor Leifsson, Dr. David Riggins and Dr. Fathi Finaish for serving on my advisory committee and enriching my useful knowledge and skills during my PhD study. Also I would like to acknowledge Dr. Leifsson for providing us the Matlab set-up for CFD runs.

I would like to thank Tyler Winter from M4 Company for his time and effort in training python software and his support while working together for the NASA STTR project.

I would also like to thank the Missouri University of Science and Technology and Aerospace Engineering Department for the education process they have provided me over the past three years. I would like to acknowledge the NASA STTR Grant NNX11CC60C for their partial support and funding throughout my graduate career. Furthermore, I want to thank the Mechanical and Aerospace Engineering Department for providing me the teaching assistant opportunity.

I also want to thank Ben Bettis, Srikanth Adya, Daoru Han, Thomas West, Harsheel R Shah and Zhen Hu for all of their sincere support while working together in the Aerospace Simulation Laboratory.

Finally, I would like to thank my family for their love and support. Without their encouragement and love, I would not able to finish my dissertation.

TABLE OF CONTENTS

LIST OF ILLUSTRATIONS

LIST OF TABLES

NOMENCLATURE

Symbol	Description
a	Length of a beam
b	Length of connecting rod
c	Maximum ordinate of the mean camberline
C_d	Drag coefficient
$\bar{\sigma}_{C_d}$	Average standard deviation of C_d
C_L	Lift coefficient
C_L^*	Desired profile lift coefficient value
C_p	Pressure coefficient
d	Diameter of a shaft
e	Offset distance
$e_{R_i}^k$	Local response surface error corresponding to i^{th} probability level at k^{th} iteration
E_{RT}^k	Total response surface error at k^{th} iteration
$f_S(\vec{S}_a)$	The joint probability function of $\vec{S}_a$
F	External force
g	Limit state function
g_i	Inequality constraints
H_{en}	Hermite polynomial
k	Factor for turbulence model
l	Length of a shaft or beam
l_c	Chordwise position of the maximum oridinate
$L_{n_{\alpha_A},k}$	Lagrange polynomial at α_{Ak}
L/D	Lift-drag ratio
M_∞	Mach number

n	Number of uncertain variables
n_{α_A}	Degree of interpolation in α_A
N	Total function evaluations
N_a	Number of aleatory uncertainties
N_{CDF}	Total number of CDF simulations required to create composite response surface
N_e	Number of epistemic uncertainties
$N^k_{samples}$	Number of samples for stochastic expansions at k^{th} iteration
N_t	Total number of expansion terms
N_{total}	Total sample size on uncertain variable design space
OSR	Over sampling ratio
p	Expansion order
$\vec{P}_a$	Aleatory parameter vector
$\vec{P}_e$	Epistemic parameter vector
R	Output performance
$\bar{R}$	Average of interval R
$\hat{R}$	Composite response surface
R^k_i	Output value obtained from exact function at check points corresponding to i^{th} probability level at k^{th} iteration
R_L	Lower bound of R
R^k_{si}	Output value obtained from response surface approximation corresponding to i^{th} probability level at k^{th} iteration
R^{av}_{si}	Average value of output obtained from response surface approximation at i^{th} probability level
R^{max}_{si}	Maximum value of output obtained from response surface approximation at i^{th} probability level

R_{si}^{min}	Minimum value of output obtained from response surface approximation at i^{th} probability level
R_U	Upper bound of R
$\vec{s}$	Epistemic variable (or deterministic design variable)
S	Yield strength
$\vec{S}_a$	Aleatory uncertain vector
$\vec{S}_e$	Epistemic uncertain vector
T	External torque
t	Thickness to chord ratio
V	Volume of a beam
w	Weight factor
$\vec{X}_a$	Aleatory design vector
$\vec{X}_d$	Deterministic design vector
$\vec{X}_e$	Epistemic design vector
α	Coefficient of stochastic expansions
α_A	Angle of attack
β	Probability of constraint satisfaction
$\delta\sigma_R$	Difference standard deviation of R
$\delta\sigma_{C_d}$	Difference standard deviation of C_d
ΔE_{RT}^k	Reduction value of total probability error at k^{th} iteration
θ	Angle of crank
$\bar{\mu}_{C_d}$	Average mean value of C_d
μ_{C_L}	Mean value of C_L
$\mu_{C_L}^{min}$	Minimum mean value of C_L
μ_R	Mean of R
$\bar{\mu}_R$	Average mean value of R

ν_t	Kinematic eddy viscosity
$\nu_{t_{SA}}$	Turbulent viscosity originally obtained with the Spalart-Allmaras
ξ	Standard random variable
$\vec{\xi}_a$	Standard aleatory variable
$\vec{\xi}_s$	Standard epistemic variable (or deterministic design variable)
$\rho(\vec{\xi})$	Weight function
σ_R	Standard deviation of R
$\bar{\sigma}_R$	Average standard deviation of R
σ_R^{max}	Maximum standard deviation of R
σ_R^{min}	Minimum standard deviation of R
Ψ	Random basis function
Ω	Integral support region

1. INTRODUCTION

In this section, first the motivation for efficient uncertainty quantification (UQ) in aerospace analysis and design is given. The following section gives the literature review which focuses on uncertainty quantification and robust design. Next, objectives of this PhD study and contribution of the current work to the literature are presented. Finally, an overview of the sections in this dissertation is presented.

1.1. MOTIVATION FOR UNCERTAINTY QUANTIFICATION

Uncertainties are general ubiquitous in analysis and design of highly complex engineering systems, such as aerospace analysis and design. Uncertainties can arise due to the ignorance, lack of knowledge and incomplete information in physical modeling (e.g., epistemic uncertainty in turbulence models) and from inherent variations in the systems (e.g., aleatory uncertainty in operating conditions). It is important to consider these uncertainties in applications such as robust design and reliable design of aerospace systems. Reliability design is to seek a design that achieves a required probability of failure (less than some acceptable and constant small value) and therefore ensures that the conditions that lead to disaster are highly unlikely. Robust design is a design methodology for improving the quality of a product by minimizing the impact of uncertainties on the product performance. The objective of robust design is to optimize the mean performance while minimizing the variation of performance caused by various uncertainties. In this study, uncertainties are mainly considered in applications of the robust design. One application is the robust aerodynamic shape optimization under aleatory and epistemic uncertainties. In the context of aerodynamic shape optimization, robust design implies that the performance (such as the lift-to-drag ratio) of the final configuration should be

insensitive to the uncertainties in the operating conditions (e.g., free-stream Mach number). Furthermore, the final design should be relatively insensitive to the physical modeling uncertainties in the computational tools used for aerodynamic analysis such as the computational fluid dynamics (CFD) codes. One very important component of robust design is the uncertainty quantification (UQ), which may increase the computational expense of the design process significantly compared to the computational work of deterministic optimization, especially when high-fidelity analysis tools are used to improve accuracy. Therefore, it is important to develop and implement computationally efficient robust design methodologies while keeping the desired accuracy level in the optimization process.

1.2. LITERATURE REVIEW

The following literature review includes two main topics. The first topic is a review of previous studies on uncertainty quantification. The second topic contains a review of various studies that have been conducted on robust design optimization.

1.2.1. UQ Methods. The goal of uncertainty quantification is to determine how random variation (aleatory) and lack of knowledge (epistemic) affect the sensitivity, performance, or reliability of the system that is being modeled. Various studies have been made on the topic of propagating aleatory uncertainty through Monte Carlo Simulation (MCS) [1, 2, 3, 4, 5], expansion-based methods (e.g., Taylor series [6, 7, 8, 9] and perturbation method [10, 11, 12]) and Non-Intrusive Polynomial Chaos (NIPC) Expansions [13, 14, 15] and propagating epistemic uncertainty through interval analysis and evidence theory [16, 17, 18, 19, 20, 21].

The MCS is the most comprehensive but expensive uncertainty quantification approach for evaluating statistical moments, reliability and quality of system response. It is a method for iteratively evaluating a deterministic model using sets of random numbers as inputs. This method is often used when the model is complex, nonlinear,

or involves large number of uncertain parameters. Maurice G. Cox et al. [3] worked on using MCS to determine the probability density function (PDF) of the output quantities. Zhao, L.Y et al. investigated uncertainty quantification of a flapping airfoil with stochastic velocity deviations by using a classic Monte Carlo method to numerically investigate the responses of the time-averaged thrust coefficient and the propulsive efficiency with respect to a stochastic flight velocity deviation under Gaussian distributions [4, 5]. Y. P. Ju et al. conducted studies on multi-point robust design optimization of wind turbine airfoils under geometric uncertainty where the MSC technique was used for simulating the geometric uncertainty in the robust optimization [22]. Although, MCS is the most popular sampling based method, it requires thousands of computational simulations (e.g., CFD, finite element analysis (FEA)) for obtaining accurate results. It is considerably expensive and can not be affordable for complex engineering simulations so that it is often used as benchmark for verification of uncertainty quantification analysis when other methods are used.

The expansion-based UQ is used to estimate the statistical moments (e.g., mean, variance, etc.) of the system response with a small perturbation to simulate the effect of the input uncertainty. The Taylor series and perturbation method are two main expansion-based UQ approaches. The Taylor series is a series expansion of a function about a point and used to approximate a function with a Taylor polynomial. For example, first order reliability method (FORM) uses the first order Taylor expansion (linearization) to approximate the uncertainty in the output [6]. There have also been some studies on Taylor series expansion techniques and applications in physics [7, 8, 9]. The perturbation method is used to find an approximate solution to a problem which cannot be solved by traditional analytical methods. It allows the simplification of complex mathematical problems [10, 11, 12]. Both Taylor series and perturbation methods have advantages when dealing with relatively small input variability and outputs that do not express high nonlinearity. However, most real-life problems

require much more difficult mathematical models, such as non-linear differential equations. Therefore, Taylor series and perturbation methods will not be a good option for uncertainty propagation in such cases.

The NIPC expansion is a spectral based technique for uncertainty quantification, which has been used recently for numerous physical models, such as elasticity and fluid mechanics [23, 24, 25]. Some studies conducted by Eldred et al. [14, 15] introduced efficient stochastic expansions based on NIPC for uncertainty quantification. In their study, they used Legendre and Hermite orthogonal polynomials to model the effect of uncertain variables described by uniform and normal probability distributions, respectively, and used Legendre orthogonal polynomials to model the effect of epistemic uncertainties. The accuracy and the computational efficiency of NIPC method applied to stochastic problems with multiple uncertain input variables were investigated by Hosder et al. [26, 27, 28].

The non-probabilistic approaches which are used for epistemic uncertainty quantification include interval analysis and evidence theory. There have been several previous studies conducted on epistemic uncertainty propagation [16, 17, 18]. The simplest way for epistemic uncertainty propagation is by interval analysis [19, 20, 21]. In interval analysis, it is assumed that nothing is known about the uncertain input variables except that they lie within certain intervals. L.P. Swiler and Thomas L. Paez [19, 20] examined three methods in propagating epistemic uncertainty including interval analysis, Dempster-Shafer evidence theory and Second-Order Probability and demonstrated examples of their use on a problem in structural dynamics and also examined the use of surrogate methods in epistemic analysis, both surrogate-based optimization in interval analysis and use of polynomial chaos expansions to provide upper and lower bound approximations. From their studies, it was proved that interval analysis can be effective in the quantification of epistemic uncertainty. Recently, there have been some studies investigating the topic of the mixed (aleatory

and epistemic) uncertainty propagation. Eldred and L.P. Swile et al. [29] proposed using Second-Order Probability for estimating the effect of mixed uncertainties. This method was used to separate the aleatory and epistemic uncertainties into inner and outer sampling loops, respectively. Moreover, they also applied this method to a cantilever beam design problem which was represented by two simple analytical functions. They utilized these analytical functions to represent ideal test cases since it was inexpensive to evaluate. Therefore, this study provided an analytical reference for validating codes used for mixed aleatory and epistemic uncertainty quantification. Bettis and Hosder applied the NIPC approach to the propagation of mixed uncertainty in hypersonic reentry problems [28, 30]. Du et al. [31] studied reliability-based design with a mixture of aleatory and epistemic variables input uncertainties. They introduced a method for dealing with a mixture of aleatory and epistemic input uncertainties by considering the reliability under the "worst case" combination of the epistemic variables. Moreover, they proposed an efficient methodology for the reliability-based design process with mixed input uncertainties such that the entire analysis process was not more computationally expensive than the reliability-based analysis involving only aleatory input uncertainties. Du and Guo [6, 32] also extended a unified uncertainty analysis framework to reliability analysis for multidisciplinary systems involving aleatory and epistemic as input uncertainties. They first applied proposed approach to a single disciplinary system and then extended the unified reliability analysis framework to multidisciplinary systems by proposing several algorithms. These algorithms were then applied to two different example problems, including a mathematical example and a low-speed aircraft wing design application.

1.2.2. Robust Design. Robust Design is a design methodology [33, 34] for improving the quality of a product by minimizing the impact of uncertainties on the product performance. Mathematically, the objective of robust design is to optimize the mean performance while minimizing the variation of performance

caused by various uncertainties. In practical applications, robust design is considered in many engineering fields to obtain high-performance products. Many studies of robust design have been investigated in the past decades [35, 36, 37, 38, 39, 40, 41, 42, 43, 44]. A comprehensive survey of robust optimization approaches is given by Beyer and Sendhoff [45]. Most of the previous stochastic design studies focused on optimization under aleatory uncertainties which utilized different approaches for uncertainty propagation. Among these studies, Eldred [46] formulated and investigated design under aleatory uncertainty with stochastic expansions. Dodson and Parks utilized polynomial chaos expansions for robust airfoil design under aleatory input uncertainties [47]. Byeng Dong Youn and K. K. Choi also developed a robust design optimization with epistemic uncertainty. For the epistemic uncertainty, the maximum likely value and equivalent variation were employed to define the new metric for the product quality loss in three different types of robust objectives [48]. There have been a number of robust design studies which considered both aleatory and epistemic uncertainties such as the work by Eldred [49], and Du et al. [50], who used a double-loop Monte Carlo sampling approach to determine the statistics of the response given in their model problems. None of the above studies investigated robust design under mixed uncertainties using the NIPC apporach. Moreover, the methods used within these studies were applied to various problems but none of them included aerodynamic optimization under mixed uncertanties. One of the main goals of this study was to implement stochastic expansions based on NIPC in robust optimization under mixed (aleatory and epistemic) uncertainties for aerodynamic shape design in transonic flow regime.

1.3. OBJECTIVES OF THE CURRENT STUDY

The primary objective of this study was to implement stochastic expansions based on NIPC in robust optimization under mixed (aleatory and epistemic)

uncertainties. This approach utilized stochastic response surfaces obtained with NIPC methods to approximate the objective function and the constraints in the optimization formulation. Both aleatory and epistemic uncertainties were considered in robust design. The objective function includes the stochastic measures, which are minimized simultaneously to ensure the robustness of the final design both to aleatory (inherent) and epistemic (model form) uncertainties. The computational efficiency and accuracy of stochastic optimization approach were demonstrated on aerodynamic optimization as well as model problems. To demonstrate the proposed approach for robust aerodynamic optimization under aleatory (Mach number) and epistemic (turbulence model) uncertainties, the NIPC response surfaces were used as surrogates in the optimization process. To create the surrogates, a combined NIPC expansion approach was utilized, which is a function of both the design and uncertain variables. Two stochastic optimization formulations were studied: (1) optimization under pure aleatory uncertainty and (2) optimization under mixed (aleatory and epistemic) uncertainty.

Besides the robust optimization approach with stochastic expansions, a new adaptive sampling approach was also introduced to refine Point-Collocation NIPC by using an over sampling ratio (OSR) between 1 and 2 based on the convergence check of the reduction of the total response surface error to further improve computational efficiency. The proposed adaptive sampling based Point-Collocation NIPC was implemented for pure aleatory uncertainty and mixed (aleatory and epistemic) uncertainty quantification, respectively. For adaptive sampling based Point-Collocation NIPC approach under mixed uncertainties, Second-Order Probability method was used with outer sampling for epistemic variables and inner sampling for aleatory variables both using the stochastic response surface approximation to generate the CDF curves of the output. Two numerical test problems demonstrated that the adaptive sampling based Point-Collocation NIPC approach can produce the

same accuracy level of the response surface obtained with over sampling ratio (OSR) of 2 using less number of function evaluations.

1.4. CONTRIBUTIONS OF THE CURRENT STUDY

The current study has three significant contributions to robust design optimization in aerospace and mechanical engineering. The first contribution is to apply the stochastic expansions based on NIPC to robust optimization problems with mixed uncertainties. The stochastic response surfaces were used to propagate the mixed aleatory and epistemic uncertainties through a "black-box simulation code in the optimization process. This proposed approach is much more efficient compared to traditional double loop MCS, since the function evaluation of the stochastic response surface is computationally less expensive than the traditional MCS.

The second contribution is the development of the adaptive sampling for Point-Collocation NIPC. To further improve computational efficiency, adaptive sampling approach was introduced to refine Point-Collocation NIPC based on the convergence check of the difference of total response surface error. Two different schemes, which include fixed check point and updated check point approaches for the calculation of the check points where the response surface error values are calculated for convergence check were also introduced. Based on this method, one can use probability level information of output performance for estimating the response surface more accurately and efficiently with less number of function evaluations. This approach was also demonstrated on two numberical model problems. The results were compared to the results that utilized double-loop MCS for the propagation mixed uncertainties for the validation of the methodology and demonstration of its computational efficiency.

The third contribution of this study is to implement and propagate a mixture of aleatory (inherent) and epistemic (model-form) uncertainties in transonic flow simulations and demonstrate robust airfoil optimization in this flow regime. The

topic of using combined stochastic expansions to propagate mixed uncertainties in transonic flows for robust optimization has not been investigated before. Therefore, the current research study can provide a detailed description on the implementation of combined stochastic expansions for mixed uncertainty propagation in transonic flow simulations for any future work on stochastic aerodynamic optimization.

1.5. DISSERTATION OUTLINE

This dissertation is composed of seven sections. In the second section, the uncertainty quantification with stochastic expansions will be presented which begins with an explanation of different types of uncertainties and different uncertainty modeling techniques. Then the theory of Polynomial Chaos, NIPC approaches and the detail description of the procedure for adaptive sampling based Point-Collocation NIPC approach will also be included in this section. The demonstration of NIPC approaches and adaptive sampling based Point-Collocation NIPC for UQ in model problems is given in Section 3. In Section 4, robust design with stochastic expansions will be discussed including the formulation of the robustness measures under different types of uncertainty and utilization of stochastic expansion for robust design with different polynomial expansion formulations. The applications of robust optimization to model problems and aerodynamic shape optimization are presented in Sections 5 and 6, respectively. Finally, all relevant conclusions and a discussion on future work will be given in the last section.

2. UNCERTAINTY QUANTIFICATION APPROACH

The purpose of this section is to describe the details of the methodology and approach used to propagate uncertainty through general computational simulations with stochastic expansions. In this section, an efficient approach will be described for mixed (aleatory and epistemic) uncertainty propagation by utilizing the NIPC method. It is important to first describe different types of uncertainty in aerospace simulations and the fundamental uncertainty quantification methods so that they can be later applied to applications in robust design optimization, as discussed in the following sections.

2.1. TYPES OF UNCERTAINTY IN AEROSPACE SIMULATIONS

In practical engineering applications, there are two types of input uncertainty that has to be considered in robust aerodynamic design studies: inherent (aleatory) uncertainty and model-form (epistemic) uncertainty [19, 51]. Aleatory uncertainty is classified as objective and irreducible uncertainty with sufficient information on input uncertainty data, whereas epistemic uncertainty is a subjective and reducible uncertainty that stems from lack of knowledge on input uncertainty data.

2.1.1. Aleatory Uncertainty. Aleatory uncertainty, which is probabilistic and irreducible, describes the inherent variation associated with a physical system (e.g., the free stream velocity, Mach number, angle of attack and operating conditions). Aleatory uncertainty is due to the random nature of input data and can be mathematically characterized by a probability density function (PDF) if there is enough information on the type of the distribution. Common examples of statistical distribution types are uniform, normal (Gaussian), lognormal, and Gamma distributions. The typical plots for these distributions are shown in Figure 2.1.

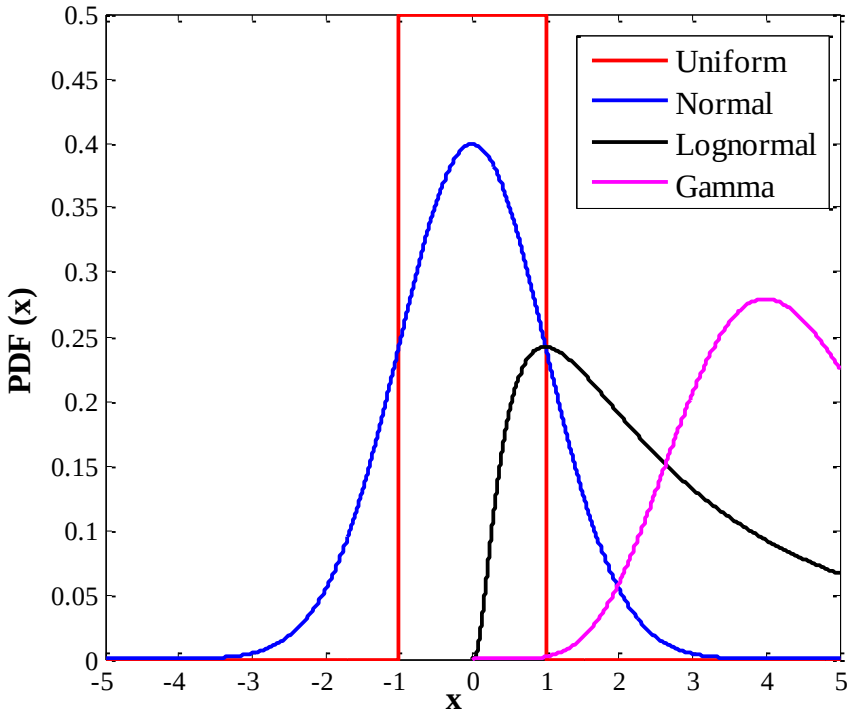

Figure 2.1. Sample probability density functions of common statistical distributions

Selecting the most appropriate and accurate distribution types for random input variables is important because it can have a significant impact when propagating the input uncertainty to the uncertainty in the output variable of interest. Aleatory uncertainty is sometimes referred as irreducible uncertainty because the uncertainty will be prevalent in the physical system because of the stochastic behavior of the input parameter. Depending upon the application, there may be numerous sources of aleatory uncertainty within a physical system. The variation of the free stream velocity, angle of attack, or manufacturing tolerances can be given as examples for aleatory uncertainty in a stochastic external aerodynamics problem.

2.1.2. Epistemic Uncertainty. Epistemic uncertainty stems from a lack of knowledge, incomplete information or ignorance in any phase or operation of a design process (e.g., turbulence models used in CFD simulations). The key

feature of this definition is that the primary cause is incomplete information of some characteristics of the system. Therefore, an increase in knowledge or information can lead to a decrease in the epistemic uncertainty. As a result, epistemic uncertainty is described as reducible uncertainty. Epistemic uncertainty fundamentally differs from aleatory uncertainty in the sense that epistemic uncertainty can be reduced and aleatory uncertainty cannot be reduced. For the characterization of epistemic uncertainty, the statistical distribution types are not suitable to be used to describe the nature of the epistemic parameter due to the lack of knowledge or information about the uncertainty. Studies conducted by Oberkampf [51] and Helton [52] show that the modeling of epistemic uncertainty with probabilistic approaches may lead to inaccurate predictions in the amount of uncertainty in the responses, due to the lack of information on the characterization of uncertainty as probabilistic. One approach to model the epistemic uncertainty is to characterize it with intervals. In this approach, the upper and lower bounds on the uncertain variable can be prescribed using either limited experimental data or expert judgment. All values within this interval are equally likely to occur due to the fact that it is not appropriate to assign a statistical distribution to epistemic uncertain variables. Examples of epistemic uncertainties associated with aerodynamic simulations can include the value of turbulence modeling parameters and fluid transport quantities.

2.1.3. Mixed Uncertainty. In many real-life engineering problems, the two types of uncertainties exist simultaneously. The problems with mixed uncertainties can have a large number of input variables and there can be many sources of aleatory and epistemic uncertainties. As a result, it is important to account for all these uncertainties in order to obtain accurate predictions of the uncertainty in the output variables of interest. For mixed uncertainty quantification, formulations that combine probabilistic methods and interval approach are sought. To such a case, the output response (e.g., the drag coefficient in an aerodynamic optimization problem) should

be in form of the combination of probability distribution due to the effect of aleatory input uncertainty and interval distribution that indicates the effect of the epistemic uncertainty.

2.2. THEORY OF POLYNOMIAL CHAOS

Polynomial Chaos, also called "Wiener Chaos expansion", is a spectral method to propagate uncertainty in a system, when there is aleatory uncertainty in the system parameters. An important aspect of spectral representation of uncertainty is that one may decompose a random function (or variable) into separable deterministic and stochastic components. The stochastic response output can be approximated by a series of orthogonal polynomials basis from Askey scheme [53] associate dwith random inputs. For example, for any random variable (i.e., R) such as velocity, density or pressure in a stochastic fluid dynamics problem, one can write,

$$R(\vec{x},\vec{\xi}) = \sum_{j=0}^{\infty} \alpha_j(\vec{x})\Psi_j(\vec{\xi}) \tag{1}$$

where, $\alpha_j(\vec{x})$ and $\Psi_j(\vec{\xi})$ are the polynomial expasions coefficients (deterministic component) and random basis function corresponding to the j^{th} mode, respectively. In the most general case, $\alpha_j(\vec{x})$ can be a function of deterministic independent variable vector $\vec{x}$ and the n-dimensional standard random variable vector $\vec{\xi} = (\xi_1, ..., \xi_n)$. Each of the $\Psi_j(\vec{\xi})$ are multivariate polynomials which involve products of the one-dimensional polynomials.

In practice, the infinite expansion can be truncated at a finite number of random variables (n) and a finite expansion oder (p) :

$$R(\vec{x},\vec{\xi}) \cong \sum_{j=0}^{P} \alpha_j(\vec{x})\Psi_j(\vec{\xi}) \tag{2}$$

where the total number of expansion terms N_t in a complete polynomial chaos expansion of any order p for a response function with n uncertain input variables is given by

$$N_t = 1 + P = \frac{(n+p)!}{n!p!} \tag{3}$$

which is a function of the order of polynomial chaos (p) and the number of random dimensions (n). The basis function ideally takes the form of multi-dimensional Hermite Polynomial to span the n-dimensional random space when the input uncertainty is Gaussian (unbounded), which was first used by Wiener [54] in his original work of polynomial chaos. To extend the application of the polynomial chaos theory to the propagation of continuous non-normal input uncertainty distributions, Xiu and Karniadakis [55] used a set of polynomials known as the Askey scheme to obtain the "Wiener-Askey Generalized Polynomial Chaos". Table 2.1 gives commonly used Hermite, Legendre, and Laguerre polynomials and the associated probability density functions (PDF) included the Askey scheme. Huyse et al. [56] have shown that Legendre, Hermite and Laguerre polynomials are optimal basis functions for uniform, normal and exponential input uncertainty distributions respectively, in terms of the convergence of the statistics. The optimality of the selection of these basis functions derives from the inner product weighting functions that correspond to the PDFs of the continuous input uncertainty distributions represented in standard form. In Table 2.1,

Table 2.1. Relationship between standard forms of continuous probability distributions and Askey scheme of continuous polynomials

Input Distribution	Density Function $f(\xi)$	Polynomials Name	Weight Function $\rho(\xi)$	Support Range (R)
Uniform	$\frac{1}{2}$	Legendre $P_n(\xi)$	1	$[-1,1]$
Norm	$\frac{1}{\sqrt{2\pi}}e^{\frac{-\xi^2}{2}}$	Hermit $H_{en}(\xi)$	$e^{\frac{-\xi^2}{2}}$	$[-\infty,\infty]$
Exponetial	$e^{-\xi}$	Laguerre $L_n(\xi)$	$e^{-\xi}$	$[0,\infty]$

the constant factor between the density and the weighting functions originate due to the requirement that the integral of the probability density function over the support range is one. Eldred et al. [14] described the detailed process of how the multivariate basis functions can be derived from the product of univariate orthogonal polynomials. Take a multivariate Hermite polynomial of order n as an example, it can be defined from

$$H_{en}(\xi_{i_1}, \cdots, \xi_{i_n}) = e^{\frac{1}{2}\vec{\xi}^T\vec{\xi}}(-1)^n \frac{\partial^n}{\partial\xi_{i_1}\cdots\partial\xi_{i_n}} e^{-\frac{1}{2}\vec{\xi}^T\vec{\xi}} \tag{4}$$

which can also be shown as a product of one-dimential Hermite polynomials $\psi_{m_i^j}(\xi)$ by using the multi-index m_i^j, as described in Equation (5) :

$$H_{en}(\xi_{i_1}, \cdots, \xi_{i_n}) = \Psi_j\left(\vec{\xi}\right) = \prod_{i=1}^{n} \psi_{m_i^j}(\xi) \tag{5}$$

For example, the first few multivariate Hermit Polynomials of a two-dimensional case (including zeroth, first, and second order terms) are obtained as:

$$\begin{aligned}
\Psi_0(\vec{\xi}) &= \psi_0(\xi_1)\,\psi_0(\xi_2) = 1 \\
\Psi_1(\vec{\xi}) &= \psi_1(\xi_1)\,\psi_0(\xi_2) = \xi_1 \\
\Psi_2(\vec{\xi}) &= \psi_0(\xi_1)\,\psi_1(\xi_2) = \xi_2 \\
\Psi_3(\vec{\xi}) &= \psi_2(\xi_1)\,\psi_0(\xi_2) = \xi_1^2 - 1 \\
\Psi_4(\vec{\xi}) &= \psi_1(\xi_1)\,\psi_1(\xi_2) = \xi_1\xi_2 \\
\Psi_5(\vec{\xi}) &= \psi_0(\xi_1)\,\psi_2(\xi_2) = \xi_2^2 - 1
\end{aligned} \tag{6}$$

If the probability distribution of each random variable is different, then the optimal multivariate basis functions can be again obtained using Equation (5) by employing the optimal univariate polynomial at each random dimension. This approach requires that the input uncertainties are independent standard random variables, which also allows the calculation of the multivariate weight functions by the product

of univariate weight functions associated with the probability distribution at each random dimension. The program listing for the polynomial chaos expansion is given in Appendix A. The generalized polynomial chaos approach can be applied to the propagation of any independent random variable included in the Askey scheme. The detailed information on polynomial chaos expansions can be found in Walters and Huyse, [57] Najm, [58] and Hosder and Walters [59]. The primary objective of the stochastic methods based on polynomial chaos is to determine the coefficient of each term ($\alpha_j(\vec{x})$, $(j = 0, 1, .., P)$) in the polynomial expansion given by Equation (2). The statistics of the response can then be calculated using the coefficients and the orthogonality of basis functions. The mean of the random solution is given by

$$\mu_R = E[R(\vec{x}, \vec{\xi})] = \int_{\Omega} R(\vec{x}, \vec{\xi})\rho(\vec{\xi})d\vec{\xi} = \alpha_0 \tag{7}$$

which indicates that the zeroth mode of the expansion corresponds to the expected value or the mean of $R(\vec{\xi})$. Similarly, the variance of the distribution can be obtained:

$$\sigma_R^2 = Var[R(\vec{x}, \vec{\xi})] = \int_{\Omega} (R(\vec{x}, \vec{\xi}) - \mu_R)^2\rho(\vec{\xi})d\vec{\xi} \tag{8}$$

or

$$\sigma_R^2 = \sum_{j=1}^{P} [\alpha_j^2(\vec{x}) < \Psi_j^2 >] \tag{9}$$

In the above equations, $\langle \Psi_j \rangle = 0$ for $j > 0$ and $\langle \Psi_i \Psi_j \rangle = \left\langle \Psi_j^2 \right\rangle \delta_{ij}$, where the inner product expression $< .. >$ represents

$$\left\langle f(\vec{\xi})g(\vec{\xi}) \right\rangle_{\vec{\xi}} = \int_{\Omega} f(\vec{\xi})g(\vec{\xi})\rho(\vec{\xi})d\vec{\xi} \tag{10}$$

written in terms of two generic functions $f(\vec{\xi})$ and $g(\vec{\xi})$ in the support region Ω of $\vec{\xi}$ with $\rho(\overrightarrow{\xi})$ being the weight function.

2.3. NON-INTRUSIVE POLYNOMIAL CHAOS

To model the uncertainty propagation in computational simulations via polynomial chaos with the intrusive approach, all dependent variables and random parameters in the governing equations are replaced with their polynomial chaos expansions. Taking the inner product of the equations yields $P + 1$ times the number of deterministic equations which can be solved by the same numerical methods applied to the original deterministic system. Although straightforward in theory, an intrusive formulation for complex problems can be relatively difficult, expensive, and time consuming to implement. To overcome such inconveniences associated with the intrusive approach, NIPC formulations have been considered for uncertainty propagation. The main objective of the NIPC method is to obtain the polynomial coefficients without making any modifications to the deterministic code. This approach treats the deterministic code as a "black-box" and approximates the polynomial coefficients with formulas based on deterministic code evaluations. The "ideal" non-intrusive method would predict the polynomial coefficients with minimum number of deterministic evaluations at the desired accuracy level for a given stochastic problem. The Quadrature-Based and Point-Collocation based NIPC are the two main NIPC approaches used for uncertainty quantification in this study. A detailed description of these two approaches is given in the following sections.

2.3.1. Quadrature-Based NIPC. To find the polynomial coefficients $\alpha_j = \alpha_j(\vec{x})$, $(j = 0, 1, .., P)$ in Equation (2) using the NIPC methods based on spectral projection, the equation is projected onto the j^{th} basis:

$$\left\langle R(\vec{x}, \vec{\xi}), \Psi_j(\vec{\xi}) \right\rangle = \left\langle \sum_{k=0}^{P} \alpha_k(\vec{x}) \Psi_k(\vec{\xi}), \Psi_j(\vec{\xi}) \right\rangle \tag{11}$$

By the virtue of orthogonality of the basis polynomials, the polynomials coefficients can obtianed by

$$\left\langle R(\vec{x},\vec{\xi}),\Psi_j(\vec{\xi})\right\rangle = \alpha_j(\vec{x})\left\langle \Psi_j^2(\vec{\xi})\right\rangle \tag{12}$$

$$\alpha_j(\vec{x}) = \frac{\left\langle R(\vec{x},\vec{\xi}),\Psi_j(\vec{\xi})\right\rangle}{\left\langle \Psi_j^2(\vec{\xi})\right\rangle} = \frac{1}{\left\langle \Psi_j^2(\vec{\xi})\right\rangle}\int_{\Omega} R(\vec{x},\vec{\xi})\Psi_j(\vec{\xi})\rho(\vec{\xi})d\vec{\xi} \tag{13}$$

The objective of the spectral projection methods is to predict the polynomial coefficients by evaluating the numerator ($\left\langle R(\vec{x},\vec{\xi}),\Psi_j(\vec{\xi})\right\rangle$) in Equation (13), since the term in the denominator ($\left\langle \Psi_j^2(\vec{\xi})\right\rangle$) can be computed analytically for multivariate orthogonal polynomials. With this non-intrusive approach, the multi-dimensional integral in the numerator term of Equation (13) is evaluated with numerical quadrature [60, 61, 14, 62]. For the integration of one-dimensional problems, the straightforward approach will be to use Gaussian quadrature points, which are zeros of orthogonal polynomials that are optimal for the given input uncertainty distribution (i.e., Gauss-Hermite, Gauss-Legendre, and Gauss-Laguerre points for normal, uniform, and exponential distributions respectively). The extension of this approach to multidimensional problems can be achieved via tensor product of one-dimensional quadrature formulas. For one-dimensional integral, if the polynomial chaos expansion degree is p, then the minimum Gaussian points required for the exact estimation of the integral will be $p+1$, because p-point Gaussian Quadrature rule will yield an exact result for polynomials degree of $2p-1$ or less and the polynomial degree of the product of function estimation and the basis polynomials in numerator in Equation(13) will be $2p$. Therefore, the number of response evaluations will be $(p+1)^n$ when the Quadrature-Based NIPC is used to construct the response surface as a function of n expansion variables. An alternative approach for more efficient evaluation of the multidimensional integrals will be to use sparse tensor product spaces instead of full-tensor product of Gauss quadrature points to cover the

multidimensional random space. The concept of sparse grids was first proposed by Smolyak [63] and recently implemented by many researchers for efficient solution of stochastic problems [64, 65, 66, 67]. As shown by Eldred et al. [14], using sparse grids can provide significant gains in terms of efficiency for the solution of smooth functions in random space with moderate number of input uncertain variables. The program listing for Quadrature-Based NIPC is given in Appendix B.

2.3.2. Point-Collocation NIPC. The Point-Collocation NIPC method starts with replacing the uncertain variables of interest with their polynomial expansions given by Equation (14). Then, $N_t = P + 1$ vectors ($\vec{\xi_j} = \{\xi_1, \xi_2, ..., \xi_n\}_j, j = 0, 1, ..., P$) are chosen in random space for a given polynomial chaos expansion with $P + 1$ modes and the deterministic code is evaluated at these points. With the left hand side of Equation (14) known from the solutions of deterministic evaluations at the chosen random points, a linear system of equations can be obtained

$$\begin{pmatrix} R(\vec{x}, \vec{\xi_0}) \\ \\ R(\vec{x}, \vec{\xi_1}) \\ \vdots \\ R(\vec{x}, \vec{\xi_P}) \end{pmatrix} = \begin{pmatrix} \Psi_0(\vec{\xi_0}) & \Psi_1(\vec{\xi_0}) & \cdots & \Psi_P(\vec{\xi_0}) \\ \\ \Psi_0(\vec{\xi_1}) & \Psi_1(\vec{\xi_1}) & \cdots & \Psi_P(\vec{\xi_1}) \\ \vdots & \vdots & \ddots & \vdots \\ \Psi_0(\vec{\xi_P}) & \Psi_1(\vec{\xi_P}) & \cdots & \Psi_P(\vec{\xi_P}) \end{pmatrix} \begin{pmatrix} \alpha_0(\vec{x}) \\ \\ \alpha_1(\vec{x}) \\ \vdots \\ \alpha_P(\vec{x}) \end{pmatrix} \tag{14}$$

The coefficients ($\alpha_j(\vec{x})$) of the stochastic expansion are obtained by solving the linear system of equations given above. The solution of the linear problem given by Equation (14) requires N_t deterministic function evaluations. If more than N_t samples are chosen, then the over-determined system of equations can be solved using the Least Squares approach. Hosder et al. [68] investigated this option on model stochastic problems by increasing the number of collocation points in a systematic way through the introduction of over sampling ratio (OSR) defined as the number of samples

divided by N_t. In the solution of stochastic model problems with multiple uncertain variables, they have used OSR = 1, 2, 3, and 4 to study the effect of the number of collocation points (samples) on the accuracy of the polynomial chaos expansions. Their results showed that using OSR of 2 gives a better approximation to the statistics at each polynomial degree. Increasing the number of collocation points help reduce the error between the polynomial chaos response surface approximation with the Point-Collocation NIPC and the representation with the exact chaos expansion. It should be noted that the Point-Collocation NIPC with OSR of 2 which required $N = 2(n+p)!/(n!p!)$ deterministic evaluations will be significantly more efficient than the full tensor product quadrature with $N = (p+1)^n$ for larger problems [68]. The Point-Collocation NIPC has the advantage of flexibility on the selection of collocation points. With the proper selection of collocation points, it has been shown that Point-Collocation NIPC can produce highly accurate stochastic response surfaces with computational efficiency. For the model problems considered in Section 5, Latin Hypercube sampling with the OSR of 1 or 2 were used to choose the collocation points. In robust airfoil optimization design problems, Latin Hypercube sampling with the OSR of 2 was used to select the collocation points to obtain more accurate solution. The number of response evaluations will be $OSR \times N_t$ when the Point-Collocation NIPC is used to construct the stochastic response surface. The program listing for Point-Collocation NIPC is given in Appendix C.

2.3.3. Mixed UQ with Stochastic Expansions. With the introduction of non-probabilistic variables $\vec{s}$ (epistemic uncertain variables or deterministic design variables) and aleatory uncertainty ($\vec{\xi_a}$), a bounded domain $\vec{s_L} \leq \vec{s} \leq \vec{s_U}$ (with no implied probability content) was assumed for the nonprobabilistic variables and a Legendre chaos basis would be appropriate for each of the dimensions in $\vec{s}$ within a polynomial chaos expansion. A combined stochastic expansions of R can be written:

$$R\left(\vec{\xi}_a, s\left(\vec{\xi}_s\right)\right) \cong \sum_{j=0}^{P} \alpha_j \Psi_j\left(\vec{\xi}_a, s\left(\vec{\xi}_s\right)\right) \tag{15}$$

In Equation (15), $\vec{\xi}_a$ is the standard aleatory random variable vector corresponding to aleatory uncertainties, whereas $\vec{s}$ are the epistemic uncertain variables in interval $[\vec{s_L}, \vec{s_U}]$, which are mapped from the associated standard variables in interval [-1,1],

$$\vec{s} = \frac{\vec{s}_U - \vec{s}_L}{2} \cdot \vec{\xi}_s + \frac{\vec{s}_U + \vec{s}_L}{2} \tag{16}$$

where, $\vec{\xi}_s$ are the standard epistemic variables (or deterministic design variables) in interval [-1,1]. For this combined variable expansion, the mean and variance are calculated by performing the expectations over only the aleatory uncertainties, which eliminates the polynomial dependence on $\vec{\xi}_a$, leaving behind the desired polynomial dependence of the moments on $\vec{s}$.

$$\mu_R\left(\vec{s}\right) = \sum_{j=0}^{P} \alpha_j \left\langle \Psi_j\left(\vec{\xi}_a, \vec{s}\right)\right\rangle_{\vec{\xi}_a} \tag{17}$$

$$\sigma_R^2\left(\vec{s}\right) = \sum_{j=0}^{P}\sum_{k=0}^{P} \alpha_j \alpha_k \left\langle \Psi_j\left(\vec{\xi}_a, \vec{s}\right) \Psi_k\left(\vec{\xi}_a, \vec{s}\right)\right\rangle_{\vec{\xi}_a} - \mu_R^2\left(\vec{s}\right) \tag{18}$$

2.3.4. Second Order Probability. Second-Order Probability [20, 69] utilizes an inner loop and an outer sampling loop as described in Figure 2.2 to propagate mixed (aleatory and epistemic) uncertainty. In the outer loop, a specific value for epistemic variable is prescribed and then passed down to inner loop. Any aleatory uncertainty propagation method may be used to perform aleatory uncertainty analysis in the inner loop for the specified value of the epistemic uncertain variable. The Second-Order Probability will produce interval bounds for the output variable of interest at different probability levels. Each iterations of the outer loop will generate one cumulative distribution function (CDF) based on the aleatory uncertainty analysis in the inner loop. As an example, 1000 different CDF curves

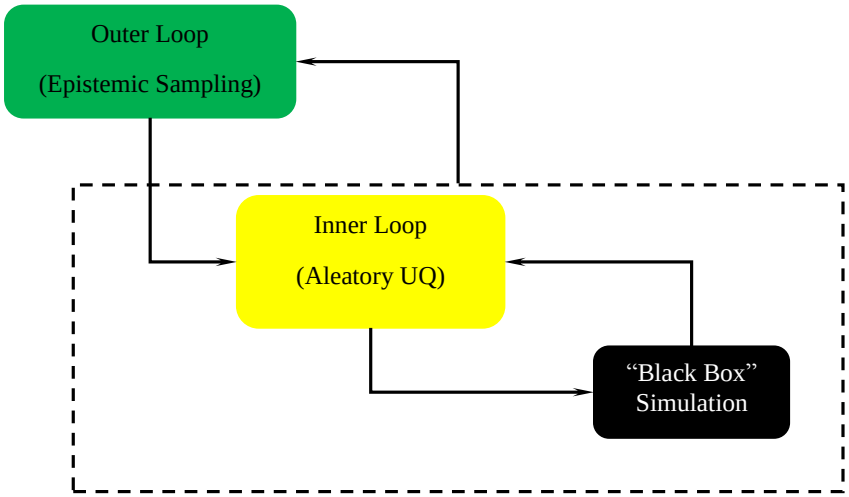

Figure 2.2. Diagram of the second-order probability sampling strategy

will be generated if there are 1000 samples in the outer loop. The main advantage of Second-Order Probability is that it is easy to separate and identify the aleatory and epistemic uncertainties. On the other hand, the double sampling loops will make this method computationally expensive, especially when traditional sampling techniques, such as MCS, are used for uncertainty propagation. Since this study is mainly focused on efficient uncertainty quantification, the NIPC method will be used to create a stochastic response surface for the output quantity of interest as a function of both aleatory and epistemic uncertain variables. The Second-Order Probability was used to determine the bounds at specified probability levels of the output in mixed uncertainty studies using stochastic expansions.

2.4. ADAPTIVE SAMPLING FOR POINT-COLLOCATION NIPC

As discussed in Section 2.2.2, Point-collocation NIPC with OSR of 2 gives a better approximation to the statistics at each polynomial degree. The error between the polynomial chaos response surface approximation with the Point-Collocation NIPC and the representation with the exact chaos expansion will be reduced by

increasing of the number of collocation points. To further improve computational efficiency and obtain the same accuracy level of the OSR= 2 results with less numbers of function evaluations, an adaptive sampling approach is introduced to refine Point-Collocation NIPC by using the OSR between 1 and 2 based on the convergence check of the difference of total response surface error. Two different schemes are considered for the calculation of the check points where the response surface error values are calculated for convergence check, including fixed check point and updated check point approaches. The fixed check points are calculated at the first iteration (OSR=1) and are not updated. The updated check points are modified in an automated way so that the response values evaluated at these points represent more accurately the probability levels where the response surface error values are intended to be calculated.

The procedure of adaptive sampling for the Point-Collocation NIPC approach is illustrated in Figure 2.3 with eight steps and the details will be discussed for pure aleatory uncertainty and mixed (both aleatory and epistemic) uncertainty in the following sections.

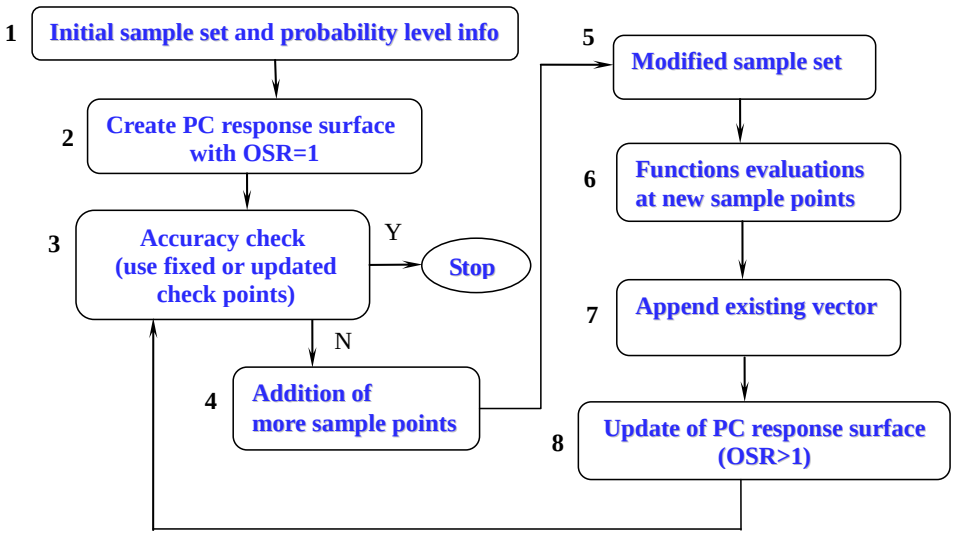

Figure 2.3. Schematic of adaptive sampling based Point-Collocation NIPC

2.4.1. Adaptive Sampling Approach for Pure Aleatory Uncertainty Propagation. As can be seen in Figure 2.3, there are eight steps in the procedure. The details of each step are described as follows:

Step 1: Generate N_{total} random samples ($N_{total} \gg N^0_{sample}$) on aleatory uncertain variable design space using Latin Hypercube sampling and specify the probability levels for check point calculations. The N^0_{sample} represents the number of collocation points used for creating the initial response surface.

Step 2: Select N^0_{sample} samples from initial sample set N_{total}, which are used to calculate the polynomial expansion coefficients and construct the initial response surface using Equantion (14).

The number of samples N^0_{sample} can be calculated by:

$$N^0_{sample} = N_t \cdot OSR^0 = \frac{(n+p)!}{n!p!} \cdot OSR^0 \tag{19}$$

where, N_t is the total number of expansion terms which is a function of polynomial expansion order p and number of uncertain variables n. OSR^0 is the initial OSR, which can be any number greater than or equal to 1 (for example, $OSR^0 = 1$ in this proposed approach).

Step 3: Check the convergence of total response surface error which includes four procedures given below:

(1) Generate the CDF curve of the output as shown in Figure 2.4 using N^a_{sample} number of samples for aleatory uncertainty variables using the stochastic response surface approximation obtained in step 2, where, $i = 1, ..., n_{check}$ and n_{check} is the total number of probability levels.

(2) Calculate the output value at each specified probability level based on the CDF results. For pure aleatory uncertain variable case, the output at specific probability level is single value as shown in Figure 2.4.

(3) Obtain the check points which are corresponding to the output values at specified probability levels by solving multi-variable non-linear equations. To solve the multi-variable non-linear equations, Trust-Region Dogleg Method was applied and implemented through Matlab code in this study. As discussed before, there are two different schemes to implement this step which are fixed check point and update check point approaches. The fixed check points are calculated at the initial iteration (OSR=1) and are not updated. The updated check points are modified in an automated way so that the response values evaluated at these points represent more accurately the probability levels where the response surface error values are intended to be calculated. The updated check points are modified based on the reduction value ΔE_{RT}^{k} of total probability error E_{RT}^{k} at k^{th} iteration (Flow chart of check point update procedure is shown in Figure 2.5) :

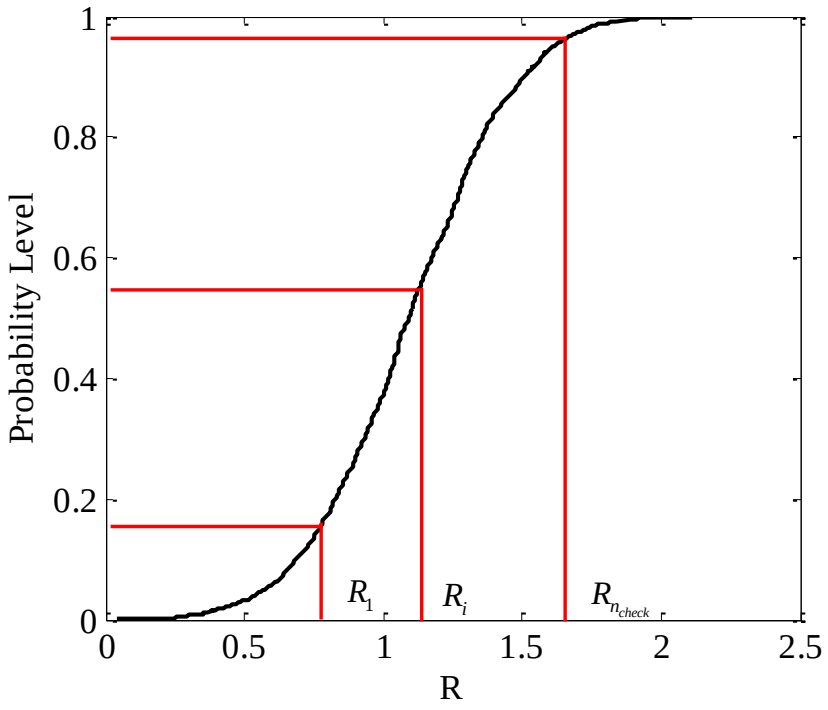

Figure 2.4. CDF curve of output from NIPC response surface showing the specified probability levels for accuracy evaluation
($i = 1, ..., n_{check}$; n_{check}: number of probability levels)

$$\text{if} \quad \begin{cases} \Delta E_{RT}^{k} > \varepsilon : & \text{update check points} \\ \Delta E_{RT}^{k} \leqslant \varepsilon : & \text{STOP updating check points} \end{cases}$$

where, ε is the user specified convergence criterion value (e.g. 0.1 represents 10% reduction). The total error reduction value ΔE_{RT}^{k} of total probability level error is calculated by

$$\begin{aligned} \Delta E_{RT}^{0} &= E_{RT}^{0} \qquad \text{(Initial setup)} \\ \Delta E_{RT}^{k} &= \left| E_{RT}^{k} - E_{RT}^{k-1} \right|, k = 1, 2, 3 \cdots \end{aligned} \tag{20}$$

where k corresponds to iteration number.

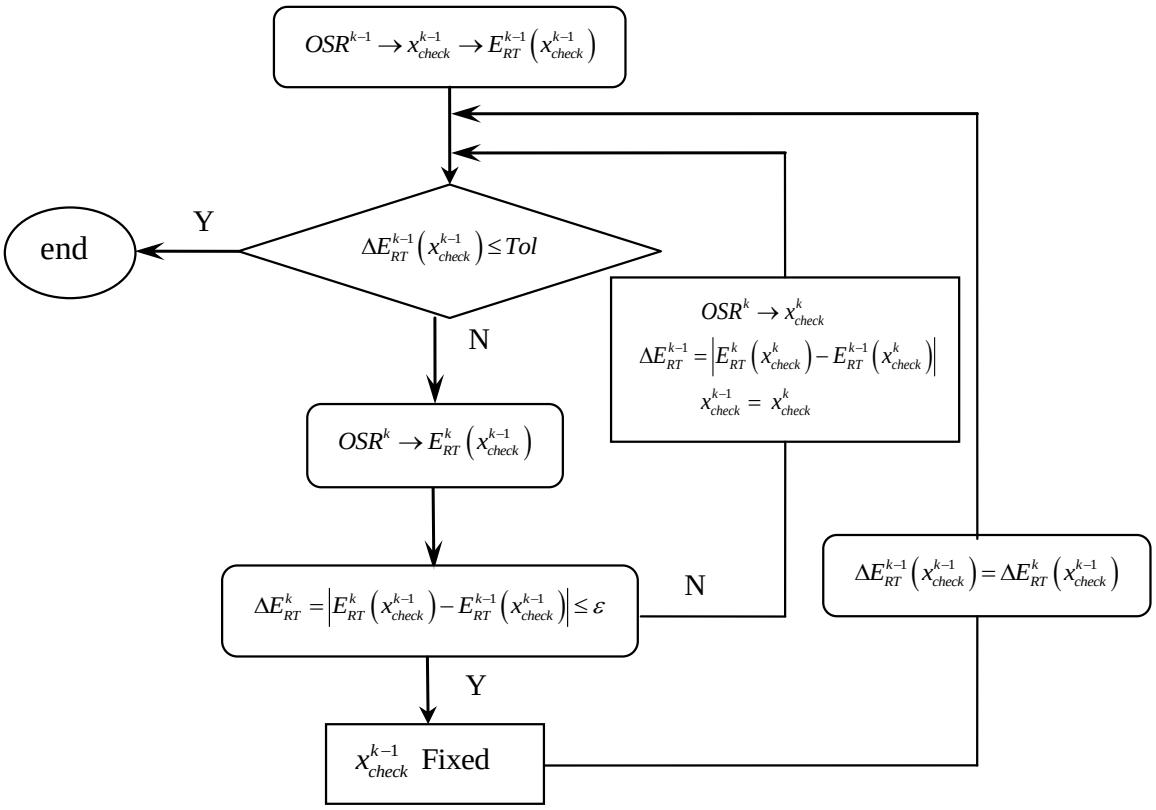

Figure 2.5. Flow chart for check point update

The local response surface error and total response surface error are computed by Equation (21) and Equation (22), respectively:

$$e_{R_i}^k = \left| \frac{R_{s_i}^k - R_i^k}{R_i^k} \right| \qquad (i = 1, ..., n_{check}) \tag{21}$$

and

$$E_{RT}^k = \sqrt{\sum_{i=1}^{n_{check}} \left(e_{R_i}^k\right)^2} \tag{22}$$

where, i represents probability level. $R_{s_i}^k$ and R_i^k are the output value obtained from response surface and exact function at check points corresponding to i^{th} probability level at k^{th} iteration, respectively.

(4) Check error of total response surface by calculating the difference between the actual function (deterministic code) and the response surface at check points that correspond to the output at specified probability level. Two different convergence criteria are considered in this approach including sample size criterion and error convergence criterion. Sample size convergence criterion limits the maximum sample size for response surface approximation to OSR of 2 as shown in Equation (23).

$$N_{sample}^k \leqslant 2 \cdot N_t \tag{23}$$

Error convergence criterion includes the definition of a predefined small tolerance value (Tol) and check if the difference of total response surface error (ΔE_{RT}^k) in successive iterations satisfy the following inequality

$$\left|\Delta E_{RT}^k\right| \leqslant Tol \tag{24}$$

If either of above convergence criteria is satisfied, then the procedure stops and the results are obtained. Otherwise, continue to step 4.

Step 4: Add N_{add} samples from previous ($N_{total} - N_t \cdot OSR^{k-1}$) subsample set, which are used to update the response surface in order to improve the accuracy of approximation.

Step 5: Modify sample set by appending the additional samples to the previous sample set. The number of samples and OSR at k^{th} iteration are given as:

$$N^k_{sample} = N_t \cdot OSR^0 + k \cdot N_{add} \tag{25}$$

$$OSR^k = \frac{N^k_{sample}}{N_t \cdot OSR^0} \tag{26}$$

where, k is the iteration number ($k = 1, 2, 3, ...$).

Step 6: Evaluate the function (deterministic code) at the added sample points.

Step 7: Append new function evaluations to the existing vector and construct new polynomial expansions matrices which were created to apply Point-Collocation NIPC as in Equantion (14).

Step 8: Evaluate the polynomial expansion coefficients based on the updated matrice and obtain the updated response surface. Perform accuracy check according to step 3 using the updated response surface.

Repeat step 3 to 8 until accuracy criteria is satisfied.

2.4.2. Adaptive Sampling Approach for Mixed Uncertainty Propagation. For Mixed uncertainty propagation, The same procedure can be implemented as shown in Figure 2.3.

Step 1: Generate N_{total} random samples ($N_{total} \gg N^0_{sample}$) on both aleatory and epistemic uncertain variable design space using Latin Hypercube sampling and specify the probability levels for check point calculations.

Step 2: Select N^0_{sample} samples from initial sample set N_{total}, which are used to calculate the polynomial expansion coefficients and construct the initial response surface. For mixed uncertainty propagation, the response surface is created based on

Equantion (15) and Equantion (14). The number of samples N^0_{sample} can be calculated using Equation (19).

Step 3: Check the convergence of total response surface error which also includes four procedures given below:

(1) Generate the CDF curves of the output as shown in Figure 2.6, where, $i = 1, ..., n_{check}$ and n_{check} is the total number of probability levels. Due to the effect of epistemic uncertainty, the output value is an interval at specific probability level. Second-Order Probability method was utilized with N^e_{sample} samples for epistemic variables (outer sampling) and N^a_{sample} samples for aleatory variables (inner sampling) both using the stochastic response surface approximation obtained in step 2 to generate the CDF curves of the output.

(2) Calculate the output value at each specified probability level based on the CDF results. For mixed uncertain variable case, the output at specific probability level is an interval. An example of CDF curves (p-box) is given in Figure 2.6. For

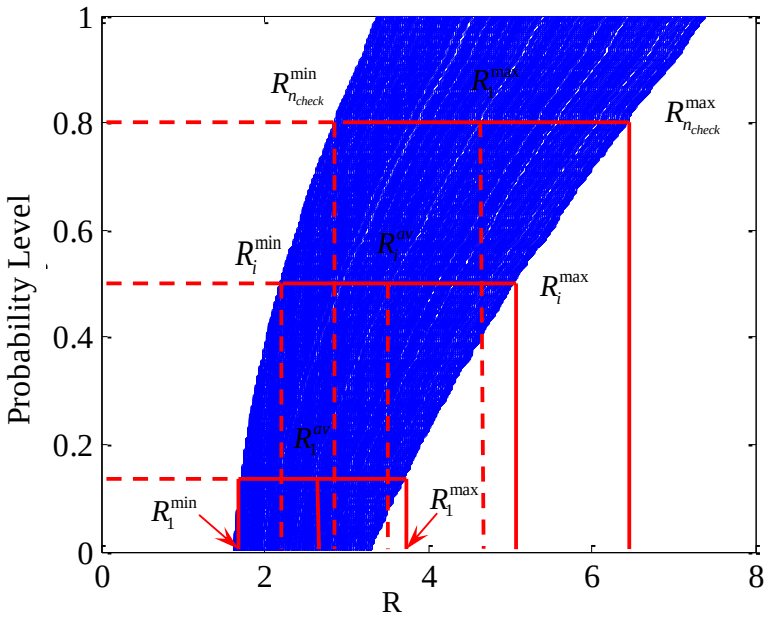

Figure 2.6. P-Box results from NIPC response surface showing the specified probability levels for accuracy evaluation
($i = 1, ..., n_{check}$; n_{check}: number of probability levels)

mixed uncertainty case, since the output value at specified probability level is an interval, check points can be calculated based on different output value such as, the maximum value of output R_{si}^{max}, minimum value of output R_{si}^{min}, or average of output value R_{si}^{av}.

The average output value at i^{th} specified probability level is calculated based on stochastic response surface approximation using Equation (27).

$$R_{si}^{av} = \frac{(R_{si}^{min} + R_{si}^{max})}{2} \tag{27}$$

(3) Obtain the check points which are corresponding to the output values at specified probability levels. The same approach was utilized to solve the multi–variable non-linear equations. As discussed in Section 2.4.1, two different schemes (fixed check point and update check point) can be used to obtain the check points.

(4) Check error of total response surface by calculating the difference between the actual function (deterministic code) and the response surface at check points that correspond to the output at specified probability level. Sample size criterion and error convergence criterion are also used as convergence criteria.

If either of these convergence criteria is satisfied, then the procedure stops and the results are obtained. Otherwise, continue to step 4.

Step 4: Add N_{add} samples from previous ($N_{total} - N_t \cdot OSR^{k-1}$) subsample set, which are used to update the response surface in order to improve the accuracy of approximation.

Step 5: Modify sample set by appending the additional samples to the previous sample set.

Step 6: Evaluate the function (deterministic code) at the added sample points.

Step 7: Append new function evaluations to the existing vector and construct new polynomial expansions matrices.

Step 8: Evaluate the polynomial expansion coefficients with the updated matrice based on Equation (14) and Equantion (15), and obtain the updated response surface. Perform accuracy check according to step 3 using the updated response surface.

Repeat step 3 to 8 until accuracy criteria is satisfied.

The program listing for adaptive sampling based Point-Collocation NIPC is given in Appendix D.

3. APPLICATIONS OF UNCERTAINTY QUANTIFICATION METHOD

Before application to design, the demonstrations of the UQ methods described in the previous section on two model problems are given in this section. Since the main purpose of this study is to apply a computationally efficient uncertainty quantification approach to robust design optimization under mixed (aleatory and epistemic) uncertainties, both model problems include mixed uncertainties (aleatory and epistemic). First, the application of Quadrature-Based and Point-Collocation based NIPC to an engineering model problem is presented, and then a numerical problem is used to demonstrate the efficiency of the adaptive sampling for Point-Collocation NIPC approach.

3.1. MODEL PROBLEM 1: SHAFT DESIGN

In this section, Quadrature-Based and Point-Collocation based NIPC approach are applied to the uncertainty quantification of a model problem (Figure 3.1), which indicates limit-state function of a shaft in a speed reducer:

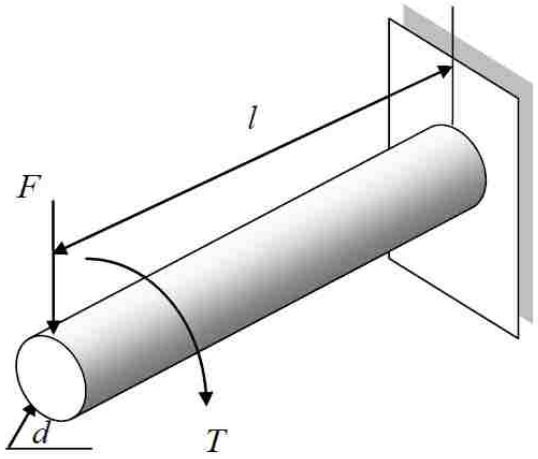

Figure 3.1. Shaft in a speed reducer used for model problem

$$g = S - \frac{16}{\pi d^3}\sqrt{4F^2l^2 + 3T^2} \tag{28}$$

where $d = 39$ mm is the diameter of the shaft, $l = 400$ mm is the length of the shaft, F is the external force, T is the external torque and S is the yield strength. The limit-state function represents the difference between the strength and the maximum equivalent stress, which has to be positive (or greater than a specified positive value) for a safe system. To demonstrate the uncertainty quantification under mixed input uncertainties, the external force F was treated as epistemic uncertainty as described in Table 3.1, external torque T and yield strength S as aleatory uncertain variables with normal distribution. The distributions of aleatory uncertain variables are given in Table 3.2. It is important to realize that the accuracy of the uncertainty propagation

Table 3.1. Limits of epistemic uncertain variable

Varibles	F_L	F_U
F	1800 N	2200 N

Table 3.2. Distribution of aleatory uncertain variables

Varibles	μ	σ	Distribution
T	450 N·m	50 N·m	Normal
S	250 Mpa	30 Mpa	Normal

approach is dependent upon the polynomial expansion order (p) used within the NIPC method. Moreover, the number of function evaluations increases with the polynomial expansion order (p). Therefore, it is important to intelligently select an appropriate expansion order p. An optimal expansion order p would be high enough to estimate accurate results while taking the smallest number of required function evaluations. To

find the optimal expansion order p, convergence studies were implemented where the mean and standard deviation of the limit-state function was analyzed as a function of polynomial order. Figure 3.2 shows the computational results for increasing expansion orders for each of the coefficient estimation approach. From Figure 3.2, it is obvious that a 2^{nd} order polynomial chaos was sufficient for convergence of the NIPC response surface. This can be seen from the fact that there is no obvious changes in both mean

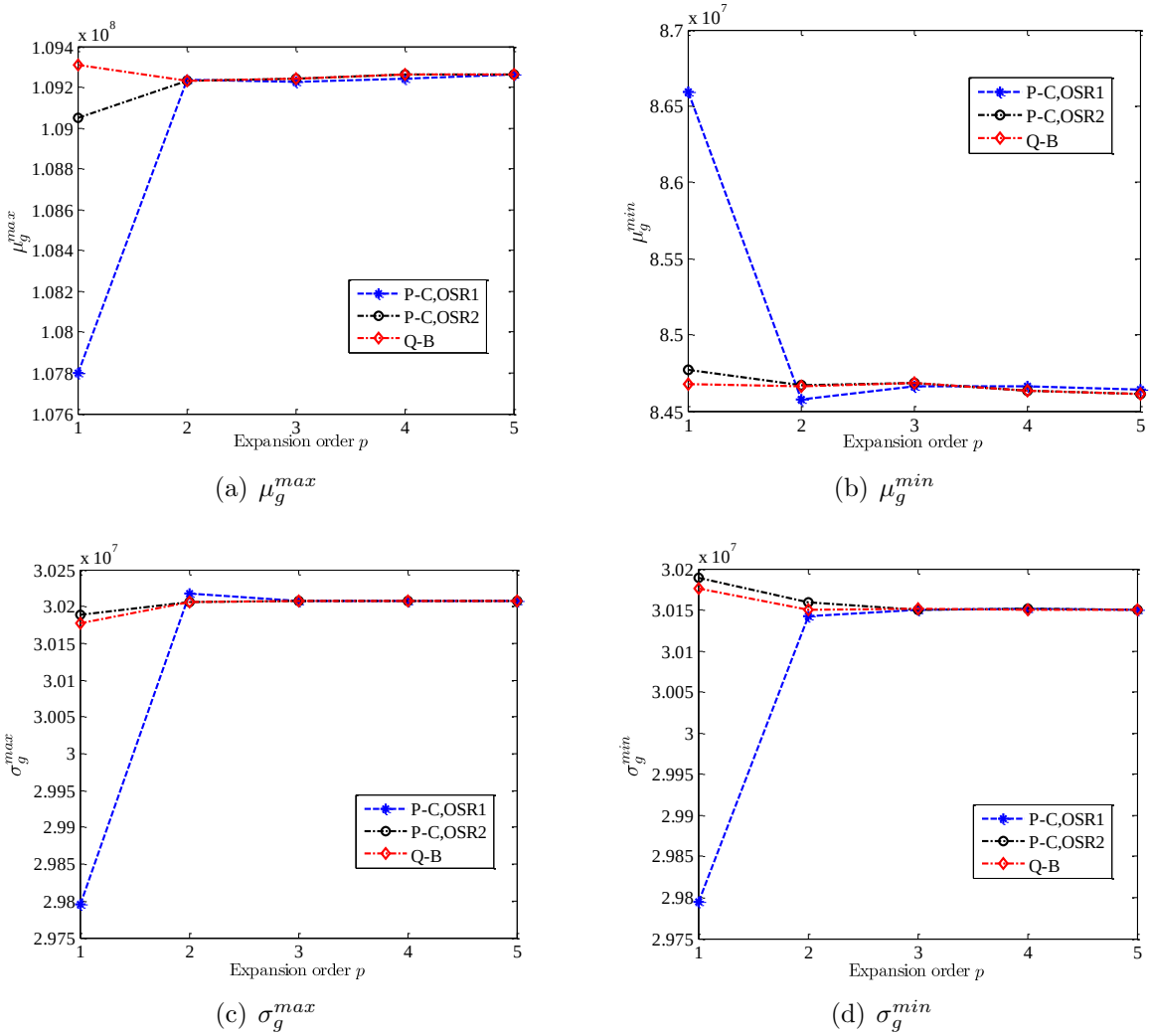

(a) μ_g^{max} (b) μ_g^{min}

(c) σ_g^{max} (d) σ_g^{min}

Figure 3.2. Convergence of NIPC for increasing expansion orders for shaft speed reducer case
(P-C: Point-Collocation, OSR: over sampling ratio, Q-B: Quadratured-Based)

and standard deviation of the limit-state function for expansion order p higher than two. Therefore, a 2^{nd} order polynomial was selected along with Quadrature-Based and Point-Collocation with the OSR of 1 and 2 which corresponded to a total of 27, 10 and 20 function evaluations needed to construct the NIPC response surface. For the Point-Collocation approach, the sample points were selected according to the respective statistical distribution of each stochastic input variable. After the convergence study had been completed, the next step was to perform the mixed aleatory-epistemic uncertainty propagation for the limit-state function. For the UQ analysis, five probability levels (2.5%, 20%, 50%, 80%, 97.5%) are considered. For this problem, Second Order Probability was used to obtain the cumulative probability. A random sample of size 100 was used for the outer loop (epistemic) sampling and 2,000 samples were utilized for the inner loop (aleatory) sampling to produce the CDF curves from the stochastic response surface. Moreover, the results obtained by direct MCS for the original function that utilized the same samples were compared to the results that were obtained by NIPC approach. The comparison of average output value at specified probability levels are shown in Table 3.3. The relative error results are given in Table 3.4, which indicate that Quadrature-based and Point-Collocation

Table 3.3. Comparison of average output values at specified probability level

		P-C, OSR1	P-C, OSR2	Q-B	MCS
Probability Level	2.5%	3.1810×10^7	3.3860×10^7	3.3883×10^7	3.3880×10^7
	20%	7.0322×10^7	7.0724×10^7	7.0716×10^7	7.0722×10^7
	50%	9.7080×10^7	9.7150×10^7	9.7146×10^7	9.7154×10^7
	80%	1.2303×10^8	1.2360×10^8	1.2358×10^8	1.2360×10^8
	97.5%	1.5768×10^8	1.5856×10^8	1.5854×10^8	1.5854×10^8
Number of FE		10	20	27	200000

(P-C: Point-Collocation, Q-B: Quadrature-Based, OSR: Over Sampling Ratio, FE: Function Evalustions, MCS: Monte-Carlo Sampling)

Table 3.4. Relative error results for each method

Probability Level	P-C, OSR1	P-C, OSR2	Q-B
2.5%	6.1088	0 .0579	0.0099
20%	0.5657	0.0027	0.0086
50%	0.0758	0.0038	0.0079
80%	0.4596	0.0015	0.0146
97.5%	0.5456	0.0095	0.0031

(P-C: Point-Collocation, Q-B: Quadrature-Based, OSR: Over Sampling Ratio)

with OSR of 2 are more accurate compared to Point-Collocation approach with OSR of 1. The relative error for each method at i^{th} probability level can be calculated by

$$Error = \left| \frac{R^i_{NIPC} - R^i_{MCS}}{R^i_{MCS}} \right| \times 100 \tag{29}$$

This result is further verified by Figure 3.3 which gives the p-box plots for Quadrature-Based, Point-Collocation NIPC and MCS approaches. Since the error is relatively small for this problem, these results are shown for probability level between 0% and 10% to make this difference easy to identify. As can be seen from the figure, the p-box plots of Quadrature-Based and Point-Collocation NIPC with OSR of 2 are overlapped and much closer to the plots obtained from MCS which indicates that Quadrature based and Point-Collocation NIPC with OSR of 2 give slightly more accurate approximation compared to the Point-Collocation NIPC with OSR of 1.

3.2. MODEL PROBLEM 2: SOBOL FUNCTION

In this section, the adaptive sampling approach for Point-Collocation NIPC is demonstrated on two numerical examples including Sobol function problem with 8 variables and 20 variables, respectively.

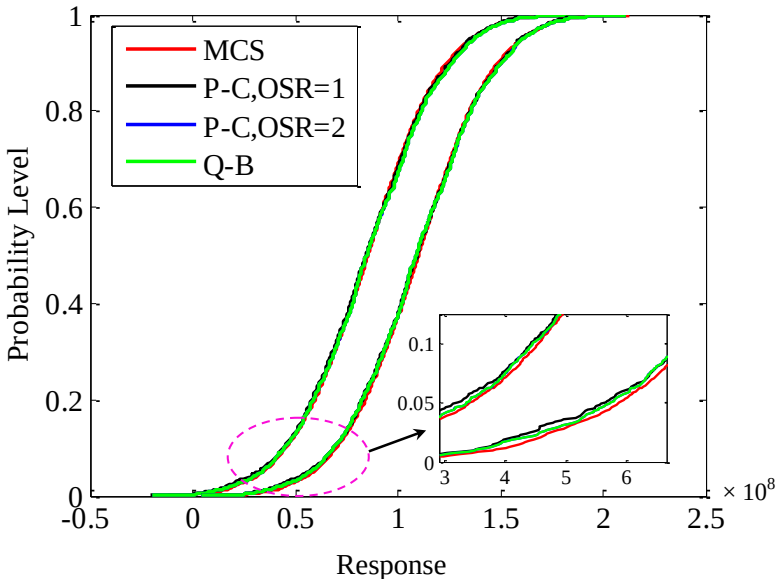

Figure 3.3. Comparison of P-box plot for NIPC and MCS

3.2.1. Sobol Function with 8 Variables. Sobol function is a common test problem in uncertainty quantification and polynomial chaos studies [70]. The expression of the function is given as follows:

$$Y = \prod_{i=1}^{n} \frac{|4x_i - 2| + a_i}{1 + a_i} \tag{30}$$

where, x_i are the input uncertain variables, $i = 1, 2, ..., n$ and a_i are nonnegative constant values. For numerical application, $n = 8$ is selected together with $\vec{a} = [1, 2, 5, 10, 20, 50, 100, 500]$ following the example in [70]. For mixed uncertainty case, x_i $(i = 1, 3, 5, 7$) are treated as aleatory uncertainty following uniform distribution with [0, 1] and x_i $(i = 2, 4, 6, 8$) are considered as epistemic uncertainty which falls in the interval [0, 1]. The application example is carried out using polynomial chaos expansion of degree 2 ($p = 2$) and the initial response surface was created by using Point-Collocation based NIPC with OSR of 1 ($OSR^0 = 1$). A total number of 1000 ($N_{total} = 1000$) Latin Hypercube sampling were generated on the variable

design space. The mixed uncertainty results for the response at five probability levels, $2.5\%, 20\%, 50\%, 80\%$ and 97.5% were analyzed following the discussion in Section 2.4.2. Two different accuracy check procedures were used which included the fixed check point and updated check point approaches. The number of check points at each iteration was corresponding to the total number of specified probability levels. Additional samples ($N_{add} = 9$) were added after each iteration to update the response surface. For mixed uncertainty case, Second Order Probability approach was used to compute the output of response surface at the specified probability levels. A random sample size of 500 was used for the outer loop (epistemic) and 2,000 samples were utilized for the inner loop (aleatory) to produce CDF results from the response surface. Moreover, the other CDF results obtained by direct MCS approach that utilized the same samples were used as benchmark to compare the results that were obtained by adaptive sampling based Point-Collocation NIPC approach. For updated check point approach, the convergence criterion value (ε) of total error reduction value was specified as 0.1 for this problem. Results obtained from these two accuracy check procedures are reported in Table 3.5 and Table 3.6. For fixed check point method, the check points were calculated only once based on the estimation of initial response surface and the total number of function evaluations for check points calculation is constant which equals to the number of specified probability levels. For the updated check point method, the check points were updated based on the total probability

Table 3.5. Probability Level Error Results at fixed check points for 8 variable case

Probability Level	OSR^0 $= 1$	OSR^1 $= 1.2$	OSR^2 $= 1.4$	OSR^3 $= 1.6$	OSR^4 $= 1.8$	OSR^5 $= 2.0$
2.5%	1.818	0.4342	0.6296	0.3695	0.5655	0.4091
20%	0.2205	0.1490	0.4019	0.4393	0.3201	0.3932
50%	0.2767	0.2128	0.0026	0.01899	0.0409	0.0542
80%	0.3790	0.1327	0.022	0.0212	0.0524	0.0239
97.5%	1.3610	0.0201	0.0650	0.1247	0.04706	0.0392
E^k_{RT}	2.3296	0.5235	0.7514	0.5881	0.6549	0.5718

Table 3.6. Probability Level Error Results at updated check points for 8 variable case

Probability Level	OSR^0 = 1	OSR^1 = 1.2	OSR^2 = 1.4	OSR^3 = 1.6	OSR^4 = 1.8	OSR^5 = 2.0
2.5%	1.8182	0.1781	0.1056	0.0777	0.0843	0.1115
20%	0.2205	0.2838	0.1824	0.1380	0.1607	0.2372
50%	0.2768	0.1586	0.0183	0.0288	0.0911	0.1712
80%	0.3790	0.0748	0.1328	0.1314	0.1248	0.0796
97.5%	1.3610	0.0309	0.0014	0.0251	0.0146	0.0467
E^k_{RT}	2.3296	0.3795	0.2497	0.2093	0.2387	0.3264

error reduction value ΔE^k_{RT} which was calculated using Equation (20). The total function evaluations of both fixed and update check point methods are given in Table 3.7. It can be seen that the total number of function evaluations for check points calculation is 10 for updated check point method in this 8 variables case. Figure 3.4 also shows the iteration history of total probability level error E^k_{RT} for both fixed and updated check points methods. For both approaches, the total probability level error started converging at the first iteration and the convergence of error achieved at iteration 2. The relative error of output value at i^{th} probability level at k^{th} iteration can be calculated by Equation (31) and the comparison results are shown in Figure 3.5.

Table 3.7. Number of function evaluations for 8 variable case

		$k=0$	$k=1$	$k=2$	$k=3$	$k=4$	$k=5$	Total
Fixed	N_{RS}	45	9	9	9	9	9	90
	N_{check}	5	0	0	0	0	0	5
Updated	N_{RS}	45	9	9	9	9	9	90
	N_{check}	5	5	0	0	0	0	10

(k: iterations, N_{RS}: number of function evaluations for response surface, N_{check}: number of function evaluations for check point)

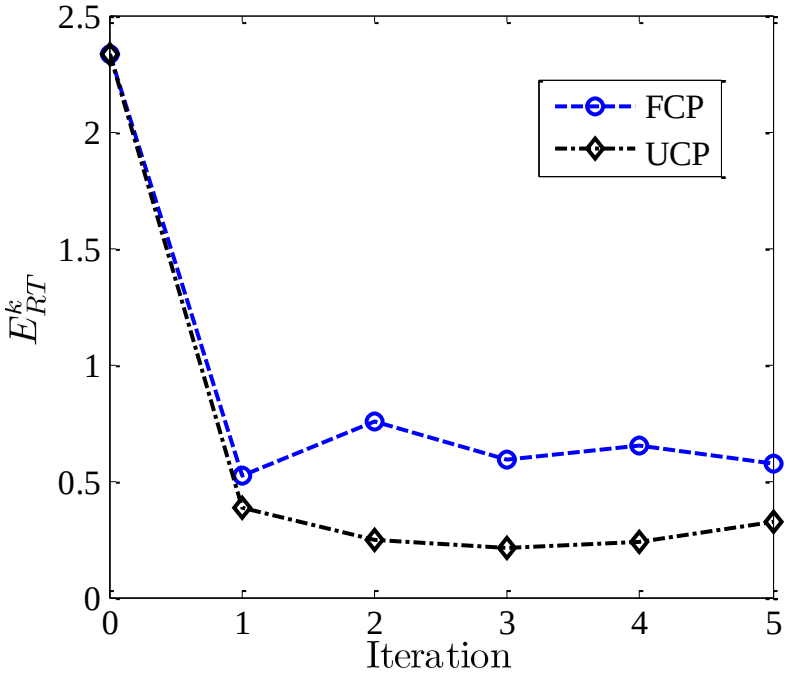

Figure 3.4. Iteration history for total probability level error for the "8 variable" sobol function problem
(FCP: Fixed Check Point approach, UPC: Updated Check Point approach)

$$Error_i^k = \left| \frac{R_{adpt}^{i,k} - R_{MCS}^{i,k}}{R_{MCS}^{i,k}} \right| \times 100 \tag{31}$$

It is obvious to see that both adaptive sampling approaches with fixed check point and updated check point converge at the second iteration at all specified probability levels which indicated that adaptive sampling based Point-Collocation approach requires much less function evaluations when compared with the Point-Collocation with OSR of 2 and can provide the same level of accuracy. The results obtained with the updated check point approach are more accurate and stable than that of fixed check points, and give a more accurate representation of the response at specified probability level. The results shown in Figure 3.6 are the p-box plots for Point-Collocation with OSR of 1 and 2, adaptive sampling based Point-Collocation at 2^{nd} iteration and MCS apporaches. As can be seen from this figure, the p-box plots of adaptive sampling

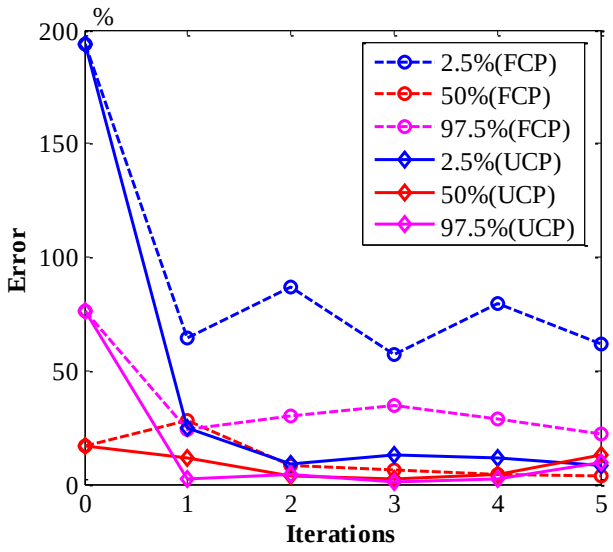

(a) Selected probability level (2.5%, 50%, 97.5%)

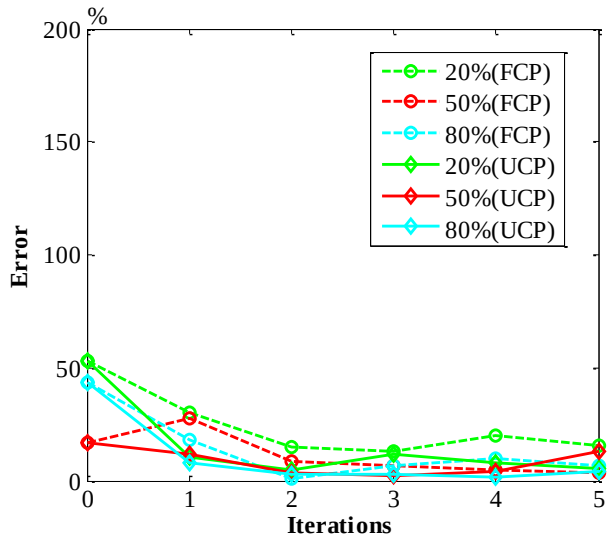

(b) Selected probability level (20%, 50%, 80%)

Figure 3.5. The error of the response with respect to MCS at specified probability levels for the " 8 variable " sobol function problem
(FCP: Fixed Check Point approach, UPC: Updated Check Point approach)

based Point-Collocation at 2^{nd} iteration and Point-Collocation with OSR of 2 are much closer to the CDF results obtained from exact function evaluations compared to OSR of 1.

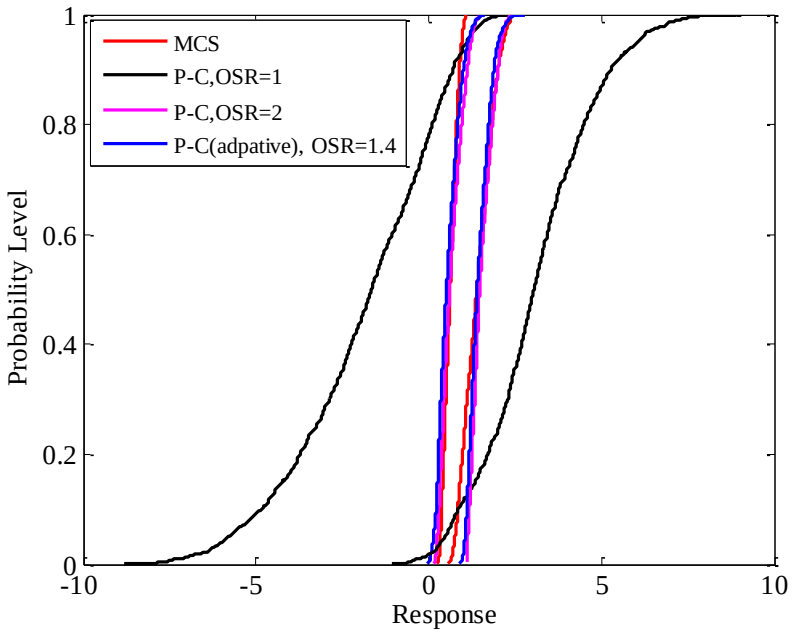

Figure 3.6. Comparison of P-box plot for NIPC and MCS methods for the 8 varible case

3.2.2. Sobol Function with 20 Variables. To demonstrate proposed adaptive sampling approach to a problem with large number of uncertain variables, the sobol function was modified by increasing the number of uncertain variables to 20 with $\vec{a} = [1, 2, 5, 10, 15, 20, 30, 45 : 5 : 105]$. For mixed uncertainty case, every x_i with an odd i was treated as aleatory uncertainty following uniform distribution with [0,1] and the even ones were considered as epistemic uncertainty which falls in the interval [0,1]. The application example was also carried out using polynomial chaos expansion of degree 2 ($p = 2$) and the initial response surface was created by using Point-Collocation based NIPC with OSR of 1 ($OSR^0 = 1$). A total number of 1000 ($N_{total} = 1000$) Latin Hypercube sampling were generated on the uncertain variable design space. The mixed uncertainty results for the response at five probability levels: $2.5\%, 20\%, 50\%, 80\%$ and 97.5% were also analyzed. Additional samples ($N_{add} = 46$) was added after each iteration to update the response surface. A random sample size

of 500 was used for the outer loop (epistemic) and 2,000 samples were utilized for the inner loop (aleatory) to generate the CDF curves from the stochastic response surface. Moreover, the results obtained by direct MCS for the original function that utilized the same samples were used as reference to compare the results that were obtained by adaptive sampling based Point-Collocation NIPC approach. For updated check point approach, the convergence criterion value (ε) of total error reduction value was specified as 0.12 for this case. Results obtained from these accuracy check procedures are given in Table 3.8 and Table 3.9. The total function evaluations of both fixed and update check point methods are given in Table 3.10. For updated check point

Table 3.8. Probability Level Error Results at fixed check points for 20 variable case

Probability Level	OSR^0 = 1	OSR^1 = 1.2	OSR^2 = 1.4	OSR^3 = 1.6	OSR^4 = 1.8	OSR^5 = 2.0
2.5%	5.1127	0.4622	0.3486	0.3359	0.3886	0.2520
20%	2.2076	0.0409	0.1906	0.3403	0.4044	0.4269
50%	0.2713	0.5046	0.4197	0.2744	0.2526	0.2062
80%	0.6114	0.1295	0.1749	0.1965	0.1959	0.1935
97.5%	1.9134	0.1200	0.0567	0.1083	0.1498	0.1245
E^k_{RT}	5.9264	0.7079	0.6065	0.5952	0.6627	0.5842

Table 3.9. Probability Level Error Results at updated check points for 20 variable case

Probability Level	OSR^0 = 1	OSR^1 = 1.2	OSR^2 = 1.4	OSR^3 = 1.6	OSR^4 = 1.8	OSR^5 = 2.0
2.5%	5.1127	0.0422	0.2621	0.3129	0.1982	0.2179
20%	2.2076	0.3714	0.3745	0.3353	0.3037	0.3002
50%	0.2713	0.0965	0.1175	0.0339	0.0411	0.0106
80%	0.6114	0.0216	0.0313	0.1358	0.1188	0.1241
97.5%	1.9134	0.0475	0.0442	0.0362	0.0403	0.0016
E^k_{RT}	5.9264	0.3896	0.4751	0.4809	0.3859	0.3913

Table 3.10. Number of function evaluations for 20 variable case

		$k=0$	$k=1$	$k=2$	$k=3$	$k=4$	$k=5$	Total
Fixed	N_{RS}	231	46	46	46	46	46	461
	N_{check}	5	0	0	0	0	0	5
Updated	N_{RS}	231	46	46	46	46	46	461
	N_{check}	5	5	0	0	0	0	10

(k: iterations, N_{RS}: number of function evaluations for response surface, N_{check}: number of function evaluations for check point)

approach, the check points were updated only once for this 20 variables case which indicated that the total number of function evaluations was 10. Figure 3.7 also gives the iteration history of total probability level error E_{RT}^{k} for both fixed and updated check point methods. For both approaches, the total probability level error started converging at 2^{nd} iteration and the convergence of error achieved at first iteration. The

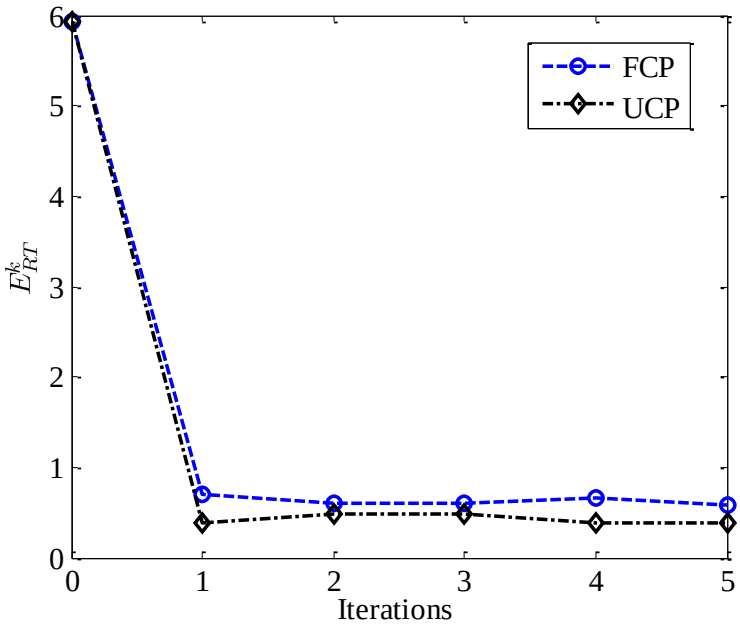

Figure 3.7. Iteration history for total probability level error for the "20 variable" Sobol function problem
(FCP: Fixed Check Point approach, UPC: Updated Check Point approach)

comparison of the relative error of the output value at specified probability levels are shown in Figure 3.8. It is obvious to see that both adaptive sampling approaches with fixed check points and updated check points converged at 2^{nd} iteration at all specified probability levels which indicated that adaptive sampling based Point-

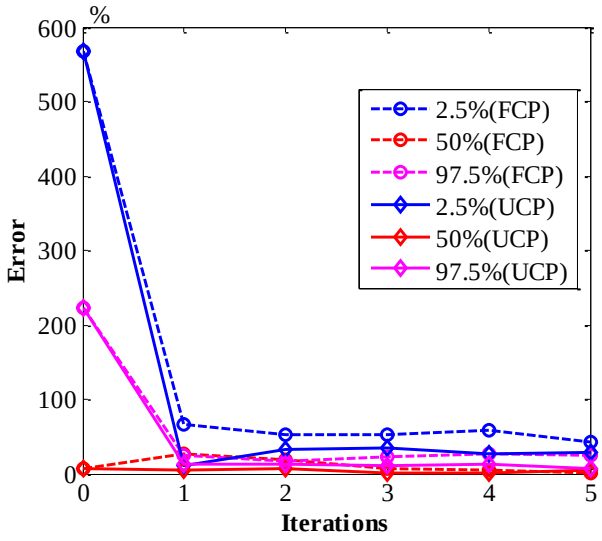

(a) Selected probability level (2.5%, 50%, 97.5%)

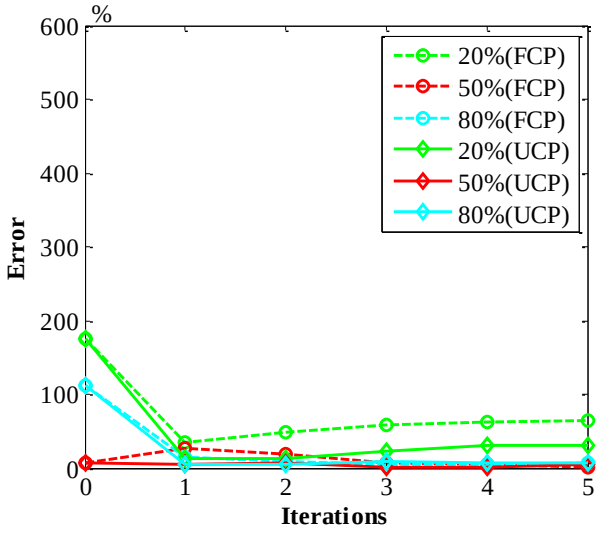

(b) Selected probability level (20%, 50%, 80%)

Figure 3.8. The error of the response with respect to MCS at specified probability levels for the " 20 variable " sobol function problem
(FCP: Fixed Check Point approach, UPC: Updated Check Point approach)

Collocation approach requires much less function evaluations when compared with the point-collocation with OSR of 2 and can provide the same level of accuracy. Figure 3.9 gives the p-box plots for Point-Collocation with OSR of 1 and 2, adaptive sampling based Point-Collocation at 2^{nd} iteration and MCS approaches. As can be seen form this figure, the p-box plots of adaptive sampling based Point-Collocation at converged iteration and Point-Collocation with OSR of 2 are much closer to the CDF obtained from exact function evaluations compared to OSR of 1, which indicate that the adaptive sampling based Point-Collocation NIPC can improve the accuracy of response surface approximation with less function evaluations.

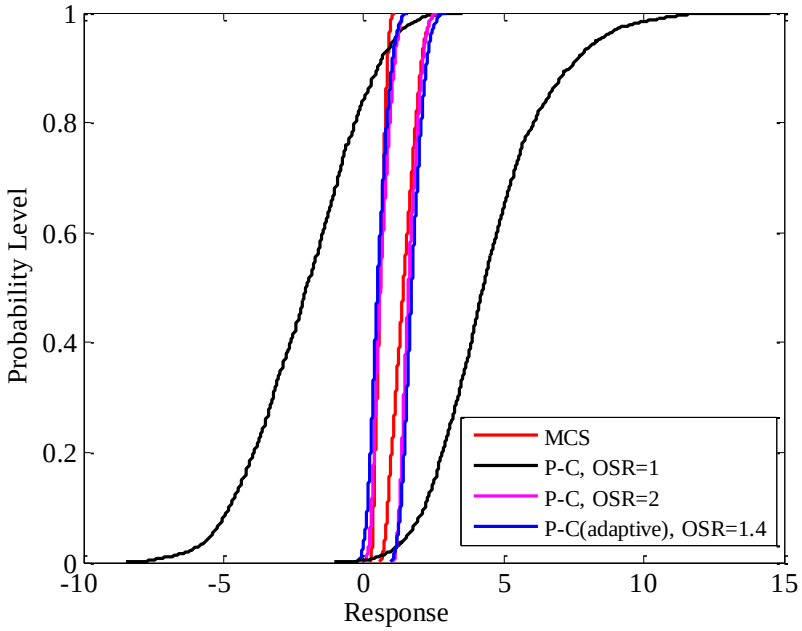

Figure 3.9. Comparison of P-box plot for NIPC and MCS methods for the 20 variable case

3.3. SUMMARY OF THE RESULTS

In this section, NIPC based stochastic expansions approach was applied to model problems under mixed uncertainties to demonstrate the application of Quadrature,

Point-Collocation and adaptive sampling based Point-Collocation approach in mixed uncertainty quantification. The UQ results for the first test problem demonstrated that Quadrature-Based and Point-Collocation NIPC approach are efficient techniques for highly accurate mixed uncertainty quantification using relatively low-order polynomial chaos expansions. The Quadratue-based NIPC is more accurate than the Point-Collocation with OSR of 1. The Quadratue-Based approach can be the preferred method when analyzing problems with less number of uncertain variables. On the other hand, the Point-Collocation method is more affordable for problems with large number of uncertain variables and can give the desired accuracy level with careful selection of the number of collocation points and the polynomial expansion order. The results of model problem 2 show that adaptive sampling approach significantly enhances the efficiency of the Point-Collocation method. Two numerical test problems demonstrate that the adaptive approach can produce the same accuracy level of the response surface obtained with OSR of 2 using significantly less numbers of function evaluations.

4. ROBUST DESIGN WITH STOCHASTIC EXPANSIONS

In this section, the details of robust design with stochastic expansions are described. First, different robustness measures for a system depending on the input uncertainty type are given following the discussion given by Du et al. [50]. The utilization of stochastic expansions in robust optimization is presented in Section 4.2.

4.1. FORMULATION OF THE ROBUST OPTIMIZATION

In this section, different robustness measures for a system are described depending on the input uncertainty type following the discussion given by Du et al. [50]: (1) purely aleatory (inherent) input uncertainty, (2) purely epistemic (model-form) input uncertainty, and (3) mixed (aleatory and epistemic) input uncertainty:

4.1.1. Aleatory Uncertainties Only. If there are only aleatory uncertainties as input variables, the response R can be described as a function of $\vec{S}_a = (S_{a_1}, S_{a_2}, ...S_{a_{N_a}})$ which is the vector consisting of N_a aleatory uncertainties and can include both aleatory design variables ($\vec{X}_a$) and aleatory parameters ($\vec{P}_a$). In this study, the aleatory uncertainty is imposed to the design variables through the statistical distribution parameters that define them (e.g., mean and variance), which vary in the design space. Figure 4.1 shows the propagation of input aleatory uncertainties through the simulation code and the uncertainty of the response, $R = f(\vec{S}_a)$. For probabilistic output uncertainty, the mean and the variance of R can be calculated by

$$\mu_R = E(R) = \int_\Omega R(\vec{S}_a)\rho(\vec{S}_a)d\vec{S}_a \tag{32}$$

$$\sigma_R^2 = E[(R-\mu_R)^2] = \int_\Omega (R(\vec{S}_a)-\mu_R)^2\rho(\vec{S}_a)d\vec{S}_a \tag{33}$$

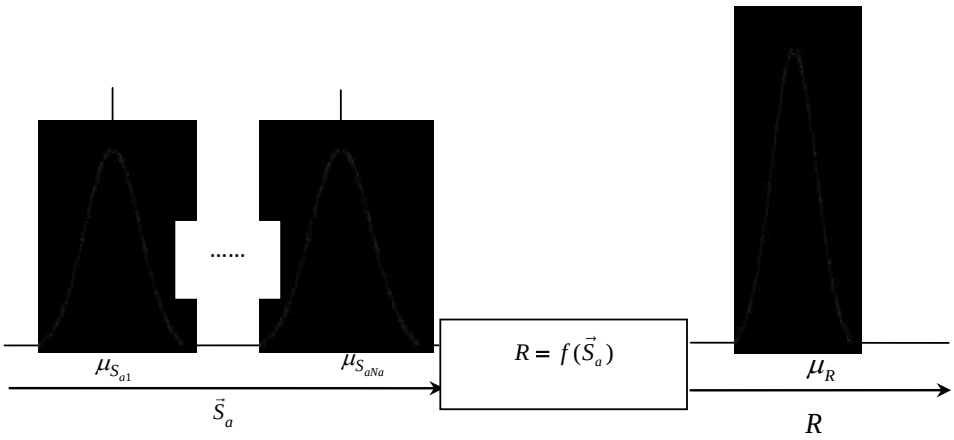

Figure 4.1. Robustness estimation of response in the presence of aleatory uncertainties only

where $\rho(\vec{S_a})$ represents the joint probability function (PDF) of $\vec{S_a}$ and Ω stands for the support region of $\vec{S_a}$. For this case, the variance (or the standard deviation, σ) of R is considered as the robustness measure.

4.1.2. Epistemic Uncertainties Only. If there are only epistemic uncertainties as input, the response will be a function of epistemic uncertainty vector $\vec{S_e} = (S_{e_1}, S_{e_2}, ..., S_{e_{N_e}})$, which may include epistemic design variables ($\vec{X_e}$) and epistemic parameters ($\vec{P_e}$) in general. In this study, the epistemic uncertainty is imposed to the design variables through the parameters that define them (e.g., average and the limits of the interval), which vary in the design space. The relationship between input epistemic uncertainties and response $R = f(\vec{S_e})$ is shown in Figure 4.2. The midpoint ($\overline{R}$) and width (δR) of interval R are the most relevant statistics of response R for this case, and given by

$$\overline{R} = \frac{1}{2}(R_L + R_U) \tag{34}$$

$$\delta R = R_U - R_L \tag{35}$$

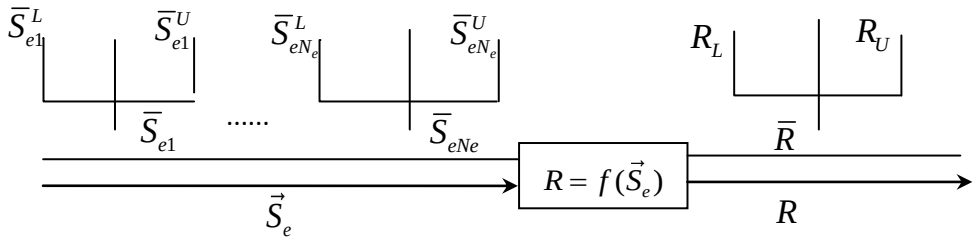

Figure 4.2. Robustness estimation of response in the presence of epistemic uncertainties only

respectively, where R_U and R_L represent the upper bound and lower bound of R. For this case, the robustness of the response is assessed by δR. For robust optimization, δR should be as low as possible, while $\overline{R}$ is equal to the desired value.

4.1.3. Mixed Uncertainties (Aleatory and Epistemic). When both aleatory uncertainties $\vec{S}_a = (S_{a_1}, ..., S_{a_{N_a}})$ and epistemic uncertainties $\vec{S}_e = (S_{e_1}, S_{e_2}, ..., S_{e_{N_e}})$ exist as input variables, the response R becomes a function of both types of uncertainty, $R = f(\vec{S}_a, \vec{S}_e)$ as shown in Figure 4.3. For this case, the uncertainty of R will be in the form of a family of probability distributions each due to the aleatory input uncertainties at a fixed value of epistemic input uncertainty vector. The intervals at each probability level will reflect the effect of epistemic uncertainties on R. The average mean value of R will be calculated by,

$$\overline{\mu}_R = \frac{1}{2}(\mu_R^{max} + \mu_R^{min}) \tag{36}$$

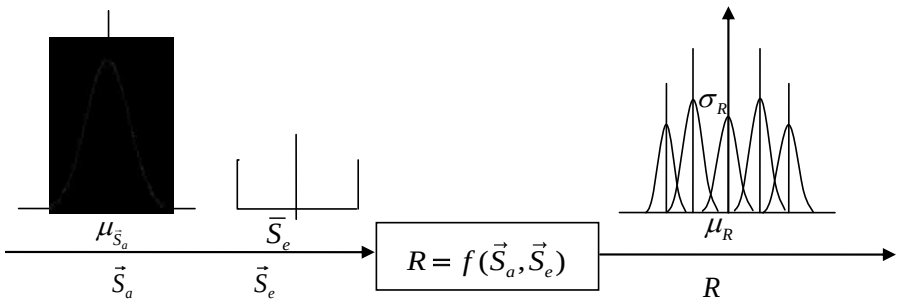

Figure 4.3. Robustness estimation of response in the presence of mixed uncertainties

where μ_R^{max} and μ_R^{min} are the maximum and minimum means of response R, respectively. The average value of the standard deviation of R ($\overline{\sigma}_R$) will be obtained by

$$\overline{\sigma}_R = \frac{1}{2}(\sigma_R^{max} + \sigma_R^{min}) \tag{37}$$

where σ_R^{max} and σ_R^{min} are the maximum and minimum standard deviations of response R, respectively. The difference between σ_R^{max} and σ_R^{min} will be computed by,

$$\delta\sigma_R = \sigma_R^{max} - \sigma_R^{min} \tag{38}$$

In this study, the average standard deviation $\overline{\sigma}_R$ will be used as a robustness measure for aleatory input uncertainties ($\vec{S}_a$), whereas we will utilize the standard deviation difference $\delta\sigma_R$ as the robustness measure for epistemic uncertainties ($\vec{S}_e$). It should be noted that one may also consider alternative measures for robustness to aleatory input uncertainties in the presence of mixed uncertainties. One approach will be to consider the maximum value of the standard deviation as a conservative measure, which in turn can be used in the robust optimization formulation described below.

4.1.4. Robust Optimization Formulation Under Mixed Uncertainties. To achieve a robust design in the presence of aleatory and epistemic uncertainties, both a lower value of $\overline{\sigma}_R$ and a lower value of $\delta\sigma_R$ are desired. To illustrate this, let us consider two designs (A and B) with performances (i.e., responses) having two different families of probability distributions represented by one blue and one red curve in Figure 4.4. From these distributions, it is obvious that $\overline{\sigma}_R$ of design A is less than that of design B, which indicates that design A is more robust than design B when only randomness of the input is considered. Now comparing $\delta\sigma_R$ of two designs, it can be seen that design A has smaller difference between the distribution variances indicating that it is also more robust to epistemic uncertainties. In the light of above discussion and following the formulation of Du et al. [50], a composite (weighted sum)

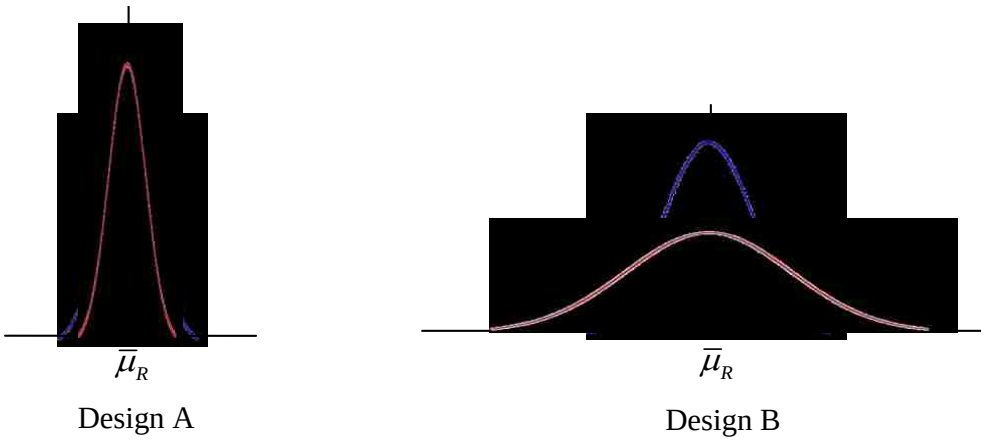

Figure 4.4. Robustness assessment of mixed uncertainty design

objective function for robust optimization under mixed uncertainties can be written as

$$F(\vec{X}_d, \vec{S}_a, \vec{S}_e) = w_1\overline{\mu}_R + w_2\overline{\sigma}_R + w_3\delta\sigma_R \tag{39}$$

where $\vec{X}_d$ is the deterministic design variable vector, $\vec{S}_a = \left\{\vec{X}_a, \vec{P}_a\right\}$, and $\vec{S}_e = \left\{\vec{X}_e, \vec{P}_e\right\}$. The values of the weight factors w_1, w_2, and w_3 should be chosen based on the emphasis on the contribution of each term to the objective function by also considering the order of magnitude of each term. While minimizing F, a feasible design should also satisfy the inequality constraints $g_i(\vec{X}_d, \vec{S}_a, \vec{S}_e)$, $(i = 1, 2, ..., N_g)$ and the side constraints for aleatory design variables $\vec{X}_a$ (specified by the lower and the upper limits of the mean of the each aleatory variable), epistemic design variables $\vec{X}_e$ (specified by the lower and the upper limits of the epistemic variable), and the deterministic design variables $\vec{X}_d$. Under mixed uncertainties, a conservative form of the satisfaction of the inequality constraints can be written as $\mu_{gi}^{max} + \beta\sigma_{gi}^{max} \leq 0$ where $\mu_{g_i}^{max}$ and $\sigma_{g_i}^{max}$ are the maximum of the mean and the maximum of the standard deviation of the constraint function g_i, respectively. Here β_i is a positive constant, which denotes the probability of constraint satisfaction.

In summary, the overall formulation for robust design optimization under aleatory and epistemic uncertainties can be written as:

$$\begin{aligned} Minimize \quad & w_1\overline{\mu}_R + w_2\overline{\sigma}_R + w_3\delta\sigma_R \\ S.t. \quad & \mu_{g_i}^{max} + \beta_i\sigma_{g_i}^{max} \leq 0, i = 1, 2, ..., N_g \\ & X_{d_j}^L \leq X_{d_j} \leq X_{d_j}^U, j = 1, 2, ..., N_d \\ & X_{e_k}^L \leq X_{e_k} \leq X_{e_k}^U, k = 1, 2, ..., N_e \\ & \mu_{X_{a_m}}^L \leq \mu_{X_{a_m}} \leq \mu_{X_{a_m}}^U, m = 1, 2, ..., N_a \end{aligned} \tag{40}$$

4.2. STOCHASTIC EXPANSIONS FOR ROBUST DESIGN

In this proposed methodology, the optimization is performed on the stochastic response surfaces obtained with NIPC methods described above. While constructing the stochastic response surfaces, a combined expansion approach will be utilized, which will expand the polynomials as a function of uncertain design variables and parameters (aleatory and epistemic) as well as the deterministic design variables. The combined expansion approach and robust optimization with stochastic expansions will be described in the following sections.

4.2.1. Formulation with Combined Expansions. With the introduction of deterministic design variables ($\vec{X}_d$), design variables with epistemic uncertainty ($\vec{X}_e$), parameters with epistemic uncertainty ($\vec{P}_e$), design variables with aleatory uncertainty ($\vec{X}_a$), and parameters with aleatory uncertainty ($\vec{P}_a$), a combined stochastic expansions of R is obtained by ultilizing the Equation (15):

$$\begin{aligned} & R(X_a(\vec{\xi}_{xa}), P_a(\vec{\xi}_{pa}), X_e(\vec{\xi}_{xe}), P_e(\vec{\xi}_{pe}), X_d(\vec{\xi}_d)) \\ = & \sum_{j=0}^{P} \alpha_j \Psi_j(\vec{\xi}_{xa}, \vec{\xi}_{pa}, \vec{\xi}_{xe}, \vec{\xi}_{pe}, \vec{\xi}_d) \end{aligned} \tag{41}$$

In this approach, multi-dimensional basis functions Ψ_j are derived from the tensor product of one-dimensional optimum basis functions for the aleatory uncertain parameters and design variables ($\vec{P}_a$ and $\vec{X}_a$) selected based on their input probability distributions (e.g., Hermite polynomials for normal uncertain variables), the Legendre polynomials for the epistemic uncertain parameters and design variables ($\vec{P}_e$ and $\vec{X}_e$), and the Legendre polynomials for the deterministic design variables ($\vec{X}_d$). The selection of the Legendre polynomials as basis functions for the epistemic uncertainties and the design variables are due to their bounded nature ($\vec{P}_e^L \leq \vec{P}_e \leq \vec{P}_e^U$, $\vec{X}_e^L \leq \vec{X}_e \leq \vec{X}_e^U$, and $\vec{X}_d^L \leq \vec{X}_d \leq \vec{X}_d^U$) and should not be interpreted as a probability assignment to these variables. In Equation (41), $\vec{\xi}_{xa}$ and $\vec{\xi}_{pa}$ correspond to standard aleatory random variable vectors associated with $\vec{X}_a$ and $\vec{P}_a$, whereas $\vec{\xi}_{xe}$, $\vec{\xi}_{pe}$, and $\vec{\xi}_d$ are the standard variables in interval [-1,1], which are mapped from the associated intervals of $\vec{X}_e$, $\vec{P}_e$, and $\vec{X}_d$ via

$$\vec{\xi}_{xe} = \left(\vec{X}_e - (\frac{\vec{X}_e^L + \vec{X}_e^U}{2}) \right) / \left(\frac{\vec{X}_e^U - \vec{X}_e^L}{2} \right) \tag{42}$$

$$\vec{\xi}_{pe} = \left(\vec{P}_e - (\frac{\vec{P}_e^L + \vec{P}_e^U}{2}) \right) / \left(\frac{\vec{P}_e^U - \vec{P}_e^L}{2} \right) \tag{43}$$

$$\vec{\xi}_d = \left(\vec{X}_d - (\frac{\vec{X}_d^L + \vec{X}_d^U}{2}) \right) / \left(\frac{\vec{X}_d^U - \vec{X}_d^L}{2} \right) \tag{44}$$

Using the combined expansion given in Equation (41), the mean and the variance of the output response are obtained by evaluating the expectations given in Equations (7) and (8) over the standard aleatory uncertain variables (including standard aleatory design variables ($\vec{\xi}_{xa}$) and standard aleatory parameters ($\vec{\xi}_{pa}$)),

$$\mu_R(\vec{\xi}_{xe}, \vec{\xi}_{pe}, \vec{\xi}_d) = \sum_{j=0}^{P} \alpha_j \left\langle \Psi_j(\vec{\xi}_{xa}, \vec{\xi}_{pa}, \vec{\xi}_{xe}, \vec{\xi}_{pe}, \vec{\xi}_d) \right\rangle_{\vec{\xi}_{xa}, \vec{\xi}_{pa}} \tag{45}$$

$$\sigma_R^2(\vec{\xi}_{xe}, \vec{\xi}_{pe}, \vec{\xi}_d) = \left(\sum_{j=0}^{P} \sum_{k=0}^{P} a_j a_k \left\langle \Psi_j \Psi_k \right\rangle_{\vec{\xi}_{xa}, \vec{\xi}_{pa}} \right) - \mu_R^2 \tag{46}$$

which will become the functions of standard epistemic design variables ($\vec{\xi}_{xe}$), standard epistemic parameters ($\vec{\xi}_{pe}$), and standard deterministic design variables ($\vec{\xi}_d$).

4.2.2. Robust Design Based On Stochastic Expansions. The flowchart of robust optimization under mixed uncertainties based on combined stochastic expansions is shown in Figure 4.5.

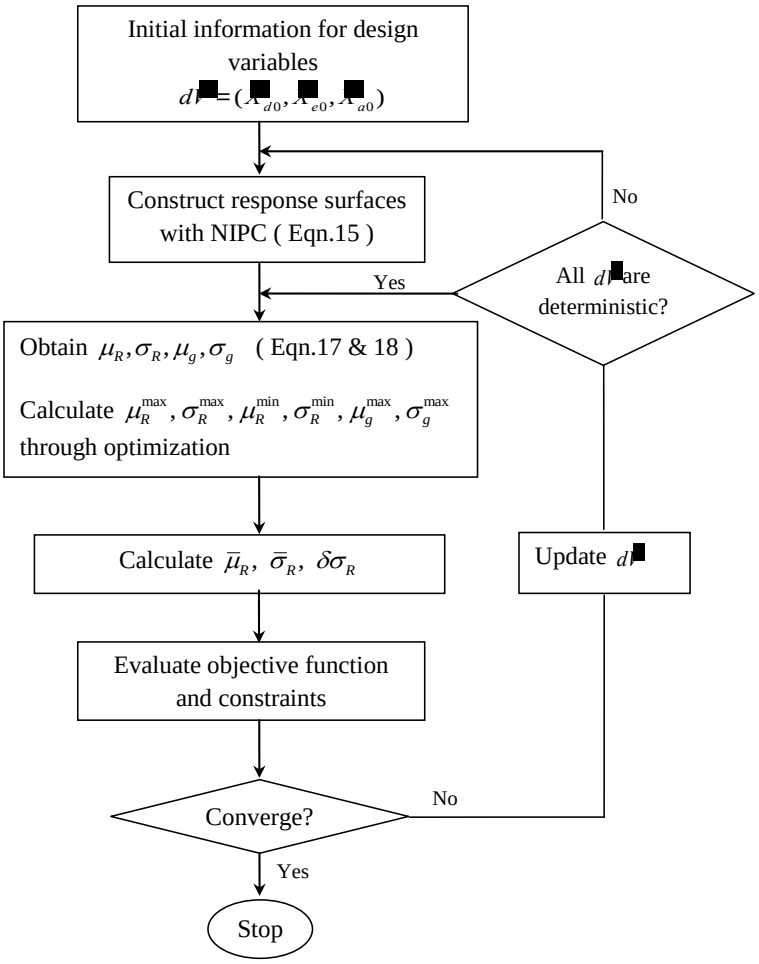

Figure 4.5. Flow chart of the robust optimization process under mixed uncertainties with combined stochastic expansions

From Equations (45) and (46) given in the previous section, it can be clearly seen that the mean and standard deviation of the response R (i.e., objective function F or constraint g_i) at a given design point is characterized by two bounds due to epistemic uncertainties with specified interval bounds $[\vec{X}_e^L, \vec{X}_e^U]$ and $[\vec{P}_e^L, \vec{P}_e^U]$. In other words, the mean and standard deviation of output (response) will also be bounded by its maximum and minimum values. In this approach, μ_R^{max}, μ_R^{min}, σ_R^{max} and σ_R^{min} are calculated at a given design point through optimization using the analytical expressions of response statistics obtained with Equation (45) and Equation (46). Then, these values are used in robust optimization formulation given by Equation (40), which is performed with Sequential Quadratic Programing (SQP) method [71]. The whole procedure is repeated until the convergence is achieved. It should be noted that when at least one design variable is uncertain (aleatory or epistemic), the stochastic response surfaces for the objective function and the constraints (if necessary) have to be re-constructed at each optimization iteration since the uncertain design variables and the associated statistics are updated at each iteration changing the bounds on which the response surfaces are created. On the other hand, if all design variables are deterministic and the uncertainties are associated with the problem parameters, only a single stochastic response surface for the objective function and a single response surface for each constraint function has to be constructed, since the bounds on the statistics of uncertain parameters and the bounds on the design variables are fixed and do not vary during the entire optimization process.

5. APPLICATION OF ROBUST OPTIMIZATION: MODEL PROBLEMS

The robust optimization methodology described in the previous section is demonstrated on two model problems: (1) the robust design of a slider-crank mechanism and (2) robust design of a beam problem.

5.1. MODEL PROBLEM 1: ROBUST DESIGN OF A SLIDER-CRANK

This design problem is taken from Du et al. [50], who also used the same problem to demonstrate their robust optimization approach under aleatory and epistemic uncertainties. The design problem includes a slider-crank mechanism (Figure 5.1) to be designed such that, for crank angles of $\theta = 10^\circ$ and $\theta = 60^\circ$, the slider distance s should be 3.5 cm and 2.5 cm, respectively. The length of the crank is a, the length of the connecting rod is b and the offset is e. Since different installation positions of the slider are needed, the offset distance e is specified within a tolerance. The robust optimization problem for two cases will be formulated and solved based on the classification of a, b, and e.

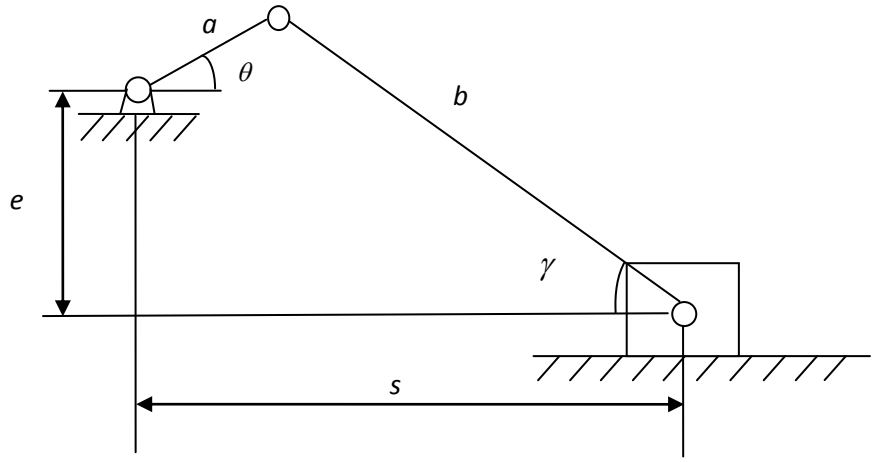

Figure 5.1. Slider-crank mechanism used in model problem 1

5.1.1. Case 1. This case corresponds to the original robust optimization problem used by Du et al. [50]. In this case, a and b are considered as design variables with aleatory uncertainty ($\vec{X}_a = \{a, b\}$) modeled with normal distributions following $\mathrm{N}(\mu_a, 1\%\mu_a)$ and $\mathrm{N}(\mu_b, 1\%\mu_b)$, respectively. The offset distance e is treated as an epistemic design variable ($\vec{X}_e = \{e\}$) with an average value ($\overline{e}$) and specified tolerance within $[\overline{e} - 5\%\overline{e}, \overline{e} + 5\%\overline{e}]$. Due to the uncertainties in a, b, and e, there will be an error in the slider distance s at crank angles $\theta = 10^\circ$ ($Z(10^\circ)$) and $\theta = 60^\circ$ ($Z(60^\circ)$) given by

$$Z(10^\circ) = [acos10^\circ + \sqrt{b^2 - (e + asin10^\circ)^2}] - 3.5 \tag{47}$$

$$Z(60^\circ) = [acos60^\circ + \sqrt{b^2 - (e + asin60^\circ)^2}] - 2.5 \tag{48}$$

To ensure robustness of the design at these two crank angles under aleatory and epistemic uncertainties of design variables, the average standard deviation $\overline{\sigma}_Z$ and difference between the maximum and minimum standard deviation $\delta\sigma_Z$ should be minimized at these angles. The design is also subject to inequality constraints given by

$$g_1 = e - (b - a) \leq 0 \tag{49}$$

$$g_2 = (e + a) - bsin45^\circ \leq 0 \tag{50}$$

Here the first constraint ensures the existence of the crank and the second constraint imposes that the transmission angle is greater than 45°. For robust design, the worst case of these constraints should be satisfied with a chosen β value of 3. The error of actual displacements at 10° and 60° at the mean values of aleatory design variables and average value of epistemic design variables are also treated as two equality constraints. Combining all these, the robust design formulation for the this problem is written as

$$
\begin{aligned}
&\underset{\vec{X}_a,\vec{X}_e}{min} \quad w_1\overline{\sigma}_Z(10^\circ) + w_2\delta\sigma_Z(10^\circ) + w_3\overline{\sigma}_Z(60^\circ) + w_4\delta\sigma_Z(60^\circ) \\
&s.t. \quad \mu_{g_i}^{max} + 3\sigma_{g_i}^{max} \leq 0 \quad i = 1,2 \\
&\qquad h_1(\vec{X}_a,\vec{X}_e) = \mu_a cos10^\circ + \sqrt{\mu_b^2 - (\overline{e} + \mu_a sin10^\circ)^2} - 3.5 \\
&\qquad h_2(\vec{X}_a,\vec{X}_e) = \mu_a cos60^\circ + \sqrt{\mu_b^2 - (\overline{e} + \mu_a sin60^\circ)^2} - 2.5 \\
&\qquad 0.1 \leq \mu_a \leq 20 \qquad 0.1 \leq \mu_b \leq 20 \qquad 0.1 \leq \overline{e} \leq 20
\end{aligned}
\tag{51}
$$

The weight factors in the multi-objective function are used to normalize (scale) each objective and correspond to the inverse of the mean value of the associated term evaluated at the deterministic optimal solution reported in Du et al. [50] (i.e., $w_1 = 33.88$, $w_2 = 4.48 \times 10^3$, $w_3 = 29.53$, and $w_4 = 1.03 \times 10^3$). Following the methodology described in the previous section, the robust optimization was performed with stochastic response surfaces representing the objective function obtained with the NIPC approach that have utilized a 2^{nd} order polynomial expansion over aleatory and epistemic design variables. Two methods, Point-Collocation and Quadrature-Based approach were implemented to obtain the stochastic response surfaces for comparison. The Point-Collocation NIPC method was evaluated with the OSR of 1 and 2 to study the effect of OSR on the accuracy of the results. The number of original function evaluations required to construct a single response surface was 10 for the Point-Collocation with OSR of 1, 20 for OSR of 2, and 27 for the Quadrature-Based method. For this case, two response surfaces were constructed to represent the multi-objective function at each optimization iteration, corresponding to the error in the slider distance at crank angles $\theta = 10^\circ$ and $\theta = 60^\circ$. No response surface was necessary for the inequality constraints in this problem due to their linear nature, which were evaluated analytically. Besides the stochastic response surface based approach, robust optimization was also performed with double-loop MCS, which was the approach used by Du et al. [50] to propagate the mixed uncertainties and obtain the maximum and

minimum value of the response statistics used in the robust optimization formulation. Following a convergence study for the double-loop MCS, the desired accuracy level was obtained by using 200 samples in the outer loop for the interval (epistemic) variables and 10000 samples in the inner loop for aleatory variables at each epistemic variable value. This procedure was repeated at each optimization iteration to determine the bounds of the statistics used in the multi-objective function, which required a separate double-loop Monte-Carlo sampling for the error at each crank angle. (i.e., 4×10^6 response evaluations per optimization iteration). Table 5.1 gives the values of the optimum design variables obtained with different methods. In this table, the total number of function evaluations to obtain the optimal solution with Monte Carlo method is the product of the original function simulations per iteration and the number of iterations required for convergence. All methods give the same optimum design variable values validating the stochastic response surface based robust optimization approach. Compared to MCS, total number of function evaluations required to create the stochastic response surfaces are significantly less indicating the computational efficiency of the approach. Although the Point-Collocation NIPC with $OSR = 1$ is more efficient than the Point-Collocation with $OSR = 2$ and Quadrature-Based NIPC in terms of the response evaluations for this problem, an OSR of 1.0 for Point-Collocation NIPC may not be accurate in general for most stochastic problems. The robustness measures that construct the multi-objective function (i.e., mean of the standard deviation and the difference in standard deviation) at the optimum design are reported on Table 5.2. These values are approximately the same for all methods and their small values indicate the robustness of the design to both aleatory and epistemic uncertainties considered in this problem.

Table 5.1. Optimum design results of the slider-crank problem for Case 1

Method	$\{\mu_a, \mu_b, \overline{e}\}$ (cm)	# of FE
MCS	$\{1.32, 2.22, 0.10\}$	8×10^7
Q-B	$\{1.32, 2.22, 0.10\}$	1,080
P-C OSR=1	$\{1.32, 2.22, 0.10\}$	800
P-C OSR=2	$\{1.32, 2.22, 0.10\}$	1,600

(MCS: Monte-Carlo Sampling, Q-B: Quadrature-Based, P-C: Point-Collocation, OSR: Over Sampling Ratio, FE: Function Evaluations)

Table 5.2. Robustness assessment of slider-crank problem for Case 1

Method	$\{\ \overline{\sigma}_Z(10°)\ ,\overline{\sigma}_Z(60°)\}$	$\{\delta\sigma_Z(10°),\delta\sigma_Z(60°)\}$
MCS	$\{\ 2.60,\ 2.70\} \times 10^{-2}$	$\{0.81,\ 10.23\ \} \times 10^{-5}$
Q-B	$\{\ 2.58,\ 2.69\ \} \times 10^{-2}$	$\{0.81,\ 10.31\ \} \times 10^{-5}$
P-C OSR=1	$\{\ 2.58,\ 2.69\ \} \times 10^{-2}$	$\{\ 0.87,\ 13.28\ \} \times 10^{-5}$
P-C OSR=2	$\{\ 2.58,\ 2.69\ \} \times 10^{-2}$	$\{\ 0.81,\ 10.30\ \} \times 10^{-5}$

(MCS: Monte-Carlo Sampling, Q-B: Quadrature-Based, P-C: Point-Collocation, OSR: Over Sampling Ratio, FE: Function Evaluations)

5.1.2. Case 2. For this case, the original model problem presented in Case 1 is modified to include only a single design variable, b (the length of the connecting rod), which is considered as deterministic ($\vec{X}_d = \{b\}$). In addition, the length of the crank a is now assumed as an aleatory parameter (($\vec{P}_a = \{a\}$)) modeled with normal distribution using $\mathrm{N}(1.2, 0.012)$ and the offset distance e is an epistemic parameter ($\vec{P}_e = \{e\}$) specified with a tolerance between $[0.095, 0.105]$. The purpose of this modification on the model problem is to demonstrate the robust optimization approach for a case when all design variables are deterministic and uncertainties are associated with the problem parameters, which will require the construction of a single stochastic response surface (for the objective function), since the bounds on the

statistics of uncertain parameters and the bounds on the design variables parameters are fixed and do not vary during the optimization process.

The objective function for this case is also modified such that the robustness of the error is now desired only at a single crank angle, $\theta = 10^\circ$ to ensure a feasible solution for the modified problem. The same inequality constraints of case 1 also apply to this problem. Since only one crank angle is considered, the equality constraint is written for this angle. With the addition of the bound on the deterministic design variable, the robust optimization statement for Case 2 is written as

$$\begin{aligned} \underset{\vec{X}_d}{min} \quad & w_1 \overline{\sigma}_Z(10^\circ) + w_2 \delta\sigma_Z(10^\circ) \\ s.t. \quad & \mu_{g_i}^{max} + \beta\sigma_{g_i}^{max} \leq 0 \quad i = 1, 2 \\ & h(X_d, P_a, P_e) = \mu_a cos10^\circ + \sqrt{b^2 - (\overline{e} + \mu_a sin10^\circ)^2} - 3.5 \\ & 2 \leq b \leq 20 \end{aligned} \tag{52}$$

The results for this case were again obtained with two robust optimization approaches as in Case 1 (optimization with stochastic response surfaces and optimization that utilize double-loop Monte Carlo). The same sample size reported in Case 1 was used for performing the double-loop MCS, which were used as reference to test the accuracy of the NIPC approaches. For this case, convergence of the NIPC response surfaces with respect to the polynomial order were performed at the optimum design point obtained with the double-loop Monte Carlo approach. Figure 5.2 shows the average standard deviation ($\overline{\sigma}\,(10^\circ)$) values obtained with Point-Collocation NIPC with $OSR = 1$ and $OSR = 2$, and Quadrature-Based NIPC at expansion orders up to 5. As can be seen from Figure 5.2, the Point-Collocation NIPC with $OSR = 1$ does not exhibit convergence whereas both the Quadrature-Based and Point-Collocation NIPC with $OSR = 2$ seem to be accurate for all polynomial degrees. Figure 5.3 shows the standard deviation difference ($\delta\sigma\,(10^\circ)$) values at the same expansion orders. From

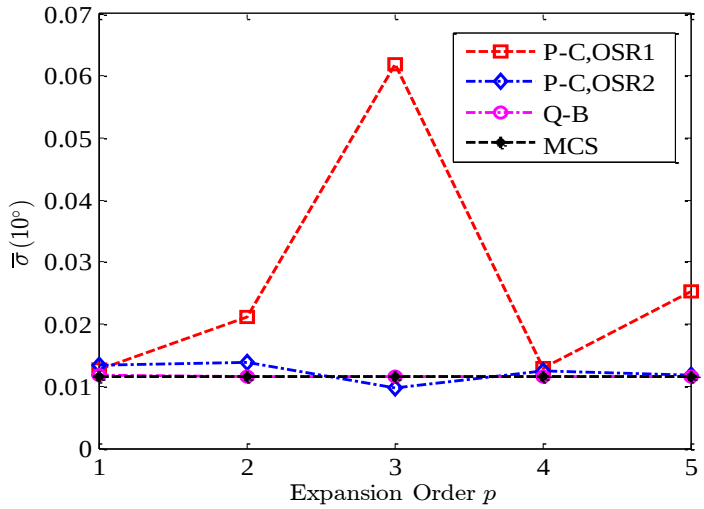

Figure 5.2. Convergence of NIPC results for $\overline{\sigma}\,(10^\circ)$ as a function of expansion order for model problem 1, case 2

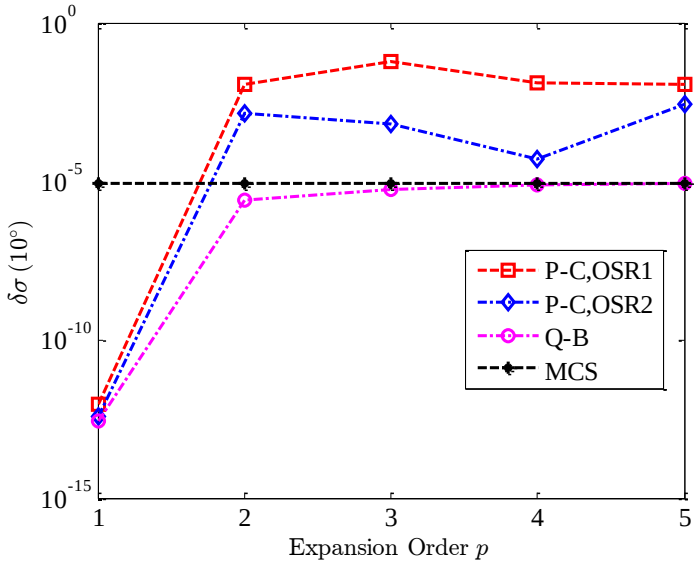

Figure 5.3. Convergence of NIPC results for $\delta\sigma\,(10^\circ)$ as a function of expansion order for model problem 1, case 2

this figure, it can be seen that all NIPC methods seem to converge at a polynomial order of 2. For this metric, the most accurate method is the Quadrature-Based approach, followed by the Point-Collocation with $OSR = 2$. Although the number

of function evaluations required for the construction of second-order NIPC expansion with Quadrature-Based approach is greater than the number required by the Point-Collocation NIPC (27 vs.20), a better accuracy level is achieved with the quadrature approach.

Following the convergence study, the optimization was performed with Point-Collocation NIPC (with OSR of 1 and 2) and Quadrature-Based approach using an expansion order of 2.0. As can be seen from Table 5.3, all methods give the same optimum value of the design variable. The computational cost of the optimization with stochastic response surface is significantly lower than the Monte Carlo approach especially considering the fact that only a single response surface is used for the whole stochastic optimization process. Table 5.4 shows the robustness measures that construct the multi-objective function (i.e., mean of the standard deviation and the difference in standard deviation) at the optimum design. For this case, the robustness measures obtained with each method is very small, however the results obtained with the Quadrature-Based NIPC method is closer to those obtained with the Monte-Carlo approach compared to the Point-Collocation NIPC results verifying the observations made in the convergence study.

Table 5.3. Optimum design results of the slider-crank problem for Case 2

Method	b (cm)	FE per RS	Total number of FE
MCS	2.339	$--$	3×10^7
Q-B	2.339	27	27
P-C OSR=1	2.339	10	10
P-C OSR=2	2.339	20	20

(MCS: Monte-Carlo Sampling, Q-B: Quadrature-Based, P-C: Point-Collocation, OSR: Over Sampling Ratio, FE: Function Evaluations)

Table 5.4. Robustness assessment of slider-crank problem for Case 2

Method	$\overline{\sigma}_Z(10°)$	$\delta\sigma_Z(10°)$
MCS	1.09×10^{-2}	8.40×10^{-6}
Q-B	1.16×10^{-2}	2.61×10^{-6}
P-C OSR=1	2.12×10^{-2}	1.16×10^{-2}
P-C OSR=2	1.39×10^{-2}	1.35×10^{-3}

(MCS: Monte-Carlo Sampling, Q-B: Quadrature-Based, P-C: Point-Collocation, OSR: Over Sampling Ratio, FE: Function Evaluations)

5.2. MODEL PROBLEM 2: ROBUST DESIGN OF A BEAM

In this model problem, which includes the uncertainties in both design variables and parameters, the robust design of a cantilever beam shown in Figure 5.4 is considered with length l, width b, and height h. The beam is subjected to a torque T and an external force F acting normal to horizontal axis of the beam at its free end. The objective is to reduce the volume ($V = lbh$) of the beam while satisfying a stress constraint given by

$$g = \sqrt{\left(\frac{6FL}{bh^2}\right)^2 + 3\left[\frac{T}{b^2h}(3 + \frac{1.8b}{h})\right]^2} - S \leqslant 0 \tag{53}$$

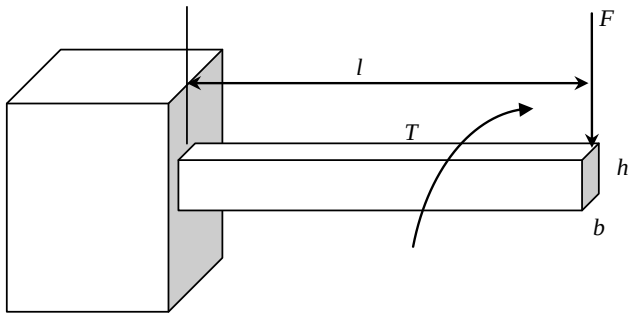

Figure 5.4. Schematic of the beam design problem of model problem 2

This equation represents the difference between the maximum equivalent stress of the beam and the yield strength S, which has to be less than or equal to zero for a safe design. In this design problem, the external force F is considered as a parameter with epistemic uncertainty and the length of the beam l is treated as an epistemic design variable (Table 5.5). The external torque T and yield strength S are treated as parameters with aleatory uncertainty, whereas the width b and the height h of the beam are modeled as aleatory design variables with statistics given in Table 5.6.

Table 5.5. Design variables (DV) and parameters (P) with epistemic uncertainty for model problem 2

DV / P	lower limit	upper limit
$\overline{l}$ (DV)	$\overline{l} - 0.1\overline{l}$	$\overline{l} + 0.1\overline{l}$
F (P)	270 lb	330 lb

Table 5.6. Design variables (DV) and parameters (P) with aleatory uncertainty for model problem 2

DV / P	Mean	Standard deviation	Distribution
h (DV)	μ_h	$1\%\mu_h$	Normal
b (DV)	μ_b	$1\%\mu_b$	Normal
S (P)	100 $kpsi$	10 $kpsi$	Normal
T (P)	450 $lb - in$	50 $lb - in$	Normal

To ensure robustness of the design under epistemic and aleatory uncertainties, the objective function, which is the weighted sum of the average mean of the volume ($\overline{\mu}_V$), the average standard deviation of the volume ($\overline{\sigma}_V$), and the standard deviation

difference of the volume ($\delta\sigma_V$) should be minimized. The inequality constraint given by Equation (53) should be satisfied at the worst case with a specified β value of 3. The robust design formulation for this problem is given as

$$\begin{aligned} \min_{d} \quad & w_1\overline{\mu}_V + w_2\overline{\sigma}_V + w_3\delta\sigma_V \\ s.t. \quad & \mu_g^{max} + \beta\sigma_g^{max} \leq 0 \\ & 0.1 \leq \mu_h \leq 0.8 \\ & 0.1 \leq \mu_b \leq 0.4 \\ & 2 \leq \bar{l} \leq 20 \end{aligned} \tag{54}$$

Considering the magnitude of $\overline{\mu}_V$, $\overline{\sigma}_V$, and $\delta\sigma_V$, the weights in the multi-objective function are chosen as $w_1 = 1$, $w_2 = 100$, and $w_3 = 500$ to ensure equal contributions to the objective function from each term (i.e., scaling them to approximately the same order of magnitude). For this problem, the double-loop MCS results were again used as reference to check the accuracy of the results obtained with two NIPC approaches. After performing a convergence study based on the inner and outer loop samples, the desired accuracy with the double-loop Monte Carlo sampling approach for the robustness measures was obtained with 500 epistemic variable samples in the outer loop and 10^5 aleatory variable samples in the inner loop. The convergence of the performance and robustness measures used in the objective function ($\bar{\mu}_V$, $\bar{\sigma}_V$, and $\delta\sigma_V$) obtained with Quadrature-Based and Point-Collocation NIPC with $OSR = 1$ and $OSR = 2$ were studied for different polynomial expansion orders at the optimum design point obtained with the Monte Carlo approach (Figure 5.5). For the same robustness measures, the error values relative to the Monte-Carlo results at each polynomial order are shown in Figure 5.6. It is evident that the convergence is rapid for $\overline{\mu}_V$ and achieved by the first order expansion for all NIPC methods. The convergence for $\overline{\sigma}_V$ and $\delta\sigma_V$ are obtained at 2^{nd} order expansion. From Figure 5.6, it

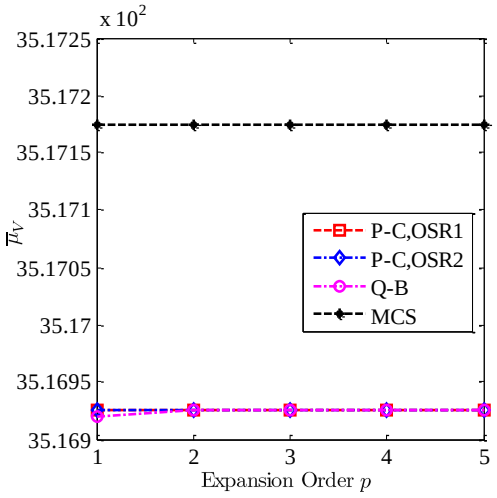

(a) Average mean of beam volume, $\bar{\mu}_V$

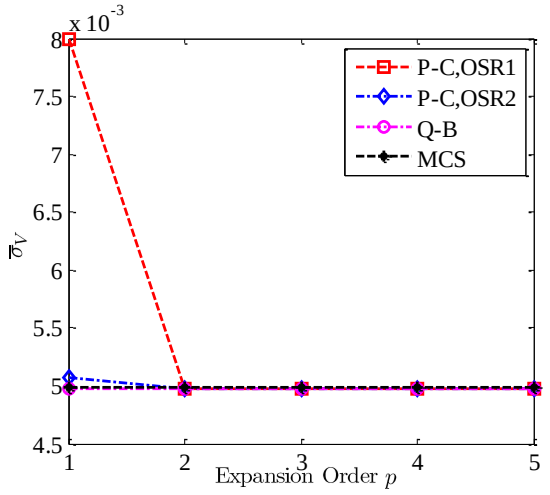

(b) Average standard deviation of beam volume, $\bar{\sigma}_V$

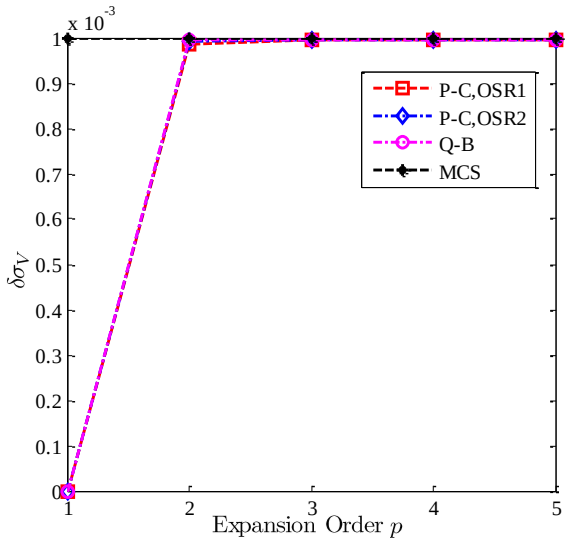

(c) Difference of standard deviation of beam volume, $\delta\sigma_V$

Figure 5.5. Convergence of NIPC results as a function of expansion order for model problem 2

can be seen that the Quadrature-Based NIPC is more accurate than Point-Collocation based approach in terms of the error levels (especially for $\delta\sigma_V$) observed at the second-order expansion. Based on the convergence results, the robust optimization was performed with stochastic response surfaces representing the objective function

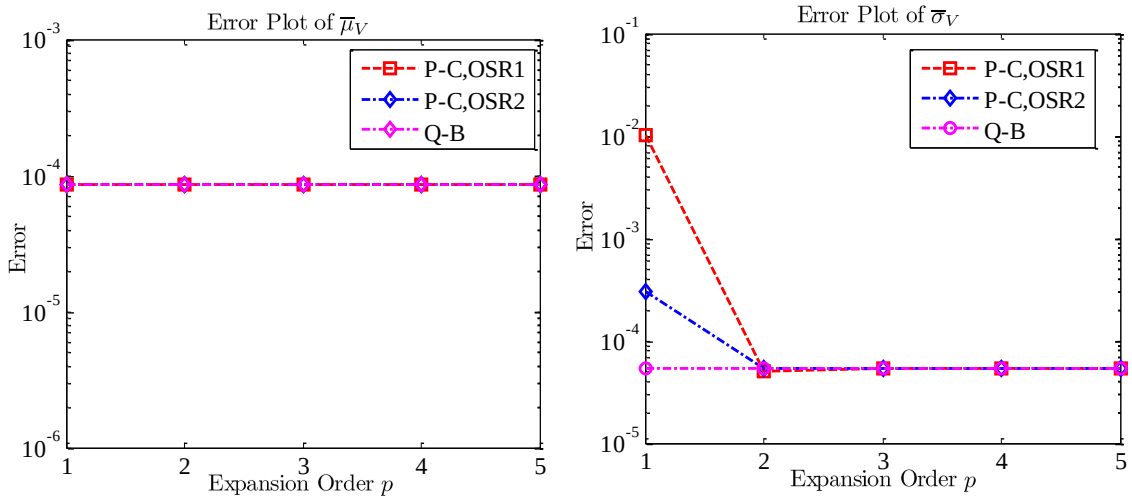

(a) Error of average mean of beam volume, $\bar{\mu}_V$ (b) Error of average standard deviation of beam volume, $\bar{\sigma}_V$

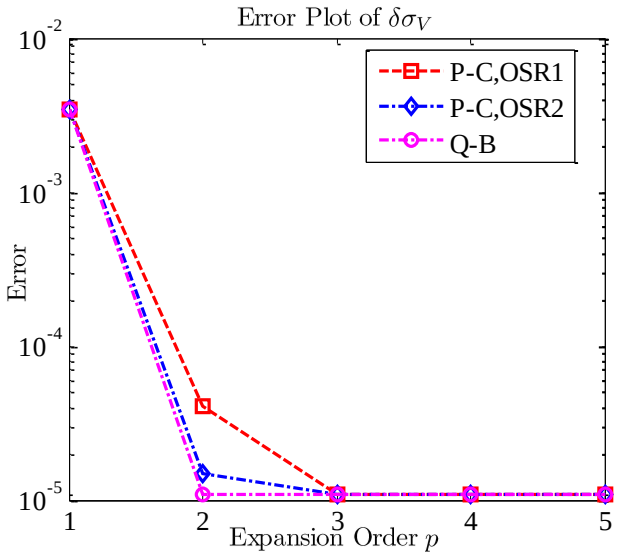

(c) Error of difference of standard deviation of beam volume, $\delta\sigma_V$

Figure 5.6. Error convergence of NIPC results as a function of expansion order for model problem 2

and the inequality constraint obtained with the NIPC approach that have utilized a 2^{nd} order polynomial expansion over aleatory and epistemic design variables and parameters. Two NIPC methods, Point-Collocation and Quadrature-Based approach were implemented to obtain the stochastic response surfaces for comparison. The

Point-Collocation method was performed with the OSR of 1 and 2. The number of original function evaluations required to construct a single response surface was 28 for the Point-Collocation Method with $OSR = 1$ and 56 with $OSR = 2$. The Quadrature-Based method required 729 function evaluations. For this case, two response surfaces were constructed at each optimization iteration, one for the objective function and the other for the inequality constraint. The optimum design variable values obtained with stochastic response surface based optimization again compare well with the result of the approach utilizing the double-loop Monte-Carlo sampling (Table 5.7) at a significantly reduced cost in terms of the total number of function evaluations, which include both the objective and constraint functions. The Point-Collocation NIPC is more efficient than the Quadrature-Based NIPC for this problem since the number of expansion variables ($n = 6$) is greater than the number of variables in the previous model problem ($n = 3$) and the computational cost of the Quadrature-Based NIPC increase exponentially with the number of expansion variables for a given polynomial degree. An alternative approach to reduce the computational expense of the Quadrature-Based approach will be to implement sparse grid and cubature techniques, which may improve the computational efficiency significantly while retaining the accuracy of the original tensor product quadrature method.

Table 5.7. Optimum design results of the beam problem

Method	$\{\mu_h, \mu_b, \bar{l}\}$ (in)	Total # of FE
MCS	{0.548, 0.327, 2.0}	23.5×10^8
Q-B	{0.542, 0.323, 2.0}	96,228
P-C,OSR=1	{0.543, 0.324, 2.0}	3,696
P-C,OSR=2	{0.542, 0.323, 2.0}	6,720

(MCS: Monte-Carlo Sampling, Q-B: Quadrature-Based, P-C: Point-Collocation, OSR: Over Sampling Ratio, FE: Function Evaluations)

Table 5.8 presents the average mean, average standard deviation, and the standard deviation difference of the beam volume at the optimum design point, which are approximately the same for all the methods.

Table 5.8. Robustness assessment of the beam problem

Method	$\overline{\mu}_V$	$\overline{\sigma}_V$	$\delta\sigma_V$
MCS	3.55×10^{-1}	5.06×10^{-3}	1.01×10^{-3}
Q-B	3.50×10^{-1}	4.96×10^{-3}	9.91×10^{-4}
P-C,OSR=1	3.52×10^{-1}	4.97×10^{-3}	9.86×10^{-4}
P-C,OSR=2	3.50×10^{-1}	4.94×10^{-3}	9.88×10^{-4}

The convergence histories of these terms are given in Figure 5.7 for the optimization process with stochastic expansions. As can be seen from this figure, all three quantities are minimized simultaneously and converge to the same final values, which validate the stochastic response surface based robust optimization approach described. Another important observation made from the same figure is that the Quadrature-Based approach seem to converge to the optimum robust design in terms of all measures at less number of iterations and in a more stable manner compared to the Point-Collocation based methods, especially the one with $OSR = 1$. This emphasizes another aspect of the importance of the accuracy of the stochastic response surfaces used in the robust optimization approach in terms of the number of iterations to converge, which may influence the computational efficiency of overall stochastic optimization process. The program listing for robust optimization under mixed uncertainties (for beam model problem) is given in Appendix E.

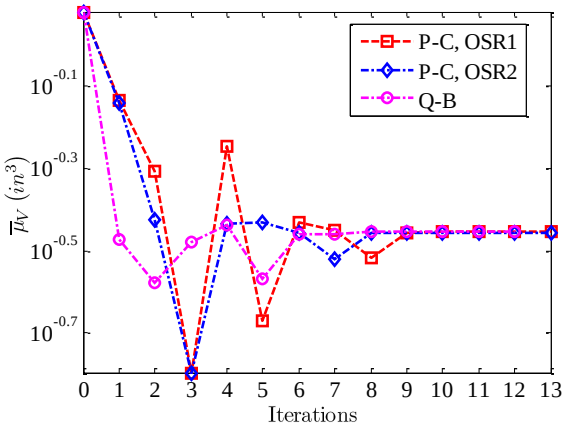

(a) Average mean of beam volume, $\bar{\mu}_V$

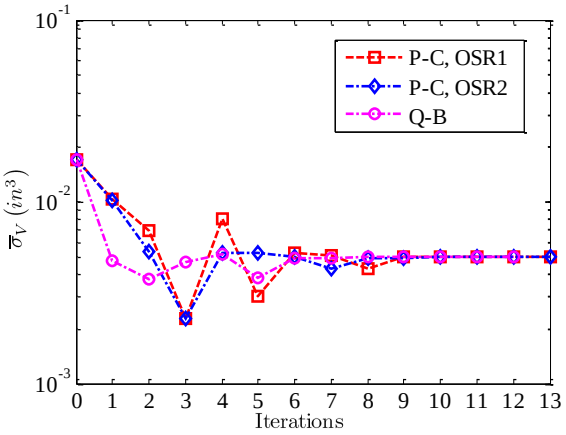

(b) Average standard deviation of beam volume, $\bar{\sigma}_V$

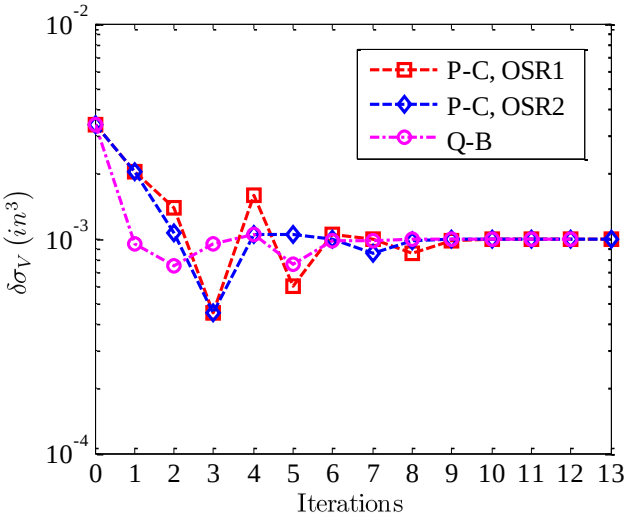

(c) Difference of standard deviation of beam volume, $\delta\sigma_V$

Figure 5.7. The convergence history of average mean, average standard deviation, and the standard deviation difference of the beam volume for the optimization process with stochastic expansions

5.3. SUMMARY OF THE RESULTS

In this section, a computationally efficient and accurate approach for robust optimization under mixed (aleatory and epistemic) uncertainties using stochastic expansions that are based on NIPC method is introduced. This approach utilizes

stochastic response surfaces obtained with NIPC methods to represent the objective function and the constraints in the optimization formulation. The objective function includes a weighted sum of the stochastic measures, which are minimized simultaneously to ensure the robustness of the final design both to inherent and epistemic uncertainties. When mixed uncertainties were propagated through a simulation code, the output response is in the form of a family of distributions described by the associated statistics (e.g., mean and the standard deviation) due to the epistemic uncertainties. In the objective function, the average of the standard deviation of the response was used as the robustness measure to aleatory uncertainties, while the difference between the maximum and the minimum value of the standard deviation is used as the robustness measure to epistemic uncertainties. In this study, a combined stochastic expansion approach was utilized to obtain the response surfaces as a function of uncertain design variables, uncertain parameters, and deterministic design variables.

The optimization approach was demonstrated on two model problems: (1) the robust design optimization of a slider-crank mechanism and (2) robust design optimization of a beam. Both problems included aleatory and epistemic uncertainties associated with design variables and problem parameters, which required the consideration of robust optimization under mixed uncertainties. The stochastic expansions were created with two different NIPC methods, Point-Collocation and Quadrature-Based approach. The Point-Collocation approach was implemented with the OSR of 1 and 2 to study the effect of this parameter on the accuracy and efficiency of the optimization process. The optimization results were compared to another robust optimization approach that utilized double-loop Monte Carlo sampling for the propagation of mixed uncertainties. The final designs obtained with two different optimization approaches agreed well in both model problems, however the number of function evaluations required for the stochastic expansion based approach

was much less than the number of function evaluations required in the Monte-Carlo based approach. This demonstrated the potential and the computational efficiency of the application of stochastic expansions to robust optimization problems with mixed uncertainties, especially to optimization problems which require the evaluation of computationally expensive high-fidelity deterministic simulations for improved accuracy.

For each model problem, the convergence of the robustness measures (statistics) used in the objective function with respect to the polynomial expansion order was studied for different NIPC methods. For the model problems considered in this section, a second order expansion was sufficient for convergence. The convergence study also indicated that the Quadrature-Based NIPC was the most accurate approach at a fixed expansion order. The accuracy of Point-Collocation NIPC with an OSR of 2 was also in desired level but the number of response function evaluations was less compared to the tensor product quadrature approach, especially for the second model problem with relatively large number of uncertainty sources. Since the number of response function evaluations for the tensor product quadrature grows significantly with the number of uncertain variables, an alternative approach to reduce the computational expense would be to implement sparse grid or cubature techniques in this approach. It has also been observed that the accuracy of the stochastic response surfaces used in robust optimization approach may reduce the number of iterations to converge to the optimum, which may influence the computational efficiency of overall stochastic optimization process. All these findings also suggest the importance of conducting convergence studies at selected design points prior to the optimization process to determine the most appropriate NIPC method and the expansion order in terms of efficiency and accuracy for robust optimization under mixed uncertainties with stochastic expansions.

6. ROBUST OPTIMIZATION FOR AERODYNAMIC DESIGN

The objective of this section is to introduce a computationally efficient approach for robust aerodynamic optimization under aleatory (inherent) and epistemic (model-form) uncertainties using stochastic expansions that are based on Point-Collocation NIPC method. The deterministic computational fluid dynamics (CFD) simulation and airfoil shape model used in the optimization studies are described in Section 6.1. Then, the robust aerodynamic optimization formulations are given in Section 6.2. The utilization of stochastic expansions in robust optimization is described in Section 6.3. The optimization results are presented in Section 6.4 and the sunmmary of results are given in Section 6.5.

6.1. CFD AND AIRFOIL SHAPE MODEL

In this section, the elements of the CFD model are described including the governing equations, numerical solution of the governing fluid flow equations (flow solver) along with the airfoil shape model and meshing of the solution domain used in our optimization studies.

6.1.1. Governing Equations. For all the optimization studies considered in this study, the flow is assumed to be steady, two-dimensional, compressible, and turbulent. The steady Reynolds-Averaged Navier-Stokes (RANS) equations are taken as the governing fluid flow equations. The fluid medium is air, assumed to be an ideal gas, with the laminar dynamic viscosity (μ) described by Sutherland's formula (see, e.g., Reference [72]). For modeling the turbulent kinematic eddy viscosity (ν_t), the turbulence model by Spalart and Allmaras [73] is used. The Spalart-Allmaras model, designed specifically for aerodynamic wall-bounded flows, is a one-equation model that solves a single conservation partial differential equation for the turbulent

viscosity. This conservation equation contains convective and diffusive transport terms, as well as expressions for the production and dissipation of ν_t. The Spalart-Allmaras model is economical and accurate for attached wall-bounded flows, and flows with mild separation and recirculation. However, the model may not be accurate for massively separated flows, free shear flows, and decaying turbulence. As described later, the turbulent viscosity is multiplied by a factor k to introduce the epistemic uncertainty in our robust optimization under mixed uncertainties problem. This is implemented in the solution through a user defined function (UDF) which is dynamically loaded with the flow solver (described below) for each CFD simulation. The whole procedure is executed automatically through scripts. The program listing for CFD simulation journal file setup is given in Appendix F.

6.1.2. Flow Solver. The flow solver is of implicit density-based formulation and the fluxes are calculated by an upwind-biased second-order spatially accurate Roe flux scheme. Asymptotic convergence to a steady state solution is obtained for each case. Automatic solution steering is employed to gradually ramp up the Courant number and accelerate convergence. Full multigrid initialization is used to get a good starting point. Numerical fluid flow simulations are performed using the computer code FLUENT [74].

The iterative convergence of each solution is examined by monitoring the overall residual, which is the sum (over all the cells in the computational domain) of the L^2 norm of all the governing equations solved in each cell. In addition to this, the lift and drag forces are monitored for convergence. The solution convergence criterion for the CFD runs is the one that occurs first of the following: a maximum residual of 10^{-6}, or a maximum number of iterations of 1000.

6.1.3. Airfoil Geometry. In this work, the NACA airfoil shapes are used. In particular, the NACA four-digit airfoil parameterization method are used, where the airfoil shape is defined by three parameters: c (the maximum ordinate of the

mean camberline as a fraction of chord), l_c (the chordwise position of the maximum ordinate as a fraction of the chord) and t (the thickness-to-chord ratio). The airfoils are denoted by NACA $mpxx$, where xx represents $(100 \times t)$, m is equal to $(100 \times c)$, and p is $(10 \times l_c)$. The shapes are constructed using two polynomials, one for the thickness distribution and the other for the mean camber line. The full details of the NACA four-digit parameterization are given in Abbott and Doenhoff [75]. A typical NACA 4-digit airfoil section is shown in Figure 6.1. The free-stream flow is at Mach number M_∞ and at an angle of attack α_A relative to the chord axis.

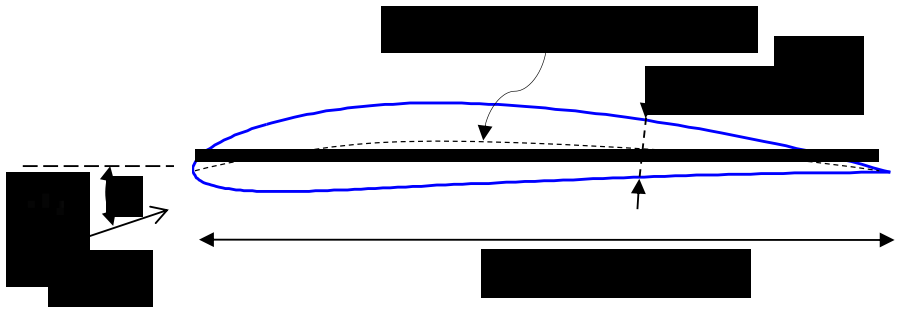

Figure 6.1. A typical NACA 4-digit airfoil section is shown

6.1.4. Grid Generation. The solution domain boundaries are placed at 25 chord lengths in front of the airfoil, 50 chord lengths behind it, and 25 chord lengths above and below it. The computational meshes are of structured curvilinear body-fitted C-topology with elements clustering around the airfoil and growing in size with distance from the airfoil surface. The non-dimensional normal distance (y^+) from the wall to the first grid point is roughly one. The free-stream Mach number, angle of attack, static pressure, and the turbulent viscosity ratio are prescribed at the farfield boundary. An example computational grid is shown in Figure 6.2. The computer code ICEM CFD [76] is used for the mesh generation.

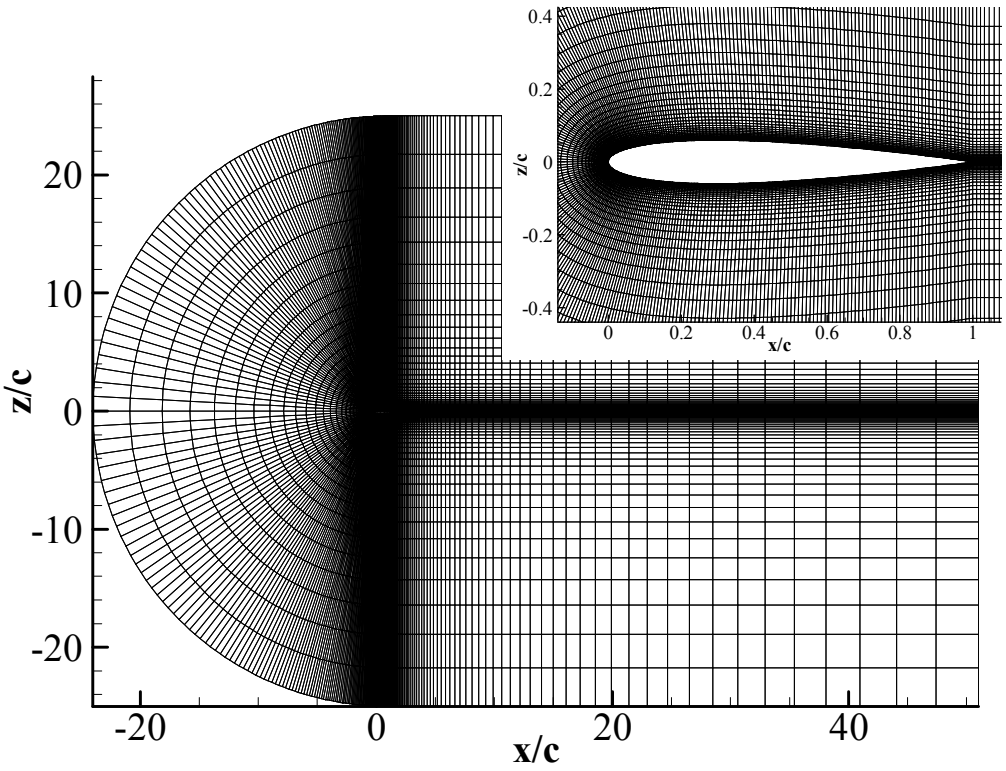

Figure 6.2. An example computational grid for the NACA0012 airfoil

6.2. ROBUST AIRFOIL OPTIMIZATION FORMULATION

In this section, robust aerodynamic optimization with stochastic expansions will be demonstrated with two cases: (1) optimization under pure aleatory uncertainty and (2) optimization under mixed (aleatory and epistemic) uncertainty. Below the optimization formulation is given for each case.

6.2.1. Optimization under Pure Aleatory Uncertainty. Based on the robustness measures discussed in Section 4, robust airfoil optimization under pure aleatory uncertainty is formulated as:

$$
\begin{aligned}
min \quad & \mu_{C_d} + \sigma_{C_d} \\
subject \quad to \quad & \mu_{C_L} \geq C_L^* \\
& 0.0 \leq c \leq 0.05 \\
& 0.3 \leq l_c \leq 0.7 \\
& 0.08 \leq t \leq 0.14
\end{aligned}
\tag{55}
$$

where $C_d = C_d(\vec{X}_d, \vec{P}_a)$ is the profile drag coefficient, which is a function of the deterministic design variable vector $\vec{X}_d$ and aleatory input uncertainty vector $\vec{P}_a$. Similarly, the lift coefficient is $C_L = C_L(\vec{X}_d, \vec{P}_a)$. In current optimization study, the deterministic design variable vector $\vec{X}_d = \{c, l_c, t\}$ is used to control airfoil shape. Note that this vector can contain the control points as the design variables when the airfoil shape is parametrized with different spline fitting techniques. The free-stream Mach number (M_∞) is treated as aleatory (inherent) input uncertainty (i.e., $\vec{P}_a = \{M_\infty\}$) and represented as a uniform random variable with bounds ($0.7 \leq M_\infty \leq 0.8$). As can be seen from the Mach number range, the transonic flow regime is considered, where the drag coefficient is very sensitive to the changes in the Mach number due to the lambda shock originating on the top surface of the airfoil. This minimization is subject to satisfying a desired profile lift coefficient (C_L^*) value or higher by the mean value of the lift coefficient adjusted by changing the angle of attack for a given design variable and uncertain variable vector value. The optimization also include geometric constraints for the profile shape, which bound the thickness, maximum camber, and the maximum camber location (note that l_c is taken as zero when $c = 0.0$). The drag coefficient and other aerodynamics characteristics of the airfoil for a given design variable vector and aleatory uncertain variable value are obtained from the CFD simulations that solve steady, two-dimensional, Reynolds-Averaged Navier-Stokes equations with Spalart-Allmaras turbulence model.

6.2.2. Optimization under Mixed Uncertainty. Robust airfoil optimization under mixed (aleatory and epistemic) uncertainties is formulated as:

$$min \quad w_1\overline{\mu}_{C_d} + w_2\overline{\sigma}_{C_d} + w_3\delta\sigma_{C_d} \tag{56}$$

$$\begin{aligned} subject \quad to \quad & \mu_{C_L}^{min} \geq C_L^* \\ & 0.0 \leq c \leq 0.05 \\ & 0.3 \leq l_c \leq 0.7 \\ & 0.08 \leq t \leq 0.14 \end{aligned}$$

where the profile drag coefficient $C_d(\vec{X}_d, \vec{P}_a, \vec{P}_e)$ is now a function of the deterministic design variable vector $\vec{X}_d$, aleatory input uncertainty vector $\vec{P}_a$, and the epistemic input uncertainty vector $\vec{P}_e$. Similarly, the lift coefficient, $C_L(\vec{X}_d, \vec{P}_a, \vec{P}_e)$, is now a function of the same variables. In the multi-objective function w_1, w_2, w_3 are the weights whose sum is equal to 1.0. In this study, equal weights are used, however one can choose different weights depending on the emphasis on each term.

In this optimization problem, airfoil shape parameters are again considered as deterministic design variable vector ($\vec{X}_d = \{c, l_c, t\}$ and the free-stream Mach number as the aleatory (inherent) input uncertainty ($\vec{P}_a = \{M_\infty\}$) with bounds ($0.7 \leq M_\infty \leq 0.8$). The kinematic eddy viscosity (ν_t) obtained from the Spalart-Allmaras turbulence model used in RANS simulations is modeled as an epistemic (model-form) input uncertainty (i.e., $\vec{P}_e = \{\nu_t\}$) through the introduction of a factor k as shown below:

$$\nu_t = k\nu_{t_{SA}} \tag{57}$$

where $\nu_{t_{SA}}$ is the turbulent viscosity originally obtained with the Spalart-Allmaras model. The range of this factor k is chosen between 0.5 and 2.0 to mimic the model-

form uncertainty due to the use of different turbulence models in RANS calculations. Figure 6.3 shows the pressure distributions of NACA2412 airfoil at $M_\infty = 0.75$,

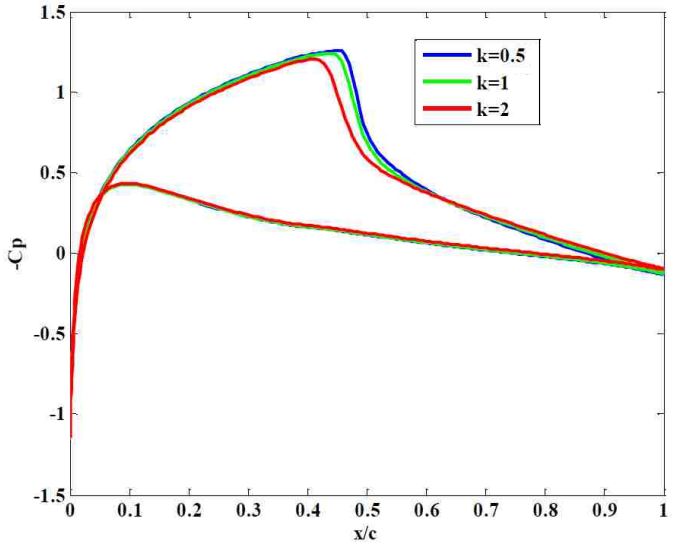

Figure 6.3. The pressure distributions of NACA2412 at M_∞=0.75, $\alpha_A = 1°$

$\alpha_A = 1°$ with different k values. From this figure, it can be seen that the " k " factor thus the turbulence model has considerable effect on the pressure distribution, especially on the shock location. This optimization is again subject to satisfying a desired profile lift coefficient (C_L^*) value or higher by the minimum of the mean value of the lift coefficient adjusted by changing the angle of attack for a given design variable and uncertain variable vector value. The optimization also includes geometric constraints for the profile shape, which bound the thickness, maximum camber, and the maximum camber location.

6.3. STOCHASTIC RESPONSE FOR ROBUST OPTIMIZATION

In this robust optimization methodology, a stochastic response surface obtained with Point-Collocation NIPC method is adopted for the propagation of aleatory and

epistemic uncertainties due to its computational efficiency and accuracy as shown in the previous studies [77, 30]. While constructing the stochastic expansions, a combined expansion approach will be utilized, which will expand the polynomials as a function of both uncertain variables (aleatory and epistemic) and deterministic design variables. The description of the Point-Collocation NIPC and combined expansion approach were given in Section 2. The utilization of the stochastic response surface in robust optimization was mainly described in this section.

Since the angle of attack has to be adjusted to satisfy the lift coefficient constraint in both optimization problems, three separate stochastic response surfaces are created with the Point-Collocation NIPC at three angles of attack ($\alpha_{A0} = 0.0°$, $\alpha_{A1} = 1.0°$, and $\alpha_{A2} = 2.0°$). Then Lagrange interpolation is applied to create a composite response surface using these three response surfaces, which is continuous and quadratic in α_A between $\alpha_A = 0.0°$ and $\alpha_A = 2.0°$ for all design variables, aleatory uncertain variables (i.e., M_∞), and the epistemic uncertain variables (i.e., k). This composite response surface $\hat{R}$ (i.e., C_d or C_L), which is now a function of α_A, $P_a(\vec{\xi}_{pa})$, $P_e(\vec{\xi}_{se})$, $X_d(\vec{\xi}_d)$ can be written as:

$$\hat{R}(\alpha_A, P_a(\vec{\xi}_{pa}), P_e(\vec{\xi}_{pe}), X_d(\vec{\xi}_d)) \cong \sum_{k=0}^{n_{\alpha_A}} R(P_a(\vec{\xi}_{pa}), P_e(\vec{\xi}_{pe}), X_d(\vec{\xi}_d))_{\alpha_{Ak}} L_{n_{\alpha_A},k}(\alpha_A) \quad (58)$$

Based on the equation above, Equations (45) and (46) can be slightly modified to calculate the mean and variance from $\hat{R}$:

$$\mu_{\hat{R}} = \mu_{\hat{R}}(\alpha_A, \vec{\xi}_{pe}, \vec{\xi}_d) = \sum_{k=0}^{n_{\alpha_A}} \sum_{j=0}^{P} \alpha_j \left(\alpha_{Ak}\right) L_{n_{\alpha_A},k}(\alpha_A) \left\langle \Psi_j(\vec{\xi}_{pa}, \vec{\xi}_{pe}, \vec{\xi}_d) \right\rangle_{\vec{\xi}_{pa}} \quad (59)$$

$$\sigma^2_{\hat{R}} = \left\{ \sum_{k=0}^{n_{\alpha_A}} \sum_{l=0}^{n_{\alpha_A}} \sum_{i=0}^{P} \sum_{j=0}^{P} L_{n_{\alpha_A},k}\left(\alpha_A\right) L_{n_{\alpha,l}}\left(\alpha_A\right) \alpha_i\left(\alpha_{Ak}\right) \alpha_j\left(\alpha_{Al}\right) \left\langle \Psi_i \Psi_j \right\rangle_{\vec{\xi}_{pa}} \right\} - \mu^2_{\hat{R}} \quad (60)$$

where α_A is the angle of attack, $n_{\alpha_A} = 2$ is the degree of interpolation in α_A, and $L_{n_{\alpha,k}}$ is the Lagrange polynomial at α_{Ak} given by

$$L_{n_{\alpha_A,k}}(\alpha_A) = \prod_{i=0, i\neq k}^{n_{\alpha_A}} \left(\frac{\alpha_A - \alpha_{Ai}}{\alpha_{Ak} - \alpha_{Ai}} \right). \tag{61}$$

Note that the introduction of α_A to the problem with the above approach indicate that it is in fact considered as a deterministic design variable within $\hat{R}$. An alternative approach to involve α_A in the response surface would be to include it among the other deterministic design variables during the original construction.

Above formulations and previous discussion in Section 4.1 clearly show that the mean and the standard deviation of response variables at a design point and angle of attack are characterized by two bounds due to epistemic uncertainties with specified interval bounds $[\vec{P}_e^L, \vec{P}_e^U]$. In other words, the mean and standard deviation of response R (i.e., C_d, or C_L) at a design point and angle of attack will also be bounded by its maximum and minimum values. Once we create the composite stochastic response surface (Equation (58)), we can use Equations (59) and (60) to calculate the mean and the standard deviation and use any standard optimization technique to determine $\mu_{c_d}^{max}$, $\mu_{c_d}^{min}$, $\sigma_{c_d}^{max}$ and $\sigma_{c_d}^{min}$ at a given design point and angle of attack. Then, these values are used in robust optimization formulations given in Section 6.2.

With the combined expansion approach, it will be straightforward to calculate the total number of CFD simulations (N_{CFD}) required to create the composite response surface $\hat{R}$ that will be used in the entire optimization process:

$$N_{CFD} = OSR \times N_t \times (n_{\alpha_A} + 1) \tag{62}$$

where, N_t is calculated from Equation (3), and n_{α_A} is the degree of interpolation in α_A used in the creation of composite response surface. It is important to note that

N_{CFD} will be the computational cost of the described optimization approach since once the response surface is created, the numerical evaluations at each optimization step will be computationally cheap due to the polynomial nature of the stochastic surrogate. It should be noted that for a stochastic optimization problem with few number of design variables (i.e., $N_d \leq 3$), the combined expansion approach described above is going to be computationally very efficient since a single response surface (a surrogate) is created which is a function of the design, aleatory and epistemic uncertain variables. The optimization can be performed using this single response surface. On the other hand, in optimization problems with large number of design variables, one can choose an alternative approach which is based on the expansion of polynomial chaos surface only on the uncertain (aleatory and epistemic) variables. With this approach a separate stochastic response surface should be created at each design point, which will increase the computational cost, however the accuracy of the response surface approximation will increase due to the reduction in the number of expansion variables.

6.4. RESULTS AND DISCUSSION

The robust airfoil optimization approach with NIPC stochastic response surface has been demonstrated on two cases: (1) optimization under pure aleatory input uncertainty and (2) optimization under mixed (aleatory and epistemic) uncertainty. The results for each case are presented below.

6.4.1. Optimization Results for the Pure Aleatory Uncertainty Case. As described with the optimization formulation in Section 6.2.1, the free stream Mach number is the only uncertain variable for this case and modeled with a uniform probability distribution between $M_\infty = 0.7$ and $M_\infty = 0.8$. The objective (Equation (55)) is to reduce the mean and the standard deviation of the drag coefficient simultaneously to obtain an airfoil shape with minimum drag that is least

sensitive to the change in Mach number in the specified range. Besides the side (geometric) constraints on the design variables, the minimization is performed such that the mean lift coefficient obtained with the optimum design is greater than or equal to 0.5. The stochastic response surfaces for the drag and the lift coefficients were created with Point-Collocation NIPC method using a quadratic polynomial expansion with OSR of 2 for 4 variables (3 deterministic design variables and 1 uncertain variable). The total number of CFD evaluations required for this case was $N_{CFD} = 90$ as can be calculated using Equation (62) along with Equation (3). It should be noted that this number is considerably low compared to the cost of alternative robust optimization formulations, which utilize Monte Carlo simulations for the calculation of the statistics. After the stochastic response surfaces for the drag and lift coefficients are created, the robust optimization is performed using the approach described in the previous section. The robust optimization was performed starting from two different initial airfoil geometries (NACA2412 and NACA0012). As can be seen from Table 6.1, both optimization runs converged to the same optimum airfoil shape with $t = 0.08$, $c = 0.0195$, and $l_c = 0.7$ (Figure 6.4). The optimum airfoil has the minimum thickness allowable and the camber is located as aft as possible to reduce the drag while satisfying the required C_L, which are typical characteristics of airfoils designed to operate at transonic speeds (e.g., supercritical airfoils). The camber value is the optimum to produce the required lift at an optimum angle of attack.

Table 6.1. Optimization results for the pure aleatory uncertainty case

	Initial Airfoil			Optimized airfoil		
	c	l_c	t	c	l_c	t
NACA2412	0.020	0.40	0.120	0.0195	0.70	0.080
NACA0012	0.0	0.0	0.120	0.0195	0.70	0.080

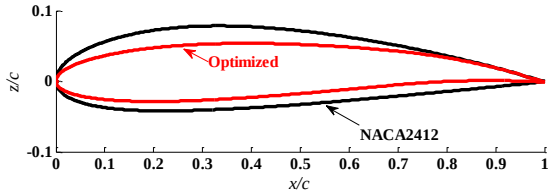

Figure 6.4. NACA2412 and the optimized airfoil shape for the pure aleatory uncertainty case

The pressure distributions of NACA2412 and optimum airfoil at M_∞=0.75 are shown in Figure 6.5 from which can be seen, at $M_\infty = 0.75$, NACA2412 airfoil has a shock wave on the top surface, whereas no shock wave exits on the optimized airfoil, due to the increase in minimum suction pressure (i.e., the decrease of the maximum value of $-C_p$) and the reduction in the maximum velocity value on the top surface giving a more flat pressure distribution. The aft camber compensates the lift that is lost in the suction region by loading the airfoil in the aft region. The optimization history of the mean and the standard deviation of the drag coefficient is given in Figure 6.6, which shows that both quantities are minimized simultaneously regardless of the initial airfoil chosen, which confirms the robust optimization approach used.

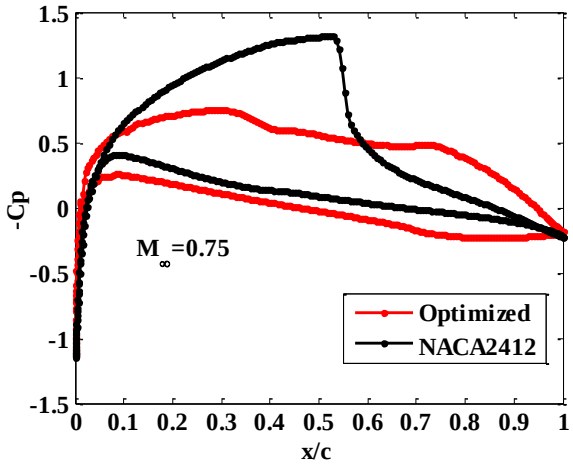

Figure 6.5. The pressure distributions of NACA2412 and optimum airfoil at M_∞=0.75 for the pure aleatory uncertainty case

This result is further verified by Figure 6.7, which gives drag vs Mach number over the uncertain Mach number range for the NACA2412 and optimized airfoil at a lift coefficient value of 0.5. As can be seen from this plot, the drag-rise of NACA2412 is significant, whereas the optimum airfoil maintains a low drag coefficient value over the uncertain Mach number range with no significant variation. The drag coefficient and L/D values for both airfoils are reported in Table 6.2, which quantifies the better aerodynamic performance of the optimum airfoil compared to NACA2412.

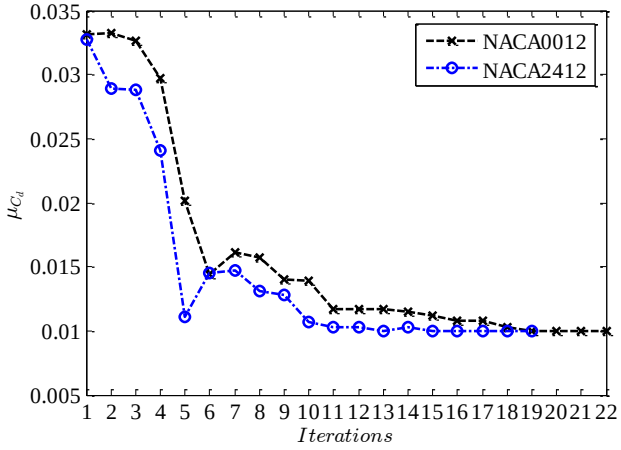

(a) Mean drag coefficient, μ_{C_d}

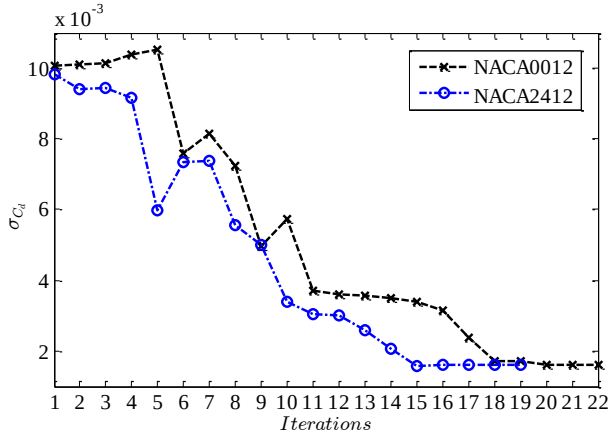

(b) Standard deviation, σ_{C_d}

Figure 6.6. The optimization history of the mean and the standard deviation of the drag coefficient for the pure aleatory uncertainty case started from two initial airfoil shapes (NACA2412 and NACA0012)

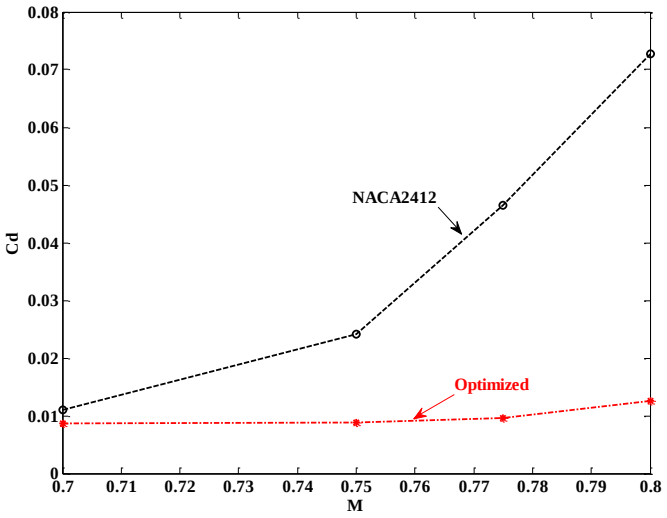

Figure 6.7. The drag coefficients of NACA2412 and optimized airfoil at C_L^*=0.5

The drag characteristics of both airfoils can also be explained by examining the Mach number contours given in Figure 6.8. As the Mach number increases, the shock wave on the top surface of NACA2412 airfoil gets stronger and eventually induces the boundary layer separation at a free-stream Mach number of 0.8 increasing the drag significantly. On the other hand, the delayed shock formation on the top surface of the optimum airfoil shape prevents a significant drag rise over the uncertain Mach number range considered. The pressure distributions of NACA2412 and optimum airfoil at M_∞= 0.7, 0.75, 0.8 are shown in Figure 6.9. It can be seen that at M_∞= 0.7, 0.75, NACA2412 airfoil has a shock wave on the top surface, whereas no shock

Table 6.2. Drag coefficient and L/D values for NACA2412 and optimum airfoil at various Mach numbers for pure aleatory uncertainty case

	Cd		L/D	
M	NACA2412	Optimized	NACA2412	Optimized
0.7	0.0110	0.0086	45.45	58.14
0.75	0.0242	0.0088	20.66	56.82
0.8	0.0727	0.0126	6.88	39.68

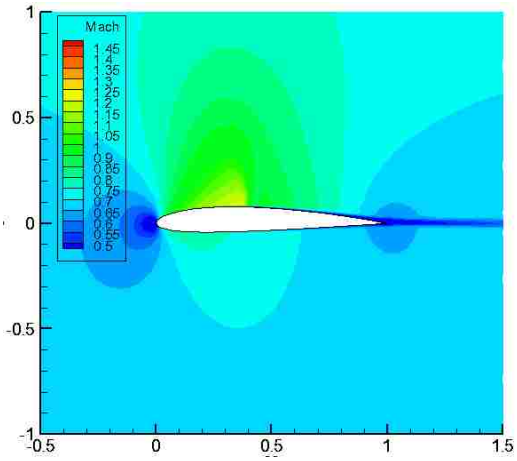

(a) $M_\infty = 0.7$, NACA2412

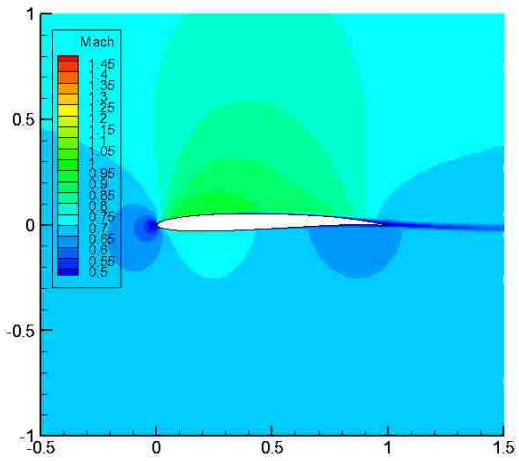

(b) $M_\infty = 0.7$, Optimum airfoil

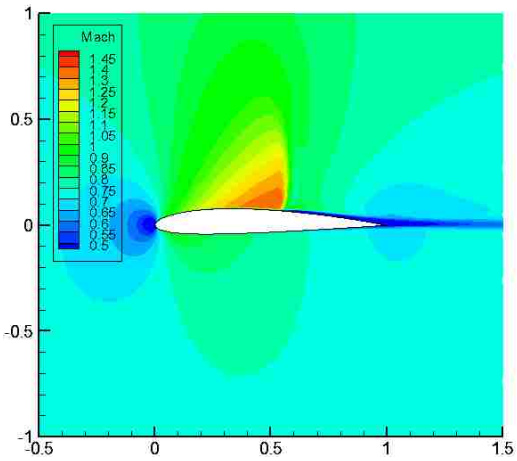

(c) $M_\infty = 0.75$, NACA2412

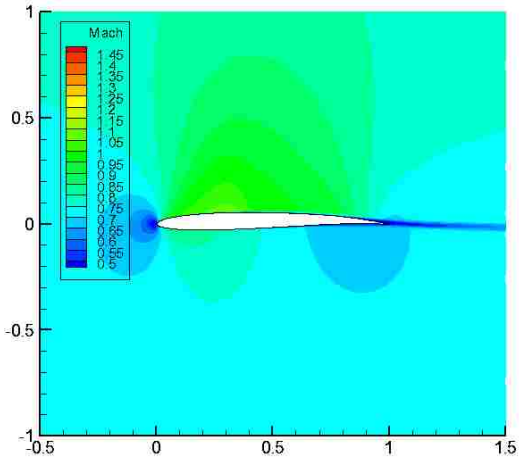

(d) $M_\infty = 0.75$, Optimum airfoil

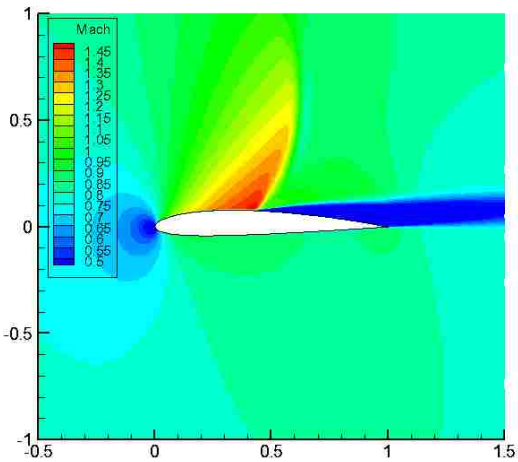

(e) $M_\infty = 0.8$, NACA2412

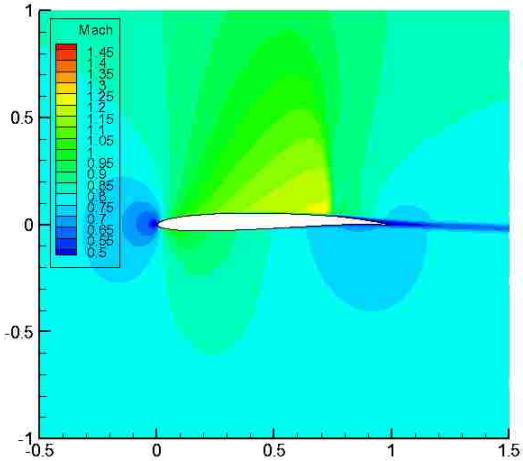

(f) $M_\infty = 0.8$, Optimum airfoil

Figure 6.8. Mach number contours for the NACA2412 and optimum airfoil shape for the pure aleatory uncertainty case

wave exits on the optimized airfoil. At $M_\infty = 0.8$, the shock wave on the optimized airfoil is much weaker compared to the shock on the NACA2412 airfoil.

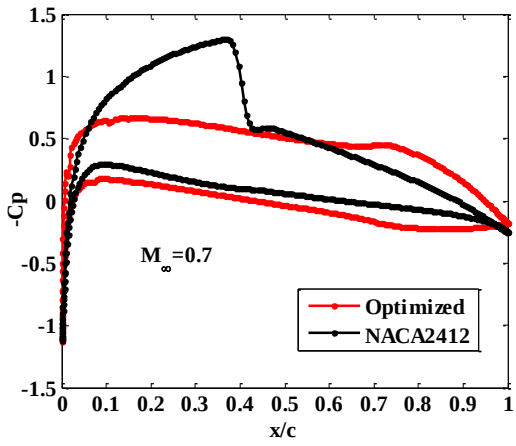

(a) $M_\infty = 0.7$

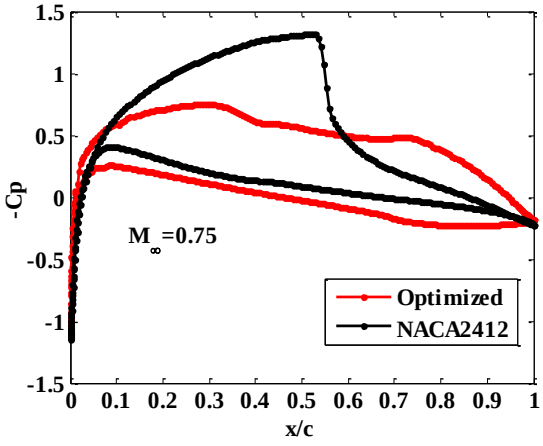

(b) $M_\infty = 0.75$

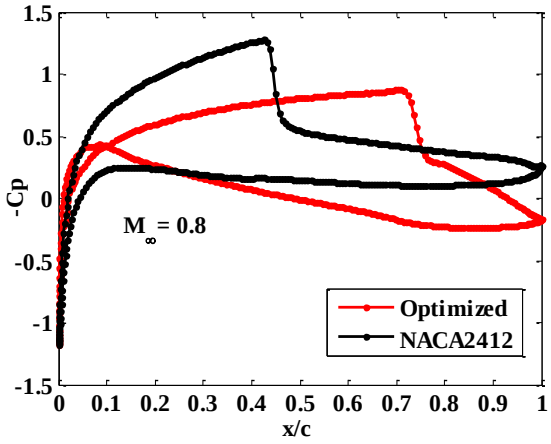

(c) $M_\infty = 0.8$

Figure 6.9. The pressure distributions of NACA2412 and optimum airfoil at M_∞=0.7, 0.75, 0.8 for the pure aleatory uncertainty case

6.4.2. Optimization Results for the Mixed Uncertainty Case. As described with the optimization formulation in Section 6.2.2, the free stream Mach number is taken as the aleatory uncertain variable for this case and modeled with a uniform probability distribution between $M_\infty = 0.7$ and $M_\infty = 0.8$, the same

as the pure aleatory case. The k factor which is multiplied with the turbulent eddy-viscosity coefficient of the Spalart-Allmaras turbulence model is the epistemic uncertain variable defined with the interval $[0.5, 2.0]$. The objective of the robust optimization under mixed uncertainties (Equation (56)) is to reduce the average of the mean ($\bar{\mu}_{C_d}$), the average of the standard deviation ($\bar{\sigma}_{C_d}$) and the standard deviation difference of the drag coefficient ($\delta\sigma_{C_d}$) simultaneously to obtain an airfoil shape with minimum drag that is least sensitive to the change in Mach number and the k factor (i.e., the turbulence model) in the range specified for each variable. Besides the side (geometric) constraints on the design variables, the minimization is performed such that the minimum of the mean lift coefficient obtained with the optimum design is greater than or equal to 0.5. The stochastic response surfaces for the drag and the lift coefficients were again created with Point-Collocation NIPC method using a quadratic polynomial expansion with an OSR of 2 for 5 variables (3 deterministic design variables, 1 aleatory uncertain variable, and 1 epistemic uncertain variable). The total number of CFD evaluations required for this case was $N_{CFD} = 126$ as can be calculated using Equation (62) along with Equation (3). Considering the fact that the propagation of an aleatory and epistemic uncertain variable are considered simultaneously, this number signifies the computational efficiency of the proposed optimization approach. After the stochastic response surfaces for the drag and lift coefficients are created, the robust optimization is performed using the approach described in the previous section.

As the result of the optimization under mixed uncertainties, the same optimum airfoil shape of the pure aleatory uncertainty case is obtained (Table 6.3). This optimum has been verified by starting the optimization from two different initial profile shapes (NACA2412 and NACA0012). This result is somehow expected since the flow field around the optimum airfoil shape does not include complex flow features such the strong shocks and shock induced separation over the range of Mach numbers

Table 6.3. Optimization results for the mixed uncertainty case

	Initial Airfoil			Optimized airfoil		
	c	l_c	t	c	l_c	t
NACA2412	0.020	0.400	0.120	0.019	0.700	0.080
NACA0012	0	0	0.120	0.019	0.700	0.080

considered to make the effect of the turbulence model (i.e., the k factor) significant on different aerodynamic quantities including the drag coefficient. Figure 6.10 gives the convergence history of average mean, average standard deviation, and the standard deviation difference of the drag coefficient for the mixed uncertainty case started from two initial airfoil shapes (NACA2412 and NACA0012). Regardless of the initial airfoil geometry used, all three quantities are reduced compared to their starting values and converge to the same final values. On the other hand, the reduction in the average mean and the average standard deviation of the drag coefficient is larger compared to the reduction in the standard deviation difference, which has already a small value for the initial airfoil shapes considered. This observation may imply that for this optimization problem, the contribution of the epistemic uncertainty (i.e., k factor) is not as much as the contribution of the aleatory uncertainty (Mach number) to the total uncertainty in the drag coefficient. Since the optimization is performed at a relatively low lift coefficient value ($C_L^* = 0.5$), one may also expect to see more contribution of the epistemic uncertainty at higher lift coefficients. Figure 6.11, which shows a carpet plot of the drag coefficient over the range of M_∞ and k factor considered also verify that the aerodynamic characteristics of the optimum airfoil is better compared to the characteristics of NACA2412 (one of the airfoils used to initiate the optimization) in the case of mixed uncertainties and no significant drag-rise (i.e., variation) is observed with the optimum geometry. This plot also shows that the uncertainty in the Mach number is the main contributor to the overall uncertainty

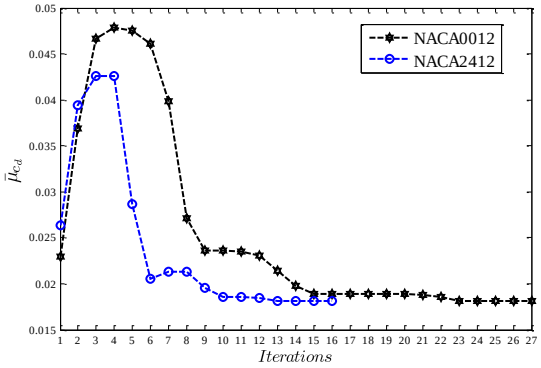

(a) Average mean of the drag coefficient, $\bar{\mu}_{C_d}$

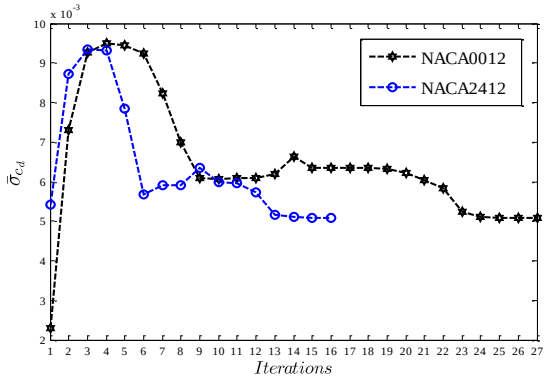

(b) Average standard deviation of the drag coefficient, $\bar{\sigma}_{C_d}$

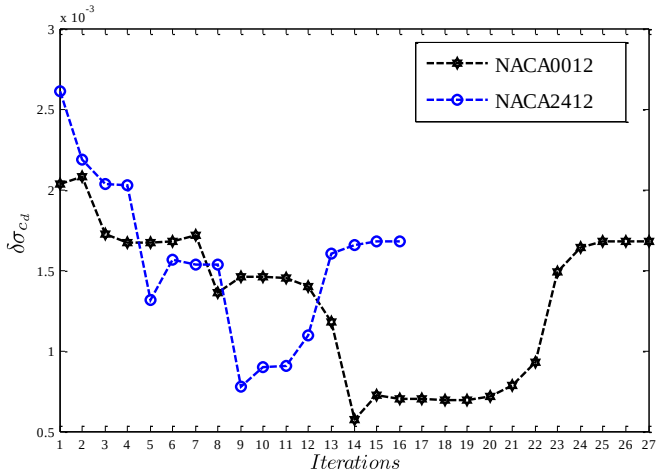

(c) Standard deviation difference of the drag coefficient, $\delta\sigma_{C_d}$

Figure 6.10. The optimization history of average mean, average standard deviation, and the standard deviation difference of the drag coefficient for the mixed uncertainty case started from two initial airfoil shapes (NACA2412 and NACA0012)

and variation in the drag coefficient, which can be quantified by the results tabulated in Table 6.4.

6.5. SUMMARY OF THE RESULTS

The objective of this section was to introduce an efficient approach for robust aerodynamic optimization under aleatory (inherent) and epistemic (model-form)

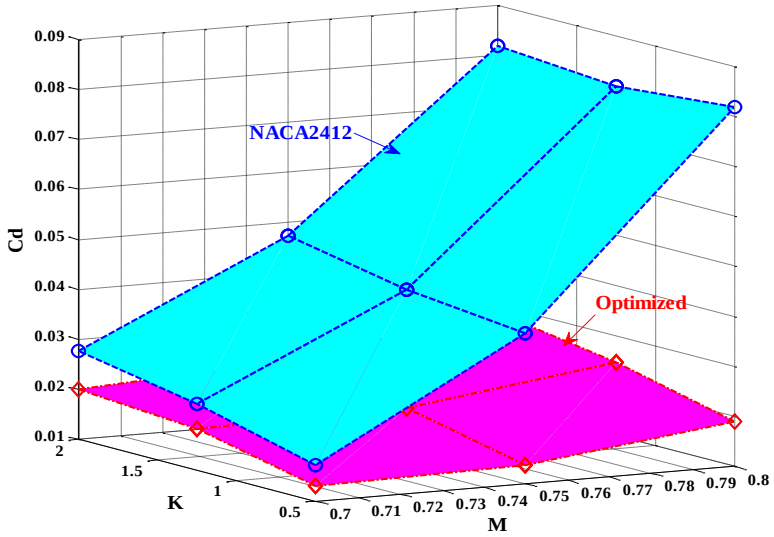

Figure 6.11. Drag coefficient values of the optimized airfoil and NACA2412 (for M_∞=[0.7,0.75 ,0.8], and k=[0.5,1.25,2.0] at C_L^*=0.5)

Table 6.4. Drag coefficient and L/D values for NACA2412 and optimum airfoil at various Mach numbers and k values for the mixed uncertainty case

		Cd		L/D	
K	M_∞	NACA2412	Optimized	NACA2412	Optimized
$K = 0.5$	0.7	0.0171	0.0131	29.22	38.17
	0.75	0.0401	0.0136	12.48	36.76
	0.8	0.0819	0.0189	6.11	26.48
$K = 1.25$	0.7	0.0233	0.0184	21.46	27.21
	0.75	0.0427	0.0190	11.71	26.37
	0.8	0.0798	0.0248	6.26	20.16
$K = 2.0$	0.7	0.0277	0.0201	18.07	24.88
	0.75	0.0474	0.0224	10.55	22.32
	0.8	0.0817	0.0286	6.12	17.51

uncertainties using stochastic expansions based on Point-Collocation Non-Intrusive Polynomial Chaos method. The stochastic surfaces were used as surrogates in the optimization process. To create the surrogates, a combined NIPC expansion approach was utilized, which is a function of both the design and the uncertain variables. In this

study, two stochastic optimization formulations were given: (1) optimization under pure aleatory uncertainty and (2) optimization under mixed (aleatory and epistemic) uncertainty. The formulations were demonstrated for the aerodynamic optimization of NACA 4-digits airfoils at transonic flow. The deterministic CFD simulations were performed with the Fluent Code to solve steady, 2-D, compressible, turbulent RANS equations.

For the pure aleatory uncertainty case, the objective was to reduce the mean and the standard deviation of the drag coefficient simultaneously to obtain an airfoil shape with minimum drag that is least sensitive to the change in Mach number in the specified range ($0.7 \leq M_\infty \leq 0.8$). Besides the side (geometric) constraints on the design variables, the minimization is performed such that the mean lift coefficient obtained with the optimum design is greater than or equal to 0.5. For the mixed uncertainty case, in addition to the aleatory uncertainty in the Mach number, a k factor which is multiplied with the turbulent eddy-viscosity coefficient of the Spalart-Allmaras turbulence model is introduced to the problem as the epistemic uncertain variable defined with the interval $[0.5, 2.0]$. The objective of the robust optimization under mixed uncertainties was to reduce the average of the mean, the average of the standard deviation, and the standard deviation difference of the drag coefficient simultaneously to obtain an airfoil shape with minimum drag that is least sensitive to the change in Mach number and the k factor (i.e., the turbulence model) in the range specified for each variable. Besides the side (geometric) constraints on the design variables, the minimization is performed such that the minimum of the mean lift coefficient obtained with the optimum design is greater than or equal to 0.5.

The results of both optimization cases confirmed the effectiveness of the robust optimization approach with stochastic expansions by giving the optimum airfoil shape that has the minimum drag over the range of aleatory and epistemic uncertainties. The optimization under pure aleatory uncertainty case required 90 deterministic CFD

evaluations, whereas the optimization under mixed uncertainty case required 126 CFD evaluations to create the stochastic response surfaces, which show the computational efficiency of the proposed stochastic optimization approach.

Although the robust aerodynamic optimization approach described in this section was demonstrated on the NACA 4-digit airfoils, the methodology described is general in the sense that it can be applied to aerodynamic optimization problems that utilize more sophisticated shape parameterization techniques. Depending on the number of design variables a combined stochastic expansion approach or an alternative approach which is based on the expansion of polynomial chaos surface only on the uncertain (aleatory and epistemic) variables can be used.

7. CONCLUSIONS AND FUTURE WORK

7.1. CONCLUSIONS

The main objective of this study was to apply a computationally efficient uncertainty quantification approach, NIPC based stochastic expansions, to robust aerospace analysis and design under mixed (aleatory and epistemic) uncertainties and demonstrate this technique on model problems and robust aerodynamic optimization.

Before the implementation of the stochastic expansions to robust optimization, the uncertainty quantification approach was applied to a model problem to demonstrate that the NIPC method is computationally more efficient than traditional Monte Carlo methods for moderate number of uncertain variables and can give highly accurate estimation of various metrics used in robust design optimization under mixed uncertainties. The proposed optimization approach utilized stochastic response surface obtained with NIPC methods to approximate the objective function and the constraints in the optimization formulation. The objective function includes the stochastic measures, which are minimized simultaneously to ensure the robustness of the final design to both aleatory and epistemic uncertainties. The optimization approach was first demonstrated on two model problems with mixed uncertainties: (1) the robust design optimization of a crank beam mechanism and (2) robust design optimization of a beam. The stochastic expansions are created with two different NIPC methods, Quadrature-Based and Point-Collocation Based NIPC. The optimization results are compared to the results of another robust optimization technique that utilized double loop Monte Carlo sampling for propagation mixed uncertainties. The optimization results obtained with two different optimization approaches agreed well in both model problems, however the number of function evaluations was much less than the number of required by Monte Carlo based

approach, indicating the computational efficiency of the optimization technique introduced.

For robust aerodynamic optimization under aleatory (Mach number) and epistemic (turbulence model) uncertainties, the NIPC response surface was also used as surrogates in the optimization process. To create the surrogates, a combined Point-Collocation NIPC approach was utilized, which is a function of both the design and uncertain variables. Two stochastic optimization formulations were studied: (1) optimization under pure aleatory uncertainty and (2) optimization under mixed (aleatory and epistemic) uncertainty. The formulations were demonstrated for the drag minimization of NACA 4-digit airfoils described with three geometric design variables over the range of uncertainties at transonic flow conditions. The deterministic CFD simulations were performed to solve steady, 2-D, compressible, turbulent RANS equations. The pure aleatory uncertainty case included the Mach number as the uncertain variable. For the mixed uncertainty case, a k factor which is multiplied with the turbulent eddy-viscosity coefficient is introduced to the problem as the epistemic uncertain variable. The results of both optimization cases confirmed the effectiveness of the robust optimization approach with stochastic expansions by giving the optimum airfoil shape that has the minimum drag over the range of aleatory and epistemic uncertainties. The optimization under pure aleatory uncertainty case required 90 deterministic CFD evaluations, whereas the optimization under mixed uncertainty case required 126 CFD evaluations to create the stochastic response surfaces, which show the computational efficiency of the proposed stochastic optimization approach. The stochastic optimization methodology described in this study is general in the sense that it can be applied to aerodynamic optimization problems that utilize different shape parameterization techniques.

To further improve computational efficiency, an adaptive sampling approach was introduced to refine Point-Collocation NIPC by using an over sampling ratio

between 1 and 2 based on the convergence check of total response surface error. Two different schemes (fixed check point and updated check point) were considered for the calculation of the check points where the response surface error values were calculated for the convergence check. The proposed adaptive sampling based Point-Collocation NIPC was implemented for mixed (both aleatory and epistemic) uncertainty quantification. Second-Order Probability method was used with outer sampling for epistemic variables and inner sampling for aleatory variables (for a fixed value of epistemic uncertain variable) both using the stochastic response surface approximation to generate the CDF curves of the output. The adaptive sampling approach was demonstrated on two model problems. The results were compared to the results that utilized double-loop Monte Carlo sampling for the propagation mixed uncertainties for the validation of the methodology and demonstration of its computational efficiency.

7.2. FUTURE WORK

There may be some potential topics that can be conducted as future work in the area of uncertainty quantification and robust design for aerospace applications. First, for mixed uncertainty quantification, one can consider alternative, more sophisticated approaches such as the Dempster-Shafer evidence theory and utilize Non-Intrusive Polynomials Chaos to represent the response in those approaches for computational efficiency. Another potential study may involve the development of a methodology which will implement global sensitivity analysis based on Sobol indices that can be calculated from NIPC expansions to reduce the number of uncertain variables by ranking the contributions of each variable to the overall output response and ignoring some uncertain variables which have least contributions. Once the number of input variables is reduced, then the robust design on the reduced problem will be computationally more efficient.

For our current study, the adaptive sampling based Point-Collocation NIPC was used just for mixed uncertainty quantification. The implementation of this approach in robust aerospace design will be one of our future works.

The refinement of the UQ/design methodology introduced here for application to the robust design of multi-disciplinary aerospace systems under mixed uncertainties should be also investigated. The integration of multi-fidelity and robust optimization methodologies should be studied for efficient and accurate stochastic design of aerospace systems.

Finally, more general shape parameterization approaches for airfoils and wings should be considered in the future robust aerodynamic shape optimization studies.

APPENDIX A

MATLAB SOURCE CODE: POLYNOMIAL CHAOS EXPANSION

```
%=========================================================
% this program is to obtain the combination polynomial
% writtend by yi zhang
%  modified 03/18/2010
%=========================================================

function  po=polynomial_combine(X,Dis_Ord,index)

dimension=size(Dis_Ord,1);

index==2; %total-tensor

P_total_expand=Dis_Ord(1,2);

% calculate the # terms of polynoimal expansion

Nt=factorial(P_total_expand+dimension)/(factorial(P_total_expand)*...
    factorial(dimension));

% select basis polynomial from the fist variable save them in cell-matrix

w=1;

for i=1:dimension
    V{i}=polynomial_basis(X(i),Dis_Ord,i);
end

% obtain the combination of the polynomial basis

for p=0:Dis_Ord(1,2)

    % obtain the combination of the polynomial basis

    [M,Nt]=basic_expand_matrix_main(size(Dis_Ord,1),Dis_Ord(1,2));

    [row,column]=size(M);

    po=ones(1,Nt);

    i_Nt=1;

    for i=1:row

        for j=1:column

            po(i_Nt)=po(i_Nt)*V{j}(M(i,j)+1);

        end

        i_Nt=i_Nt+1;

    end

end
```

APPENDIX B

MATLAB SOURCE CODE: UNCERTAINTY QUANTIFICATION WITH QUADRATURE-BASED NIPC

```
%=========================================================================
% This program is used to obtain the stochastic expansion coefficients by
% using Quadratured based NIPC approach
% written by Yi Zhang
% Modified on 11-10-2009
%=========================================================================

function [coe,Nt,Dis_Ord]=coe_R(Nd,Nu,Na,dis_Xr,k,index,expand_index,X_0)

Ne=Nu-Na;

if expand_index==2 %%combined expansion

 dis_X_expand=dis_Xr(1:Na+Nd+Ne);

elseif expand_index==1%uncertain expansion

    dis_X_expand=dis_Xr(1:Na);

end

%%%determin expasion information%%%


dim_vari=length(dis_X_expand);


for i=1:dim_vari

    Dis_Ord(i,:)=[dis_X_expand(i),P_order];

end

N_total=size(Dis_Ord,1);

[Root_int,Weight_int]=Root_legend(Dis_Ord);

[XR]=R_respond_initial_points(X_0,Root_int,Dis_Ord,Nu,Nd,Na);

%%%calculate the expansion sample points

if expand_index==1

N_expand=Nd+Nu;

elseif expand_index==2

    N_expand=Nu;

end

if index==1 % tailored_tensor

    Nt=1;
```

```
    for i=1:N_expand
        Nt=Nt*(Dis_Ord(i,2)+1);
    end
elseif index==2 %total-tensor

P_total_expand=Dis_Ord(1,2);

%calculate the terms of polynoimal expansion
Nt=factorial(P_total_expand+N_expand)/(factorial(P_total_expand)...
    *factorial(N_expand));
end
[number_gaussian_point,number_expand_varible]=size(Root_int);
%start Gauss-Quadrature intergration
num_fun=2;
for k=1:num_fun
    polynomial_basic_integral=0;
    polynomial_po_basic_integral=0;
    R_basic_integral=0;
    for i=1:number_gaussian_point^number_expand_varible
        polynomial_basic=polynomial_combine(roots(i,:),Dis_Ord,index);
        polynomial_po_basic=polynomial_basic.^2;
        polynomial_R(k,:)=polynomial_basic.*fun([R_values(i,:),X_0],k);
        weight_total=1;
        for j=1:number_expand_varible
            weight_total=weight_total*weights(i,j);
        end
     polynomial_basic_integral=polynomial_basic_integral+weight_total...
            *polynomial_basic;
     polynomial_po_basic_integral=polynomial_po_basic_integral+...
            weight_total*polynomial_po_basic;
```

```
        R_basic_integral=R_basic_integral+weight_total*polynomial_R(k,:);
    end
    coe(k,:)=R_basic_integral./polynomial_po_basic_integral;
end
```

APPENDIX C

MATLAB SOURCE CODE: UNCERTAINTY QUANTIFICATION WITH POINT-COLLOCATION BASED NIPC

```
%=========================================================================
% This program is used to obtain the stochastic expansion coefficients by
% using Point-Collocation based NIPC approach
% written by Yi Zhang
% Modified on 03-10-2010
%=========================================================================
format long;

clear all;

close all;

clc;

rand('state',0)

% boundary information for design variables

lb_or=[0.000005  0.3  0.08];% lower bound of aleatory

ub_or=[0.05  0.7   0.14 ];% lower bound of aleatory

% boundary for aleatory: M, aleatory parameter M~U(0.7,0.8)

Pa_lb_or=[0.7];% lower bound of aleatory

Pa_ub_or=[0.8 ];% upper bound of aleatory

% boundary for epistemic: k,[0.5,2.0]

k_mu_lb_or=0.5;% lower bound of epistemic

k_mu_ub_or=2.0;% upper bound of epistemic

% general format of parameters

P_lb_or=[Pa_lb_or,k_mu_lb_or];

P_ub_or=[Pa_ub_or,k_mu_ub_or];

% p_order:expansion order

P_order=2;

% expansion approach:2-total;1-tailed;

index=2;


% expansion method for variables:2-combined; 1-aleatory uncertain;

expand_index=2;

%# of deterministic design
```

```
Nd=3;

% #of aleatory parameter
Na=1;

% #of epistemic parameter
Ne=1;

% distribution of determinstic variables and aleatory parameter...
2-uniform:Na Na and epistemic:-uniform

dis_Xr=[2,2,2,2,2];

% Over sampling ratio for point-collocation NIPC

ratio=2;

%=========================================================================
% NACA airfoil definitions

alpha = 0;                              % Angle of attack [deg]
c = 1.0;                                   % Airfoil chord length [m]
p = 43765;                                 % Atmospheric static pressure [Pa]
T = 300;                                   % Atmospheric static temperature [K]
tm = 's-a';                             % Turbulence model: 's-a' or 'kw-sst'
m = [7 200 200 200 100 80 10E-6*c];% [ALE AUS ALS Wake BL IL ymin]
N_itder = 600;

%=========================================================================

%Response surface coefficients calculations

[coe,Nt,Dis_Ord,CL,Cd,Cp]=linear_regression(Nd,Na,Ne,lb_or,ub_or,...
    P_lb_or,P_ub_or,dis_Xr,P_order,index,expand_index,ratio,m,N_itder,...
    alpha,c,p,T,tm);

%=========================================================================
% subfunction :Point_Collocation NIPC approach to obtain estimate
% coefficients of RS
%=========================================================================

function [coe,Nt,Dis_Ord,CL,Cd,Cp]=linear_regression(Nd,Na,Ne,lb,ub,...
    P_lb,P_ub,dis_Xr,P_order,index,expand_index,ratio,m,N_itder,alpha,...
    c,p,T,tm)

if expand_index==2 %%combined expansion

 dis_X_expand=dis_Xr(1:Na+Nd+Ne);

elseif expand_index==1%uncertain expansion

    dis_X_expand=dis_Xr(1:Na);

end
```

```
%%%determin expasion information%%%
dim_vari=length(dis_X_expand);

for i=1:dim_vari

    Dis_Ord(i,:)=[dis_X_expand(i),P_order];

end

%%%%determine sample number%%
N_total=size(Dis_Ord,1); % total expand variables

if index==1 %% tailored_tensor

    Nt=1;

    for i=1:N_total

        Nt=Nt*(Dis_Ord(i,2)+1);

    end

elseif index==2 %% total-tensor

P_total_expand=Dis_Ord(1,2);

%calculate the terms of polynoimal expansion

Nt=factorial(P_total_expand+N_total)/(factorial(P_total_expand)...
          *factorial(N_total));
end

S=ratio*Nt;  %% set the # of samples

[Baic_points,R_input_points]=input_initial_values(Nd,Na,Ne,lb,ub,P_lb,...
    P_ub,dis_Xr,P_order,index,expand_index,S);

[points_variables,number_varibles]=size(Baic_points);

%substitute sample points into expansion formulas and respond formula

for i_p=1:points_variables

    % basic points follow standard distribution

   poly_basic(i_p,:)=polynomial_combine(Baic_points(i_p,:),Dis_Ord,index);
end

for i=1:points_variables

    i_iter=i

    M=R_input_points(Nd+Na,i);
```

```
    K=R_input_points(Nd+Na+Ne,i);
    R= RANS(R_input_points(1:Nd,i)',M,alpha,c,p,T,tm,K,m,N_itder,i);
    CL(i,1)=R.Cl;
    Cd(i,1)=R.Cd;
    Cp(i,:)=-R.Cp;
    respond_out=[CL,Cd];
end

for i_dim=1:2
coe(:,i_dim)=regress(respond_out(:,i_dim),poly_basic)';
end
```

APPENDIX D

MATLAB SOURCE CODE: ADAPTIVE SAMPLING BASED POINT-COLLOCATION NIPC

```
%=========================================================================
%Adaptive Sampling based Point-Collocation NIPC method
%written by yi zhang
%Date:02/07/2012
%=========================================================================
clear all;

close all;

format long

% Define global parameters

global Sample_point psi_rand

% Input date

tic;
% Total expansion (all the expanded varibles expand at the same order)

index=2;

% # of epstemic uncertain and aleatory variables,respectively
Npe=4;

Npa=4;

Nd=0;

Nda=0;

Nde=0;

% Define the distribution of expand variables 1==hermit;2==Legendre;...
%  length of vector denotes the dimension of variables

dis_Xr=[2*ones(1,Npa),2*ones(1,Npe)];


% Expand way:2==combined expansion;1==aleatory uncertain expansion
expand_index=2;

% uncetrain parameters' distribution:Pa_lb(mean or lower bounds)and ...
% Pa_ub(std or upper bounds)

P_lb_orig=[0*ones(1,Npa),0.0*ones(1,Npe)];

P_ub_orig=[1*ones(1,Npa),1*ones(1,Npe)];

% Define the probability level

Pro_level=[0.025,0.2,0.5,0.8,0.975];

% Expand order
```

```
P_order=2;

Nadd=9;

N_dimension=Npe+Npa+Nd+Nda+Nde;

% # of samples of aleatory variables
N_aleatory=15000;

% # of intervals of epistemic variables
N_epistemic=0;

% Total number of samples
N_total=500;

% initialized OSR(over sampling ratio)
OSR(1)=1;


for i=1:length(Pro_level)
  weights_pro_level(i)=1/length(Pro_level);
end

rand('state',0)

% Total standard samples for Ep and determinstic--maxmin
psi_rand_LHS_original=lhsdesign(N_total,Nda+Npa+Nde+Npe+Nd,'criterion',...
    'maximin');

psi_rand_LHS=psi_rand_LHS_original;

err_R=1;% Initialize the stop criterion parameter

Tol=10^(-6);% Stop criterion

poly_basic=[];

respond_out=[];

A_temp=0;

iter=0;

it=0; % used for update linear regression matrix

[coe,Nt,Dis_Ord,poly_basic,respond_out]=linear_regression(dis_Xr,Nda,...
    Nde,Nd,Npa,Npe,P_lb,P_ub,expand_index,index,ratio,P_order,...
    psi_rand_total);

 while err_R>Tol
%=========================================================================
% Calculate check points at specified probability level
% Step1_1: NIPC method to calculate the estimate response surface
```

```
% obtain coefficients of response surface using P-T method
%=========================================================================

if it~=0
    [coe,poly_basic,respond_out]=linear_regression_update(Nda,Nde,Nd,...,
        Npa,Npe,Dis_Ord,Nt,N_total,P_lb_orig,P_ub_orig,expand_index,...,
        index,ratio,P_order,poly_basic,respond_out,it,Nt_Iter,iter,...,
        Nadd,psi_rand_total,A_IX,RS_check_points);

    [R_estimate,X_S,X_U]=sampling_coe_R(Nda,Nde,Nd,Npa,Npe,...
     P_lb_orig,P_ub_orig,N_aleatory,N_epistemic,S,U,coe,Dis_Ord,Nt,index);

end

% STEP2: find out the output bounds values at specified prabability level

if iter==0

[R_estimate,X_S,X_U]=sampling_coe_R(Nda,Nde,Nd,Npa,Npe,P_lb_orig,...,
    P_ub_orig,N_aleatory,N_epistemic,S,U,coe,Dis_Ord,Nt,index);

% Calculate the Output at specified probability level
% Second order probability approach

   for j=1:N_epistemic

       R_estimate_order= sort(R_estimate(j,:))';

       for m = 1:N_aleatory

           R_point_estimate(m,j) = R_estimate_order(m);

           cdf_R_estimate(m,j) = m/N_aleatory;

       end

       for i=1:length(Pro_level)

         for j=1:N_epistemic

             R(i,j)=interp1q(cdf_R_estimate(:,j),R_point_estimate(:,j),...
                    Pro_level(i));

         end

           R_out_bounds(i,:)=[min(R(i,:)),max(R(i,:))];

           R_average_pro_level(i)= (min(R(i,:))+max(R(i,:)))/2;

       end

       for pro_i=1:length(Pro_level)

        for i=1:N_epistemic
```

```
            for j=1:N_aleatory
                diff_R(i,j)=abs(R_estimate(i,j)-R_average_pro_level(pro_i));
            end
        end
            min_diff_R=min(min(diff_R));
            [row,column]=find(diff_R==min_diff_R);
            S_check_initial(pro_i,:)=[S(column(1),:),U(row(1),:)];
        end
    end
% Calculate the initial input variables at specified probability level
% find out the check points by solving nonlinear equations
 if iter==0
 for pro_i=1:length(Pro_level)
 options=optimset('Display','off');% option to dispaly output
 [SU_check,fval]=fsolve('check_coe_R',S_check_initial(pro_i,:)',[],Nda,...
     Nde,Nd,Npa,Npe,P_lb_orig,P_ub_orig,coe,Dis_Ord,Nt,index,...
     R_average_pro_level,pro_i,options);
 S_check_points(pro_i,:)=SU_check;
 x_check=S_transfer_X(SU_check,Nda,Nde,Nd,Npa,Npe,P_lb_orig,P_ub_orig,...
     Dis_Ord);
 RS_check_points(pro_i,:)=x_check';
 R_exact_check(pro_i)=fun(x_check);
 err_check(pro_i)=abs((R_exact_check(pro_i)-R_average_pro_level(pro_i))...
     /R_exact_check(pro_i));
 end
 R_estimate_fix_check{iter+1}=R_average_pro_level;
 else
     for pro_i=1:length(Pro_level)
         R_estimate_check_update(pro_i)=check_coe_R_update...
             (RS_check_points(pro_i,:)',Nda,Nde,Nd,Npa,Npe,P_lb,P_ub,...,
```

```
            coe,Dis_Ord,Nt,index,R_average_pro_level,pro_i);

        err_check(pro_i)=abs((R_exact_check(pro_i)-...
            R_estimate_check_update(pro_i))/R_exact_check(pro_i));

    end

    R_estimate_fix_check{iter+1}=R_estimate_check_update;

end

 % Update the information for addition of more sample points
iter=iter+1;

it=Nt*ratio+iter*Nadd;

if it>2*Nt

    break

end


toc
```

APPENDIX E

MATLAB SOURCE CODE: ROBUST OPTIMIZATION UNDER MIXED UNCERTAINTIES (For Beam Molde Problem)

```
%=========================================================================
%Beam case: uncertain design and parameter uncertainties Robust
%optimization design
%written by yi zhang
%Date:09/06/2010
%case 1 --- aleatory design, epistemic design,three uncertain parameters
%=========================================================================
clear all;

close all;

format long

% Expansion order

k=2;

% Define the distribution of expand variables 1==hermit;2==Legendre;

dis_Xr=[1 1 1 1 2 2];

% expansion option: 1-tailed ;2-total

index=2;

% # of deterministic, uncertain and aleatory variables,respectively

Nd=0;

Ndu=3;

Nda=2;

Npa=2;

Npe=1;

% expansion way:1==combined expansion;2==aleatory uncertain expansion

expand_index=1;

% mean and std of aleatory uncetrain parameters

Pa_mean=[ 450 100e3];Pa_std=[50 10e3];

% Bound of epistemic parameter

Pe_lb=270;Pe_ub=330;

% h-b-l%initinal input design variable

 X_0=[0.6 0.4 5];

% Bounds of design variables
```

```
lb=[0.1  0.1  2  ];

ub=[0.8  0.4  20];

%==================outer optimization loop=======================

option=optimset('display','iter','Algorithm','sqp');

[X_optim,f_obj]=fmincon('obj_robust',X_0,[],[],[],[],lb,ub,...
'constraint_robust',option,dis_Xr,Nda,Ndu,Nd,Npa,Npe,Pa_mean,Pa_std,...
Pe_lb,Pe_ub,expand_index,index,k)

%=============================================================
% Subfunction: objective function for beam case
%=============================================================

function obj=obj_robust(X_optim,dis_Xr,Nda,Ndu,Nd,Npa,Npe,Pa_mean,...
    Pa_std,Pe_lb,Pe_ub,expand_index,index,k)

i_fun=1;

% Obtain coefficients of response surface of objective function

[coe,Nt,Dis_Ord]=coe_R(Nd,Ndu,Nda,Npa,Npe,Pa_mean,Pa_std,Pe_lb,Pe_ub,...
    dis_Xr,k,index,expand_index,X_optim,i_fun);

% Specify input design variables

 X_e0=X_optim(Nda+1:Ndu);

 lb_ep=X_e0-X_e0/10;ub_ep=X_e0+X_e0/10;

 % Initialize the epistemic variables

 X_ep0=[0.0,0.0];

 lb_Xep=[lb_ep,Pe_lb]; ub_Xep=[ub_ep,Pe_ub];

% Inner optimal loop

option=optimset('display','iter','Algorithm','sqp');

[X_ep,obj_std_max]=fmincon('fun_max_std',X_ep0,[],[],[],[],lb_Xep,...
    ub_Xep,[],option,X_optim,coe,Dis_Ord,Nt,1,lb_Xep,ub_Xep);

[X_ep,obj_std_min]=fmincon('fun_min_std',X_ep0,[],[],[],[],lb_Xep,...
    ub_Xep,[],option,X_optim,coe,Dis_Ord,Nt,1,lb_Xep,ub_Xep);

% Calculate objectives: obtain the maximin and minimum values ofobjective

average_mean_obj=X_optim(1)*X_optim(2)*X_optim(3);

max_std_obj=-obj_std_max;
```

```
min_std_obj= obj_std_min;

ave_std_obj=(max_std_obj+min_std_obj)/2;

sdiff_obj=max_std_obj-min_std_obj;

obj =1*average_mean_obj+100*ave_std_obj+500*sdiff_obj;

%=========================================================
% Subfunction: constraints function for beam case
%=========================================================

function [c,ceq]=constraint_robust(X_optim,dis_Xr,Nda,Ndu,Nd,Npa,Npe,...
    Pa_mean,Pa_std,Pe_lb,Pe_ub,expand_index,index,k)

i_fun=2;

ceq=[];

% Obtain coefficients of response surface of constriants

[coe,Nt,Dis_Ord]=coe_R(Nd,Ndu,Nda,Npa,Npe,Pa_mean,Pa_std,Pe_lb,Pe_ub,...
    dis_Xr,k,index,expand_index,X_optim,i_fun);

X_e0=X_optim(Nda+1:Ndu);

lb_ep=X_e0-X_e0/10;ub_ep=X_e0+X_e0/10;

% Initialize the epistemic variables
X_ep0=[0,0];

lb_Xep=[lb_ep,Pe_lb]; ub_Xep=[ub_ep,Pe_ub];

% Inner optimal loop

option=optimset('display','iter','Algorithm','sqp');

[X_ep,con_mean_max]=fmincon('fun_max_mean',X_ep0,[],[],[],[],lb_Xep,...
    ub_Xep,[],option,X_optim,coe,Dis_Ord,Nt,2,lb_Xep,ub_Xep);

[X_ep,con_std_max]=fmincon('fun_max_std',X_ep0,[],[],[],[],lb_Xep,...
    ub_Xep,[],option,X_optim,coe,Dis_Ord,Nt,2,lb_Xep,ub_Xep);


k=3; % define the worst case probability index

% obtain the maximin values  of constraints

g1_mean_max=-con_mean_max;

g1_std_max=-con_std_max;

c=g1_mean_max+k*g1_std_max;
```

APPENDIX F

MATLAB SOURCE CODE: CFD SIMULATION JOURNAL FILE SETUP
(Modified from the original code provided by Dr. Leifur Thor Leifsson)

```
%=========================================================================
%The purpose of the program is to setup matlab journal file for CFD
%running. After CFD runs, the ouput values can be used as response surface
%calculation by using Point-Collocation based NIPC approach.
%=========================================================================
% Define Parameters
%=========================================================================
% NACA airfoil
alpha = 0;                                  % Angle of attack [deg]
c = 1.0;                                    % Airfoil chord length [m]
p = 43765;                                  % Atmospheric static pressure [Pa]
T = 300;                                    % Atmospheric static temperature [K]
tm = 's-a';
% Turbulence model: 's-a' or 'kw-sst'
m = [7 200 200 200 100 80 10E-6*c]; % [ALE AUS ALS Wake BL IL ymin]
N_itder = 600;                              % convergence iterations for CFD run
%%%%%%%%%%%%%%%%%%%%%%%%%%%%%%%%%%%%%%%%%%%%%%%%%%%%%%%%%%%%%%%%%%%%%%%%%%%%
%%%%%%%%%%%%%%%%%%%%%%%%%%%%%%%%%%%%%%%%%%%%%%%%%%%%%%%%%%%%%%%%%%%%%%%%%%%%

x_0_or=[0.02 0.4 0.12]; % initialize airfoil shape parameters
tic;
function R = RANS(x,M,alpha,c,p,T,tm,K,m,N,i)
airfoil(x,c);                                       % Generate airfoil shape
icemcfd(m,c);                                       % Generate mesh
[X,Y,Cp,Cf] = fluent_RANS(M,c,alpha,p,T,N,tm);
% Solve flow and get data
R = aero(M,p,T,c,alpha,x,X,Y,Cp,Cf);% Calculate aerodynamic characteristics
toc;

%=========================================================================
%The matlab code below is to run CFD (Solve flow and get data)
%=========================================================================

function [x,y,Cp,Cf] = fluent_RANS(M,c,alpha,p,T,N,tm,K,i)

% Generate fluent journal file

fluent_RANS_journal(M,c,alpha,p,T,N,tm,K,i);

% Fluid flow analysis

system('del airfoil.cp');
system('del airfoil.xy');
system('del airfoil.cf');
system('del airfoil.tke');
system('del airfoil.omg');
system('del airfoil_drag.frp');
system('del airfoil_lift.frp');
system('del airfoil.cas');
system('fluent 2ddp -hidden -i fluent.jou');

% Read output

[x,y,Cp,Cf] = fluent_read_output;
```

```
%=========================================================================
%Fluent RANS journal file generator.
%=========================================================================
function fluent_RANS_journal(M,c,alpha,p,T,N,tm,K,i)

% Input:    M - Mach number.
%           c - Airfoil chord length [m].
%           alpha - Angle of attack [deg].
%           p - Atmospheric static pressure [Pa].
%           T - Atmospheric static temperature [K].
%           N - Number if iterations.
%           tm - Turbulence model: 's-a' or 'kw-sst'
%           K - Turbulent viscosity factor
% Output:   Fluent journal file fluent.jou.

fid = fopen('fluent.jou','w+');

fprintf(fid,';FLUENT Journal File\n');
fprintf(fid,'\n');
fprintf(fid,';Read in the mesh file\n');
fprintf(fid,'file read-case airfoil.msh\n');
fprintf(fid,'\n');

fprintf(fid,'/define/models/solver density-based-implicit\n');
fprintf(fid,';Enable density-based-implicit solver? [yes]\n');
fprintf(fid,'yes\n');
fprintf(fid,';No change.\n');
fprintf(fid,'\n');

switch tm
    case 's-a'

    fprintf(fid,';Specify modeling approach.\n');
    fprintf(fid,'/define/models/viscous spalart-allmaras\n');
    fprintf(fid,'yes\n');
    fprintf(fid,'\n');

    fprintf(fid,'/define/models/viscous sa-alternate-prod\n');
    fprintf(fid,';Strain/vorticity production for S-A model? [yes]\n');
    fprintf(fid,'yes\n');
    fprintf(fid,'\n');

    %-----------------------------------------------------------------------
    if ~isempty(K)
     fluent_turb_visc(K);
     fprintf(fid,'/define/user-defined interpreted-functions\n');
     fprintf(fid,';UDF Source File Name ["..\turb_visc.c"]\n');
     fprintf(fid,'turb_visc.c\n');
     fprintf(fid,';CPP Command Name ["cpp"]\n');
     fprintf(fid,'"cpp"\n');
     fprintf(fid,';virtual machine stack size [10000]\n');
     fprintf(fid,'10000\n');
     fprintf(fid,';display assembly code listing? [yes]\n');
```

```
        fprintf(fid,'yes\n');
        fprintf(fid,'\n');

        fprintf(fid,'/define/models/viscous user-defined\n');
        fprintf(fid,';Viscous user-defined functions:("none" "user_mu_t")\n');
        fprintf(fid,';Enter turbulent viscosity function ["none"]\n');
        fprintf(fid,'"user_mu_t"\n');
        fprintf(fid,';Enter TKE Prandtl number function ["none"]\n');
        fprintf(fid,'"none"\n');
        fprintf(fid,'\n');
      end
      %-------------------------------------------------------------------------

end
......
......
......

fprintf(fid,';Write case and data files.\n');
fprintf(fid,'file write-case-data\n');
fprintf(fid,';case file name [""]\n');
str = ['airfoil_', num2str(i), '.cas'];
fprintf(fid, str,'\n');
fprintf(fid,'\n');
fprintf(fid,';Exit Fluent.\n');
fprintf(fid,'exit\n');

fclose(fid);
```

BIBLIOGRAPHY

[1] G. S.n Fishman. *Monte Carlo: Concepts, Algorithms, and Applications.* New York: Springer. ISBN 0-387-94527-X, 1995.

[2] T. Botev Z.I. Kroese, D. P. Taimre. *Handbook of Monte Carlo Methods.* New York: John Wiley. p. 772. ISBN 0-470-17793-4., 2011.

[3] Siebert B.R.L. Cox, M.G. The use of a monte carlo method for evaluating uncertainty and expanded uncertainty. *Metrologia*, 43(4):S178–S188, 2006.

[4] L.Y. Zhao and X.Q. Zhang. Uncertainty quantification of a flapping airfoil with a stochastic velocity deviation based on a surrogate model. *Advanced Materials Research*, 201-203:1209–1212, 2011.

[5] L. Zhao and X. Zhang. Uncertainty quantification of a flapping airfoil with stochastic velocity deviations using the response surface method. *Open Mechanical Engineering Journal*, 5(1):152–159, 2011.

[6] X. Du. Unified uncertainty analysis by the first order reliability method. *Journal of Mechanical Design, Transactions of the ASME*, 130(9):0914011–09140110, 2008.

[7] S. Sujecki. Extended taylor series and interpolation of physically meaningful functions. *Optical and Quantum Electronics*, pages 1–14, 2012.

[8] Z.-J. Chen and H. Xiao. The taylor series multipole boundary element method (tsm-bem) and its applications in rolling engineering. *Chongqing Daxue Xuebao/Journal of Chongqing University*, 35(5):57–63, 2012.

[9] C. Shu, Y. Peng, C.F. Zhou, and Y.T. Chew. Application of taylor series expansion and least-squares-based lattice boltzmann method to simulate turbulent flows. *Journal of Turbulence*, 7:1–12, 2006.

[10] S. Rahman and B.N Rao. A perturbation method for stochastic meshless analysis in elastostatics. *Internatinal Journal for Numerical Methods in Engineering*, 50:1961–1991, 2001.

[11] R.R. Waiboer, R.G.K.M. Aarts, and J.B. Jonker. Application of a perturbation method for realistic dynamic simulation of industrial robots. *Multibody System Dynamics*, 13(3):323–338, 2005.

[12] S.K. Khattri. Series expansion of functions with he's homotopy perturbation method. *International Journal of Mathematical Education in Science and Technology*, 43(5):677–684, 2012.

[13] S.H. Lee and W. Chen. A comparative study of uncertainty propagation methods for black-box-type problems. *Structural and Multidisciplinary Optimization*, 37(3):239–253, 2009.

[14] M. S. Eldred, C. G. Webster, and P. G. Constantine. Evaluation of non-intrusive approaches for wiener-askey generalized polynomial chaos, AIAA-paper 2008-1892. In 10^{th} *AIAA Non-Deterministic Approaches Forum*, Schaumburg, IL, April, 2008.

[15] M.S. Eldred and J. Burkardt. Comparison of non-intrusive polynomial chaos and stochastic collocation methods for uncertainty quantification, AIAA 2009-0976. In 47^{th} *AIAA Aerospace Sciences Meeting*, Orlando, FL, January 2009.

[16] D. Veneziano, A. Agarwal, and E. Karaca. Decision making with epistemic uncertainty under safety constraints: An application to seismic design. *Probabilistic Engineering Mechanics*, 24(3):426–437, 2009.

[17] H.-Z. Huang and X. Zhang. Design optimization with discrete and continuous variables of aleatory and epistemic uncertainties. *Journal of Mechanical Design, Transactions of the ASME*, 131(3):0310061–0310068, 2009.

[18] M. Dolek. Simplified method for seismic risk assessment of buildings with consideration of aleatory and epistemic uncertainty. *Structure and Infrastructure Engineering*, 8(10):939–953, 2012.

[19] L. P. Swiler, T. Paez, and R. Mayes. Epistemic uncertainty quantification tutorial. In *SAND 2008-6578C, paper 294 in the Proceedings of the IMAC XXVII Conference and Exposition on Structural Dynamics, Society for Structural Mechanics*, Orlando, FL, Feb. 2009.

[20] L. Swiler, T. Paez, R. Mayes, and M. Eldred. Epistemic uncertainty in the calculation of margins, AIAA 2009-2249. In 50^{th} *AIAA/ASME/ASCE/AHS/ASC Structures, Structural Dynamics, and Materials Conference*, Palm Springs, CA, May 2009.

[21] X. Du. Reliability-based design optimization with dependent interval variables. *International Journal for Numerical Methods in Engineering*, 91(2):218–228, 2012.

[22] Y.P. Ju and C.H. Zhang. Multi-point robust design optimization of wind turbine airfoil under geometric uncertainty. *Proceedings of the Institution of Mechanical Engineers, Part A: Journal of Power and Energy*, 226(2):245–261, 2012.

[23] E. Haro Sandoval, F. Anstett-Collin, and M. Basset. Sensitivity study of dynamic systems using polynomial chaos. *Reliability Engineering and System Safety*, 104:15–26, 2012.

[24] J. Didier, B. Faverjon, and J.-J. Sinou. Analysing the dynamic response of a rotor system under uncertain parameters by polynomial chaos expansion. *JVC/Journal of Vibration and Control*, 18(5):712–732, 2012.

[25] H. Cheng and A. Sandu. Efficient uncertainty quantification with the polynomial chaos method for stiff systems. *Mathematics and Computers in Simulation*, 79(11):3278–3295, 2009.

[26] S. Hosder, R. W. Walters, and M. Balch. Efficient sampling for non-intrusive polynomial chaos applications with multiple input uncertain variables.

[27] S. Hosder, R. W. Walters, and R. Perez. A non-intrusive polynomial chaos method for uncertainty propagation in cfd simulations, AIAA 2006-891. In 44^{th} *AIAA Aerospace Sciences Meeting and Exhibit*, Reno, NV, January 2006.

[28] B. Bettis and S. Hosder. Quantification of uncertainty in aerodynamic heating of a reentry vehicle due to uncertain wall and freestream conditions, AIAA 2010-4642. In 10^{th} *AIAA Joint Thermophysics and Heat Transfer Conference*, Chicago, IL, June 2010.

[29] M.S. Eldred, L.P. Swiler, and G. Tang. Mixed aleatory-epistemic uncertainty quantification with stochastic expansions and optimization-based interval estimation. *Reliability Engineering and System Safety*, 96(9):1092–1113, 2011.

[30] S. Hosder and B. Bettis. Uncertainty and sensitivity analysis for reentry flows with inherent and model-form uncertainties. *Journal of Spacecraft and Rockets*, 49(2):193–206, 2012.

[31] X. Du, A. Sudjianto, and B. Huang. Reliability-based design with the mixture of random and interval variables. *Journal of Mechanical Design, Transactions of the ASME*, 127(6):1068–1076, 2005.

[32] J. Guo and X. Du. Reliability analysis for multidisciplinary systems with random and interval variables. *AIAA Journal*, 48(1):82–91, 2010.

[33] G. Taguchi, S. Chowdhury, and S. Taguchi. *Robust Engineering*. McGraw Hill, New York, 2000.

[34] G. Taguchi. *Taguchi on Robust Technology Development: Bringing Quality Engineering Upstream*. ASME Press, New York, 1993.

[35] D.I. Papadimitriou and K.C. Giannakoglou. Third-order sensitivity analysis for robust aerodynamic design using continuous adjoint. *International Journal for Numerical Methods in Fluids*, 2012.

[36] J.H. Wiebenga, A.H. Van Den Boogaard, and G. Klaseboer. Sequential robust optimization of a v-bending process using numerical simulations. *Structural and Multidisciplinary Optimization*, 46(1):137–153, 2012.

[37] X. Du and W. Chen. Efficient uncertainty analysis methods for multidisciplinary robust design. *AIAA Journal*, 40(3):545–552, 2002.

[38] M. Karpel, B. Moulin, and M. Idan. Robust aeroservoelastic design with structural variations and modeling uncertainties. *Journal of Aircraft*, 40(5):946–954, 2003.

[39] B. Ramakrishnan and S.S. Rao. A general loss function based optimization procedure for robust design. *Engineering Optimization*, 25(4):255–276, 1996.

[40] J. Patel A. Kumar J.K. Allen A. Ruderman, S.K. Choi. Variable sensitivity-based deterministic robust design for nonlinear system. *Journal of Mechanical Design, Transactions of the ASME*, 132:0645021–0645027, 2010.

[41] H. Choi, D.L. McDowell, J.K. Allen, D. Rosen, and F. Mistree. An inductive design exploration method for robust multiscale materials design. *Journal of Mechanical Design, Transactions of the ASME*, 130(3), 2008.

[42] A. Ruderman, S.-K. Choi, J. Patel, A. Kumar, and J.K. Allen. Simulation-based robust design of multiscale products. *Journal of Mechanical Design, Transactions of the ASME*, 132(10), 2010.

[43] T. Ray A. Saha. Practical robust design optimization using evolutionary algorithms. *Journal of Mechanical Design, Transactions of the ASME*, 133, 2011.

[44] H.X. Li X. Lu. Perturbation theory based robust design under model uncertainty. *Journal of Mechanical Design, Transactions of the ASME*, 131:1110061–1110069, 2009.

[45] H-G. Beyer and B. Sendhoff. Robust optimization−a comprehensive survey. *Computer Methods in Applied Mechanics and Engineering*, 196(33-34):3190–3218, 2007.

[46] M. S. Eldred. Design under uncertainty employing stochastic expansion methods. *International Journal for Uncertainty Quantification*, 1(2):119–146, 2011.

[47] M. Dodson and G. T. Parks. Robust aerodynamic design optimization using polynomial chaos. *Journal of Aircraft*, 46(2):635–646, 2009.

[48] B.D. Youn, K.K. Choi, L. Du, and D. Gorsich. Integration of possibility-based optimization and robust design for epistemic uncertainty. *Journal of Mechanical Design, Transactions of the ASME*, 129(8):876–882, 2007.

[49] M.S. Eldred. Recent advances in non-intrusive polynomial chaos and stochastic collocation methods for uncertainty analysis and design. 2009.

[50] X. Du, P. K. Venigella, and D. Liu. Robust mechanism synthesis with random and interval variables. *Mechanism and Machine Theory*, 44(7):1321–1337, 2009.

[51] W. L. Oberkampf, J. C. Helton, C. A. Joslyn, S. F. Wojtkiewicz, and S. Ferson. Challenge problems: uncertainty in system response given uncertain parameters. *Reliability Engineering and System Safety*, 85(1-3):11–19, 2004.

[52] J. C. Helton, J. D. Johnson, and W. L. Oberkampf. An exploration of alternative approaches to the representation of uncertainty in model predictions. *Reliability Engineering and System Safety*, 85(1-3):39–71, 2004.

[53] Askey. R. and Wilson. J. *Some Basic Hypergeometric Polynomials that Generalize Jacobi Polynomials*. Amer Mathematical Society, Providence, RI, 1985.

[54] N.Wiener. The homogeneous chaos. *American Journal of Mathematics*, 60(4):897–936, 1994.

[55] D. Xiu and G. E. Karniadakis. Modeling uncertainty in flow simulations via generalized polynomial chaos. *Journal of Computational Physics*, 187(1):137–167, May, 2003.

[56] L. Huyse, A.R. Bonivtch, J.B. Pleming, D.S. Riha, C. Waldhart, and B.H. Thacker. Verification of stochastic solutions using polynomial chaos expansions. volume 7, pages 4885–4893, 2006.

[57] R. W. Walters and L. Huyse. Uncertainty analysis for fluid mechanics with applications. Technical report, ICASE 2002-1, NASA/CR-2002-211449, NASA Langley Research Center, Hampton, VA, 2002.

[58] H. N. Najm. Uncertainty quantification and polynomial chaos techniques in computational fluid dynamics. *Annual Review of Fluid Mechanics*, 41:35–52, 2009.

[59] S. Hosder and R. W. Walters. Non-intrusive polynomial chaos methods for uncertainty quantification in fluid dynamics, AIAA-paper 2010-0129. In 48^{th} *AIAA Aerospace Sciences Meeting*, Orlando, FL, January 4-7, 2010.

[60] B. J. Debusschere, H. N. Najm, P. P. Pebay, O. M. Knio, R. G. Ghanem, and O. P. L. Maitre. Numerical challenges in the use of polynomial chaos representations for stochastic processes. *SIAM Journal on Scientific Computing*, 26(2):698–719, 2004.

[61] M.Y. L. Mathelin and T. Z. Hussaini. Stochastic approaches to uncertainty quantification in cfd simulations. *Numerical Algorithms*, 38(1):209–236, March 2005.

[62] D. Lucor, C. Enaux, H. Jourdren, and P. Sagaut. Stochastic design optimization: Application to reacting flows. *Computational Methods in Applied Mechanics and Engineering*, 196(49), 2007.

[63] S. Smolyak. Quadrature and interpolation formulas for tensor products of certain classes of functions. *Soviet Math. Dokl.*, 12(4):240–243, 1963.

[64] M. S. Eldred and B. J. Bichon. Second-order reliability formulations in dakota/uq. In *Collection of Technical Papers - AIAA/ASME/ASCE/AHS/ASC Structures, Structural Dynamics and Materials Conference*, volume 4, pages 2897–2919, 2006.

[65] D. Xiu and J.S. Hesthaven. High-order collocation methods for differential equations with random inputs. *SIAM Journal on Scientific Computing*, 27(3):1118–1139, 2006.

[66] F. Nobile, R. Tempone, and C.G. Webster. An anisotropic sparse grid stochastic collocation method for partial differential equations with random input data. *SIAM Journal on Numerical Analysis*, 46(5):2411–2442, 2008.

[67] F. Nobile, R. Tempone, and C.G. Webster. A sparse grid stochastic collocation method for partial differential equations with random input data. *SIAM Journal on Numerical Analysis*, 46(5):2309–2345, 2008.

[68] S. Hosder, R. W. Walters, and M. Balch. Efficient sampling for non-intrusive polynomial chaos applications with multiple input uncertain variables, AIAA-paper 2007-1939. In 9^{th} *AIAA Non-Deterministic Approaches Conference*, Honolulu, HI, April, 2007.

[69] M. Eldred and L. Swiler. Efficient algorithms for mixed aleatory-epistemic uncertainty quantification with application to radiation-hardened electronics. *Sandia National Laboratories Report*, SAND2009-5805, September, 2009.

[70] B. Sudret. Global sensitivity analysis using polynomial chaos expansions. *Reliability Engineering and System Safety*, 93(7):964–979, 2008.

[71] G. N. Vanderplaats. *Numerical Optimization Techniques For Engineering Design*. Vanderplaats Research and Development, Colorado Springs, CO, 3 edition, 1999.

[72] J. D. Anderson. *Fundamentals of Aerodynamics,* 4^{th} *Edition*. McGraw-Hill, New York, 2010.

[73] P. R. Spalart and S. R. Allmaras. A one equation turbulence model for aerodynamic flows, aiaa-paper-92-0439. In 38^{th} *AIAA Aerospace Sciences Meeting and Exhibit*, Reno, NV, January 6-9, 1992.

[74] *FLUENT, ver. 13.0*. ANSYS Inc., Southpointe, 275 Technology Drive, Canonsburg, PA 15317, 2011.

[75] I. H. Abbott and A. E. Von Doenhoff. *Theory of Wing Sections*. Dover Publications, 1959.

[76] *ICEM CFD, ver. 13.0.* ANSYS Inc., Southpointe, 275 Technology Drive, Canonsburg, PA 15317, 2011.

[77] S. Hosder, R. W. Walters, and M. Balch. Point-collocation nonintrusive polynomial chaos method for stochastic computational fluid dynamics. *AIAA Journal*, 48(12):2721–2730, 2010.

VITA

Yi Zhang is from Shanxi where is the western part of P. R. China. She completed her undergraduate study in the Department of Aerospace Engineering at Northwestern Polytechnical University, Xian, P. R. China, and received a B.S. degree in July 2003. She continued her study in a master degree program of the same department and received her M.S. degree in May 2006. In September 2005, she started the degree of Doctor of Philosophy in the Department of Aerospace Engineering at Northwestern Polytechnical University. From September 2007 to September 2008 she worked with Dr. Xiaoping Du in the Department of Mechanical and Aerospace Engineering at Missouri University of Science and Technology as a visiting student. Yi started to pursue the degree of Doctor of Philosophy in Aerospace Engineering in the Department of Mechanical and Aerospace Engineering at Missouri University of Science and Technology under Dr. Serhat Hosder since January 2009. She conducted research in the areas of uncertainty quantification and robust design optimization. She expects to receive her Ph.D. degree in May 2013. She has been a member of the American Society of Mechanical Engineers (ASME) since 2009 and a member of the American Institute of Aeronautics and Astronautics (AIAA) since 2009.